UNIVERSITÀ DEGLI STUDI DI PADOVA

Dipartimento di Fisica e Astronomia "Galileo Galilei"

Corso di Laurea Magistrale in Fisica

Tesi di Laurea

Hadronic Contributions

to Muon-Electron Scattering at NNLO

Relatore

Dr. Massimo Passera

Laureando

Marco Vitti

Anno Accademico 2017/2018

Contents

Introduction

Goal of this thesis is the evaluation of the hadronic contribution to the cross section of muon-electron scattering at next-to-next-to-leading order (NNLO). This contribution is essential for the interpretation of data coming from the recently proposed MUonE experiment at CERN [1,2], which aims to provide a novel determination of the hadronic leading-order (HLO) contribution to the anomalous magnetic moment of the muon.

The anomalous magnetic moment of the muon is one of the most precisely measured quantities in particle physics. Yet, the theoretical Standard Model prediction for the value of the muon g-2 deviates from the experimental measurement by 3-4σ. This long-standing discrepancy has led to speculations about possible effects of new physics, motivating a new generation of experiments at Fermilab and J-PARC. The new E989 Muon g-2 experiment at Fermilab is now taking data and its first result is expected next year.

In order to match the progress on the experimental side, an improvement in precision is required also for the theoretical prediction, whose main source of uncertainty comes from non-perturbative hadronic contributions, especially from hadronic vacuum polarization. The calculation of the leading hadronic contribution to the muon g-2, a_μ^{HLO}, traditionally relies on a dispersive integral which relates it to a complicated integration of the measured cross section for e^+e^- annihilation into hadrons.

An alternative determination of a_μ^{HLO} recently proposed in [1] involves the hadronic contribution to the running of the electromagnetic coupling, $\Delta\alpha_{\text{had}}(t)$, where t is a space-like variable. The MUonE experiment [2] could extract $\Delta\alpha_{\text{had}}(t)$ by determining the complete running of the fine-structure constant, $\Delta\alpha(t)$, from the measurement of the differential cross section $d\sigma/dt$ of elastic muon-electron scattering. On the theoretical side, the evaluation of $d\sigma/dt$ would then be needed up to NNLO. The present work is devoted to the calculation of the hadronic contributions to this cross section.

In Ch. 1 we introduce the anomalous magnetic moment of the muon and the current status of its theoretical prediction, and we discuss the MUonE proposal. In Ch. 2 we move to the study of the differential cross section for elastic muon-electron scattering. Specifically, we analyze the QED corrections up to NLO, which will serve as a benchmark for the hadronic NNLO calculation. Ch. 3 is dedicated to the theory of dispersion relations and its application, in conjunction with the optical theorem, to the evaluation of a_μ^{HLO}. In Ch. 4 we finally study the hadronic contributions to muon-electron scattering at NLO and NNLO, making use of the dispersive approach previously introduced. Conclusions are drawn in Ch. 5.

Chapter 1

The Anomalous Magnetic Moment of the Muon

Magnetic dipole moments arise as classical properties of physical systems: one important example is that of an orbiting charged particle with charge q, producing a circulating current. If m is the mass of the particle and $\vec{L} = m\vec{r} \times \vec{v}$ is its orbital angular momentum, then the associated magnetic dipole moment is

$$\vec{\mu}_L = \frac{q}{2mc}\vec{L}\,. \tag{1.1}$$

When spin is introduced as the intrinsic angular momentum of a particle in the consideration of quantum systems, it is possible to define the particle's magnetic dipole moment as

$$\vec{\mu} = g\,\mu_B \frac{\vec{\sigma}}{2} \tag{1.2}$$

where σ_i ($i = 1, 2, 3$) are the Pauli spin matrices, $\mu_B = \frac{e\hbar}{2mc}$ is the Bohr magneton and the proportionality factor g is the *gyromagnetic ratio* or g-factor.

The anomalous magnetic moment of a lepton, a_l, is defined as the deviation from the value of its gyromagnetic ratio predicted by the Dirac theory

$$a_l = \frac{g_l - 2}{2} \tag{1.3}$$

as a consequence of radiative corrections arising in quantum field theory (QFT).

1.1 Historical Introduction

The study of the anomalous magnetic moment of leptons has accompanied the evolution of the Standard Model (SM) of particle physics since its early developments. When Uhlenbeck and Goudsmit [3,4] postulated the spin of the electron to be $\hbar/2$, the experimental results coming from atomic spectroscopy could be explained setting $g_e = 2$. This was puzzling, since if the spin $\vec{S} = (\hbar/2)\vec{\sigma}$ is assumed to be an analogous of the orbital angular momentum $\vec{L}$, then the value $g_e = 1$ would be expected. The solution to this conundrum arrived with Dirac's relativistic extension of the quantum-mechanical theory of the electron [5], which naturally predicted the value $g_e = 2$.

The First Anomaly In 1948, twenty years after Dirac's prediction, Kusch and Foley [6] presented their results for the precision measurement of the magnetic moment of the electron, from the study of the hyperfine structure of atomic spectra, proposing the value $g_e = 2.00238(10)$. The discrepancy with Dirac's result was accounted for theoretically later the same year, within the framework of Quantum Electrodynamics (QED) and the renormalization program. The famous calculation by Schwinger [7]

$$a_e = \frac{\alpha}{2\pi} \simeq 0.00116 \tag{1.4}$$

was one of the first great achievements obtained by QED, together with the interpretation of the Lamb-shift [8]. The success in determining the leading contribution to a_e sparked an interest in the calculation of higher-order terms that is still vivid: the anomalous magnetic moment of the electron is now measured with an astounding precision of 0.22 parts per billion [9], and the experimental determination matches the theoretical prediction up to five loops in the perturbative expansion [10], a remarkable result that has provided the strictest test for QED.

The Muon Anomaly In 1956 Berestetskii et al. [11–13] showed that in a broad class of Beyond Standard Model (BSM) theories the sensitivity of a_l to short-distance effects is expressed by the relation

$$\frac{\delta a_l}{a_l} \sim \frac{m_l^2}{\Lambda^2} \tag{1.5}$$

where δa_l is the deviation from the theoretical prediction, m_l is the mass of the lepton and Λ represents the scale of new physics[1]. Therefore, provided the same experimental accuracy, the muon anomaly is possibly much better suited to the study of unknown effects[2] compared to a_e, by a factor $(m_\mu^2/m_e^2) \sim 4 \times 10^4$. This observation drew attention on a possible measurement of a_μ, but at that time there was no idea on how to perform such a measurement, since the technique employed until then for the electron required the ability to produce polarized leptons.

In 1957, however, the discovery of parity violation [15] led to a method of determining a_μ, in which longitudinally polarized muons are produced through pion decay and are trapped in a magnetic field, causing spin precession; the latter is then analyzed in order to extract a_μ by looking at the decay electrons/positrons of the muons. This opened the way to a series of increasingly precise measurements [16–20] in about fifty years, culminating in the E821 experiment at Brookhaven [21], which has measured a_μ with a relative precision of 0.54 parts per million (ppm). Moreover, the new E989 experiment is now in progress at Fermilab [22, 23], and it works with ultra-relativistic muons like the previous muon storage rings, while the conceptually new E34 experiment [24] at J-PARC may use ultra-cold muons, therefore providing a test for potential sources of systematic errors in the first method.

1.2 Present Theoretical Prediction of a_μ

The SM prediction for the muon anomaly is [25]

$$a_\mu^{SM} = 116591776(44) \times 10^{-11} \tag{1.6}$$

and the comparison with the latest experimental measurement of a_μ performed at BNL [26]

$$a_\mu^{exp} = 116592091(63) \times 10^{-11} \tag{1.7}$$

points out a discrepancy of about 4 standard deviations.

From the theoretical point of view, the SM prediction for the anomalous magnetic moment of the muon is typically splitted in three parts: the QED, the electroweak and the hadronic contributions

$$a_\mu^{SM} = a_\mu^{QED} + a_\mu^{EW} + a_\mu^{had} \tag{1.8}$$

which are discussed in the following. Updated results are taken from Jegerlehner's recent review [27].

1.2.1 QED Contribution

The QED contribution arise from diagrams involving the three charged leptons (e, μ, τ) interacting with the photon. It is the dominant contribution, accounting for more than 99.99% of the value of

---

[1]BSM theories in which this scaling is violated are discussed in [14].

[2]Unfortunately, although a_τ would provide even greater sensitivity to new physics, the short lifetime of the tau lepton forbids at present an experimental measurement at the required accuracy.

the entire prediction. Since three mass scales are associated to the different lepton masses (m_e, m_μ, m_τ), the QED contribution can be expressed as [28]

$$a_\mu^{\text{QED}} = A_1 + A_2\left(\frac{m_\mu}{m_e}\right) + A_2\left(\frac{m_\mu}{m_\tau}\right) + A_3\left(\frac{m_\mu}{m_e}, \frac{m_\mu}{m_\tau}\right) \tag{1.9}$$

where A_1 is related to diagrams involving photons and muon loops only. More generally, A_1 represents diagrams in which the leptons flowing in closed loops are the same as the external lepton. Indeed, A_1 is a universal contribution, valid for the electron and tau g-2 as well. The contributions to A_2 begin to appear at two loops while the first contribution to A_3 is related to a three-loop diagram with both an electronic and tauonic vacuum polarization insertions.

The A_i ($i = 1, 2, 3$) terms are expressed as a perturbative expansion in powers of α/π

$$A_i = A_i^{(2)}\left(\frac{\alpha}{\pi}\right) + A_i^{(4)}\left(\frac{\alpha}{\pi}\right)^2 + A_i^{(6)}\left(\frac{\alpha}{\pi}\right)^3 + A_i^{(8)}\left(\frac{\alpha}{\pi}\right)^4 + A_i^{(10)}\left(\frac{\alpha}{\pi}\right)^5 + \dots \tag{1.10}$$

where each $A_i^{(j)}$ is computed order by order in renormalized perturbation theory. Once the results for a given order L are collected in the coefficient of the $(\alpha/\pi)^L$ term

$$C_L = A_1^{(2L)} + A_2^{(2L)}\left(\frac{m_\mu}{m_e}\right) + A_2^{(2L)}\left(\frac{m_\mu}{m_\tau}\right) + A_3^{(2L)}\left(\frac{m_\mu}{m_e}, \frac{m_\mu}{m_\tau}\right) \tag{1.11}$$
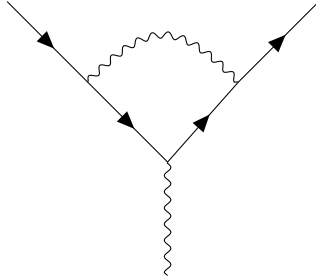
the result for a_μ^{QED} is written as

$$a_\mu^{\text{QED}} = \sum_L C_L \left(\alpha/\pi\right)^L \ . \tag{1.12}$$

In the following we present the main results for the QED contributions, which have been calculated up to five loops, i.e. $\mathcal{O}((\alpha/\pi)^5)$ in the perturbative expansion.

One-Loop Contribution

The only one-loop diagram contributing to a_μ^{QED} is depicted below

and its contribution was first evaluated by Schwinger [7], with the result

$$C_1 = A_1^{(2)} = \frac{1}{2} \tag{1.13}$$

and $A_2^{(2)} = A_3^{(2)} = 0$.

Two-Loop Contribution

Nine diagrams are related to a_μ^{QED} at two-loop level. Seven of them involve only muons and photons, thus contributing to $A_1^{(4)}$, while the vacuum polarization diagrams with an electron and a tau loop contribute to $A_2^{(4)}\left(\frac{m_\mu}{m_e}\right)$ and $A_2^{(4)}\left(\frac{m_\mu}{m_\tau}\right)$ respectively. The $A_1^{(4)}$ term was first calculated by Petermann

and Sommerfield [29, 30], while the mass-dependent ones were computed analytically in [31] (for a simplified expression see [32]): results are

$$A_1^{(4)} = 0.32847896557919378\ldots$$
$$A_2^{(4)}\left(\frac{m_\mu}{m_e}\right) = 1.0942583092(72)$$
$$A_2^{(4)}\left(\frac{m_\mu}{m_\tau}\right) = 0.000078079(14)$$

(1.14)

and $A_3^{(4)} = 0$. Errors in the last two lines of Eq.(1.14) are due to the uncertainty in the measurement of the lepton masses. The coefficient C_2 then reads

$$C_2 = A_1^{(4)} + A_2^{(4)}\left(\frac{m_\mu}{m_e}\right) + A_2^{(4)}\left(\frac{m_\mu}{m_\tau}\right) = 0.765857423(16)$$

(1.15)

where the errors on $A_2^{(4)}(m_\mu/m_e)$ and $A_2^{(4)}(m_\mu/m_\tau)$ have been added in quadrature, since the uncertainties in the lepton masses can be treated as independent. The total contribution to a_μ is

$$a_\mu^{(4)\,\text{QED}} = C_2\left(\frac{\alpha}{\pi}\right)^2 \simeq 413217.627(9) \times 10^{-11} \,.$$

(1.16)

Three-Loop Contribution

The three-loop contribution to a_μ arise from more than a hundred diagrams: for all of them an analytical evaluation has been completed in the late 1990s. Besides, numerical methods were developed in parallel by Kinoshita and his collaborators [33].

The $A_1^{(6)}$ term receives contribution from 72 diagrams, whose computation is due to Remiddi and his collaborators [34–43], while the evaluation of the $A_2^{(6)}$ terms was completed by Laporta and Remiddi in 1993 [44, 45] (see also [46]). Moreover, at three loops the two-mass-scale term $A_3^{(6)}(m_\mu/m_e, m_\mu/m_\tau)$ shows up for the first time: this has been evaluated in 1999 [47]. Results are

$$A_1^{(6)} = 1.181241456587\ldots$$
$$A_2^{(6)}\left(\frac{m_\mu}{m_e}\right) = 22.86838000(17)$$
$$A_2^{(6)}\left(\frac{m_\mu}{m_\tau}\right) = 0.00036063(12)$$
$$A_3^{(6)}\left(\frac{m_\mu}{m_e}, \frac{m_\mu}{m_\tau}\right) = 0.00052776(10)$$

(1.17)

with the value of the C_3 coefficient

$$C_3 = 24.05050982(28)$$

(1.18)

where the errors from the A_2 terms are added in quadrature and the one from A_3 linearly, taking account of correlations. The sixth-order QED contribution to a_μ is then

$$a_\mu^{(6)\,\text{QED}} = C_3\left(\frac{\alpha}{\pi}\right)^3 \simeq 30141.9022(4) \times 10^{-11} \,.$$

(1.19)

Four-Loop Contribution

More than a thousand diagrams are involved in the computation of the four-loop contribution. A complete analytical result is still missing, but a numerical evaluation has been possible thanks to the efforts of Kinoshita and collaborators. The calculation of the $A_1^{(8)}$ term, coming from 891 diagrams, has been recently accomplished [48], yielding

$$A_1^{(8)} = -1.91298(84)$$

(1.20)

with the theoretical error coming from the Monte-Carlo integration. Moreover, a quasi-exact result for this universal term has been obtained by Laporta [49]

$$A_1^{(8)} = -1.9122457649264455741526471674398300540608733906587253345\ldots \tag{1.21}$$

with an accuracy of 1100 digits. For what concerns the mass-dependent terms, results obtained in [50] read

$$A_2^{(8)}\left(\frac{m_\mu}{m_e}\right) = 132.6852(60)$$

$$A_2^{(8)}\left(\frac{m_\mu}{m_\tau}\right) = 0.04234(12) \tag{1.22}$$

$$A_3^{(8)}\left(\frac{m_\mu}{m_e}, \frac{m_\mu}{m_\tau}\right) = 0.06272(4)$$

and the sum of the $A_i^{(8)}$ terms then yields

$$C_4 = 130.8734(60) \tag{1.23}$$

for a total contribution

$$a_\mu^{(8)\ \mathrm{QED}} = C_4 \left(\frac{\alpha}{\pi}\right)^4 \simeq 380.990(17) \times 10^{-11}\ . \tag{1.24}$$

We emphasize that this four-loop contribution is about 6 times the error from the measurement of Eq.(1.7), therefore an accurate computation is essential to interpret consistently the experimental results.

Five-Loop Contribution

At five-loop level one has to consider more than 10.000 diagrams (12672 contribute to $A_1^{(10)}$ only). A complete numerical evaluation has been obtained by Aoyama et al. [51] with the result

$$C_5 \simeq 751.917(932) \tag{1.25}$$

and therefore

$$a_\mu^{(10)\ \mathrm{QED}} = C_5 \left(\frac{\alpha}{\pi}\right)^5 \simeq 5.0845(63) \times 10^{-11}\ . \tag{1.26}$$

Final Result for the QED Contribution

Summing up all the previous results, the total QED contribution is

$$a_\mu^{\mathrm{QED}} = 116584718.859(.026)(.009)(.017)(.006) \times 10^{-11} \tag{1.27}$$

where the uncertainties are due, respectively, to the errors in the measurement of the fine-structure constant and of the mass ratios, and to the numerical errors associated to the four- and five-loop terms. It is worth noting that the value of α used in the computation is the most precisely measured, and is determined from the measurement of the anomalous magnetic moment of the electron [9].

1.2.2 Electroweak Contribution

Electroweak contributions are known to be suppressed by a factor (m_μ^2/m_W^2) compared to the pure QED terms. Indeed, sensitivity to the measurement of a_μ^{EW} was reached only with the recent BNL experiment. Nonetheless, results for the one-loop term were first presented in 1972 [52–56], after the renormalizability of the SM was established. Today, the one-loop term amounts to three times the experimental uncertainty, and is therefore sizeable.

One-Loop Contribution

The analytical result for the one-loop contribution can be written as

$$a_\mu^{(2)\,\text{EW}} = \frac{5 G_F m_\mu^2}{24\pi^2\sqrt{2}} \left[1 + \frac{1}{5}\left(1 - 4\sin^2\theta_W\right)^2 + \mathcal{O}\left(\frac{m_\mu^2}{m_{Z,W,H}^2}\right) \right] \tag{1.28}$$

where G_F is the Fermi constant, θ_W is the Weinberg angle and $m_{Z,W,H}^2$ are the masses of the Z, W and Higgs boson, respectively. The $\mathcal{O}(m_\mu^2/m_{Z,W,H}^2)$ term gives a negligible contribution. Formula (1.28) yields the value

$$a_\mu^{(2)\,\text{EW}} = (194.81 \pm 0.01) \times 10^{-11} \tag{1.29}$$

where the error is due to the uncertainty in $\sin^2\theta_W$.

Two-Loop Contribution

Two-loop EW contributions arise from QED corrections or fermionic loop insertions in the one-loop EW diagrams. Surprisingly, they are the same order of magnitude of the one-loop result: this is due to the presence of $\log(m_{Z,W}/m_f)$ terms [57] associated to fermion triangular-loops, where m_f is the mass scale of the fermion in the loop, very small compared to $m_{Z,W}$. As a result, the one-loop contribution is sensibly diminished by the two-loop term [58–60]. We report the result in [27]

$$a_\mu^{(4)\,\text{EW}} \simeq (-41.23 \pm 0.22[m_H, m_t] \pm 0.72[\text{had}]) \tag{1.30}$$

where the first error is due to the uncertainties in the Higgs and top masses, while the second is due to hadronic uncertainties.

1.2.3 Hadronic Contribution

The hadronic contribution is related to pure QED diagrams with the addition of quark loops. Since quarks interact strongly at low energies, a behavior that forbids a perturbative calculation, non-perturbative techniques must be employed in the prediction of a_μ^{had}.

Leading-Order Contribution

The leading hadronic contribution a_μ^{HLO} arise from the $\mathcal{O}(\alpha^2)$ diagram in Fig. 1.1, where the hadronic vacuum polarization (HVP) insertion is depicted as a red "blob". It was shown [61–64] that this contribution can be calculated from hadronic e^+e^- annihilation data. Indeed, using dispersion relations together with the optical theorem, one obtains[3] the dispersive representation

$$a_\mu^{\text{HLO}} = \frac{\alpha}{3\pi} \int_{m_\pi^2}^{\infty} \frac{ds}{s} K_\mu^{(2)}(s) R_{\text{had}}(s) \tag{1.31}$$

where $K_\mu^{(2)}(s)$ is a smooth kernel function, m_π is the pion mass and

$$R_{\text{had}}(s) = \frac{\sigma^{(0)}(e^+e^- \to \gamma^* \to \text{hadrons})}{\sigma(e^+e^- \to \gamma^* \to \mu^+\mu^-)} \tag{1.32}$$

is the ratio of the inclusive cross section for e^+e^- annihilation into hadrons, with electromagnetic radiative corrections subtracted off, and the cross section for muon-pair production in the high energy limit. It must be noted that also hadronic final states involving photons (although related to higher order terms) are conventionally included in the leading contribution. The latest result for the theoretical prediction, obtained via the dispersion integral Eq.(1.31), is [27, 65]

$$a_\mu^{\text{HLO}} = (688.07 \pm 4.14) \times 10^{-10} \tag{1.33}$$

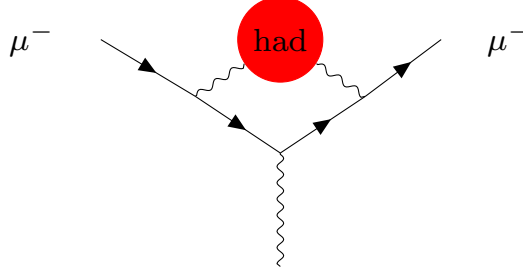[3]A more detailed account of the dispersive approach is given in Ch. 3

Figure 1.1: hadronic leading-order contribution to a_μ.

showing that the leading contribution is about a hundred times the present experimental uncertainty. The error on a_μ^{HLO} is mainly due to the experimental errors from the measurement of the cross section. As a result, the error on a_μ^{HLO} dominates the total theoretical uncertainty, and constitutes the main problem in the interpretation of the experimental results: in order to match the improved precision of the future experiments, progress in the evaluation of a_μ^{HLO} is essential.

Higher-Order Contributions

The hadronic contributions at higher order are usually split into two terms

$$a_\mu^{\text{HHO}} = a_\mu^{\text{HHO}}(\text{vp}) + a_\mu^{\text{HHO}}(\text{lbl}) \tag{1.34}$$

where the first term includes QED corrections to the HVP diagram of Fig. 1.1, while the second term arise from hadronic light-by-light diagrams. While $a_\mu^{\text{HHO}}(\text{vp})$ can be evaluated using the dispersive approach discussed above and is under control concerning the required accuracy, $a_\mu^{\text{HHO}}(\text{lbl})$ cannot be extracted from experimental data, and specific models have to be employed in its determination. Indeed, the error on $a_\mu^{\text{HHO}}(\text{lbl})$ is the second largest contribution to the theoretical uncertainty. For the vacuum polarization we have [66]

$$a_\mu^{\text{HHO}}(\text{vp}) = (-8.70 \pm 0.06) \times 10^{-10} \tag{1.35}$$

while the light-by light contribution is [67]

$$a_\mu^{\text{HHO}}(\text{lbl}) = (10.34 \pm 2.88) \times 10^{-10} \ . \tag{1.36}$$

1.3 The MUonE proposal

As discussed in the previous section, a major problem in the calculation of a_μ comes from the HLO contribution. Apart from the dispersive method, a possibility consists in lattice QCD calculations [68–73]. While very important, this approach has not yet reached the desired accuracy. A new way to address the problem has been recently investigated [1], leading to the proposal of the MUonE experiment at CERN [2]. It has been shown [74] that an alternative representation for a_μ^{HLO} is given by

$$a_\mu^{\text{HLO}} = \int_0^1 dx \, (1-x) \Delta\alpha_{\text{had}}[t(x)] \tag{1.37}$$

where $t(x) = m_\mu^2 x^2/(x-1)$ is the space-like squared momentum transfer ($t(x) < 0$ in the x-range of integration) and $\Delta\alpha_{\text{had}}(t)$ is the hadronic contribution to the running of the fine-structure constant[4]

$$\alpha(t) = \frac{\alpha(0)}{1 - \Delta\alpha(t)} \ . \tag{1.38}$$

---

[4]The total running receives contribution from the three leptons, the top and the lighter quarks

$$\Delta\alpha(t) = \Delta\alpha_{\text{lep}}(t) + \Delta\alpha_{\text{had}}(t) + \Delta\alpha_{\text{top}}(t) \ .$$

Note, however, that the neat distinction in the above expression is consistent only up to two loops, since at three loops diagrams involving both hadronic and leptonic vacuum polarizations begin to appear.

The MUonE experiment will determine $\Delta\alpha(t)$ by measuring the differential cross section $d\sigma/dt$ for elastic muon-electron scattering; the hadronic contribution will then be extracted by subtracting the leptonic part, which is well-known in perturbation theory. If a competitive measurement of a_μ^{HLO} has to be obtained with this new approach, the experimental uncertainties in the measurement of the cross section need to be of the order of 10 ppm. On the theory side, the implementation of Monte Carlo simulations requires the knowledge of the differential cross section for muon-electron scattering up to NNLO.

The process of muon-electron scattering has not been deeply investigated so far experimentally nor theoretically. Measurements have been performed in the 60s using both accelerators [75–78] and cosmic rays [79–82], and later a method to polarize muons through the scattering on electrons was studied [83, 84]. Moreover, theoreticians have mainly analyzed the QED [85–91] and the electroweak [92–94] corrections at NLO. The QED corrections at NNLO have been tackled only very recently [95–97], with the evaluation of the master integrals for both planar and non-planar graphs.

For a correct interpretation of the MUonE results, also the hadronic contributions at NNLO, related to the hadronic blob in Fig. 1.1 must be considered. This thesis is devoted to the analysis of these kind of contributions. While we will employ the dispersive approach in the calculation, an evaluation of the same contributions using the hyperspherical method has been recently presented [98].

Chapter 2

The Muon-Electron Scattering Cross Section up to NLO

2.1 Preliminary Kinematics

We start to consider the elastic process of $\mu^- e^-$ scattering with the following definitions of momenta

$$\mu^-(p_1) + e^-(p_2) \to \mu^-(q_1) + e^-(q_2).$$

The MUonE experiment will be studied in the lab frame, with the electron at rest, but we will often take advantage of the simplifications of moving to the center of mass (CM) frame.

Mandelstam variables are defined as

$$
\begin{aligned}
s &= (p_1 + p_2)^2 = (q_1 + q_2)^2 \\
t &= (q_1 - p_1)^2 = (q_2 - p_2)^2 \\
u &= (q_1 - p_2)^2 = (q_2 - p_1)^2
\end{aligned}
\tag{2.1}
$$

and satisfy the relation

$$s + t + u = 2m_e^2 + 2m_\mu^2. \tag{2.2}$$

The experiment will use a muon beam of energy around $E_\mu^{\mathrm{lab}} = 150$ GeV, from which we can extract directly the value of s looking at the lab frame

$$s = m_\mu^2 + 2m_e E_\mu^{\mathrm{lab}} \simeq 0.164 \text{ GeV}^2. \tag{2.3}$$

In our calculations we will refer to the differential cross section $d\sigma/dt$, which is given by the general formula

$$\frac{d\sigma}{dt} = \frac{1}{16\pi} \frac{1}{\lambda(s, m_\mu^2, m_e^2)} \mathcal{X}, \tag{2.4}$$

where $\lambda(x, y, z)$ is the Källen function $\lambda(x, y, z) = x^2 + y^2 + z^2 - 2xy - 2xz - 2yz$ and the quantity $\mathcal{X}$ is defined as the squared matrix element summed over the final spins and averaged over the initial ones

$$\mathcal{X} = \frac{1}{4} \sum_{\mathrm{spin}} |\mathcal{M}|^2. \tag{2.5}$$

The expression of Eq.(2.4) can be derived from the well-known formula for the differential cross section for a $2 \to 2$ elastic scattering in the CM frame

$$\left(\frac{d\sigma}{d\Omega}\right)_{\mathrm{CM}} = \frac{1}{64\pi^2 s} \mathcal{X} \tag{2.6}$$

by noting that

$$\cos\theta_{\mathrm{CM}}(t) = \frac{1}{\lambda(s, m_\mu^2, m_e^2)} \left[2st + \lambda(s, m_\mu^2, m_e^2)\right], \tag{2.7}$$

from which

$$\left(\frac{d\Omega}{dt}\right)_{\text{CM}} = 2\pi \frac{d\left(\cos\theta_{\text{CM}}\right)}{dt} = \frac{4\pi s}{\lambda(s, m_\mu^2, m_e^2)}. \tag{2.8}$$

Note that the differential cross section (2.4) is Lorentz-invariant. The Mandelstam variable t is constrained to the range $\left[-\lambda(s, m_\mu^2, m_e^2)/s, 0\right]$, where the minimum value for t is $t_{min} \simeq -0.143$ GeV^2.

2.2 Cross Section at LO

In this section we briefly discuss the LO cross section for the process, calculating only the contributions relevant for the experiment. Indeed, in the SM we can consider three diagrams contributing to the amplitude at LO, namely the photon, Z boson and Higgs boson diagrams of Fig.2.1 (whenever not specified, the top fermion line in a diagram is understood to be the muon one). Thus we would have to consider six total contributions in order to write the LO cross section, namely the squared diagrams plus the interference contributions. However, an estimate of the magnitude of each diagram's amplitude is sufficient to let us focus only on the QED diagrams in the evaluation of the NLO contributions.

2.2.1 QED Contribution

The amplitude for the scattering mediated by a photon is given by the Feynman rules of Appendix A.1

$$i\mathcal{M}_0 = ie^2 \frac{\bar{u}(q_1)\gamma^\mu u(p_1) \; \bar{u}(q_2)\gamma_\mu u(p_2)}{t} \tag{2.9}$$

from which we obtain the pure QED contribution

$$\mathcal{X}_0 = \frac{64\pi^2\alpha^2}{t^2} \left[(m_\mu^2 + m_e^2)^2 - su + t^2/2\right]. \tag{2.10}$$

We will express our results for all the remaining contributions using $\mathcal{X}_0$ as a normalization factor, since it is the dominant contribution to the cross section, as we will show in the following. A generic contribution $\mathcal{X}_i$ can then be written as

$$\mathcal{X}_i = \mathcal{X}_0 \times \delta_i \tag{2.11}$$

with the dimensionless quantity

$$\delta_i = \frac{\mathcal{X}_i}{\mathcal{X}_0}. \tag{2.12}$$

Summing over all contributions, the differential cross section then will read

$$\frac{d\sigma}{dt} = \frac{1}{16\pi} \frac{1}{\lambda(s, m_\mu^2, m_e^2)} \mathcal{X}_0 \left[1 + \sum_i \delta_i\right]. \tag{2.13}$$

We now point out that the expected sensitivity of the MUonE experiment for the measurement of the differential cross section is 10 ppm, thus any δ_i expected to be smaller than 1×10^{-5} can be neglected. Indeed, this is the case for the Higgs contribution, as we show below.

2.2.2 Z Contribution

Using the Feynman rules of App. A.1, the amplitude for the Z boson diagram is

$$i\mathcal{M}_Z = -i\left(\frac{g}{2\cos\theta_W}\right)^2 \bar{u}(q_1)\gamma^\alpha(g_{\text{V}} - g_{\text{A}}\gamma^5)u(p_1) \; \bar{u}(q_2)\gamma^\beta(g_{\text{V}} - g_{\text{A}}\gamma^5)u(p_2)$$

$$\times \frac{\left(-g_{\alpha\beta} + \frac{(q_1-p_1)_\alpha(q_1-p_1)_\beta}{m_Z^2}\right)}{t - m_Z^2} \tag{2.14}$$

where g is the $SU(2)$ coupling, θ_W is the Weinberg angle, m_Z is the mass of the Z boson and g_V and g_A are the purely vector and axial couplings, respectively, defined as

$$g_V = \sin^2\theta_W - \frac{1}{4} \qquad\qquad g_A = -\frac{1}{4}$$

and assumed to be equal for electron and muon. Then the interference contribution can be written as

$$\mathcal{X}_{Z\gamma} = \frac{1}{4}\sum_{\text{spin}} 2\text{Re}(\mathcal{M}_0^*\mathcal{M}_Z)$$
$$= \mathcal{X}_0 \times \delta_{Z\gamma} \tag{2.15}$$

where

$$\delta_{Z\gamma} = \frac{1}{\pi\sqrt{2}}\left(\frac{tG_F}{\alpha}\right)\frac{m_Z^2}{t-m_Z^2}\left[g_V^2 - \frac{g_A^2}{2}\frac{t(s-u)}{(m_\mu^2+m_e^2)^2 - su + t^2/2}\right] \tag{2.16}$$

and G_F is the Fermi constant. $\delta_{Z\gamma}$ represents the relative contribution to the cross section with respect to the dominant QED contribution obtained above. The resonance at $t \simeq m_Z^2$ is very far from the t-range considered for the experiment, over which $\delta_{Z\gamma}$ is at most 1.5×10^{-5} (in correspondence to the value $t = t_{min}$), therefore the $Z - \gamma$ interference is barely detectable. Moreover, we can safely omit the pure Z contribution, connected to $|\mathcal{M}_Z|^2$, since its relative contribution is expected to be $\mathcal{O}(G_F^2)$.

2.2.3 Higgs contribution

The amplitude for diagram (c) of Fig.2.1 is easily written as

$$i\mathcal{M}_H = -i\frac{m_\mu m_e}{v^2}\bar{u}(q_1)u(p_1)\frac{1}{t-m_H^2}\bar{u}(q_2)u(p_2) \tag{2.17}$$

where v is the v.e.v. of the Higgs field and is proportional to m_Z. If we neglect the $(q_1-p_1)_\alpha(q_1-p_1)_\beta$ term in the massive vector boson propagator[1] of Eq.(2.14), we can see that the ratio between $\mathcal{M}_H$ and $\mathcal{M}_Z$ goes like

$$\frac{\mathcal{M}_H}{\mathcal{M}_Z} \propto \frac{m_\mu m_e}{m_Z^2}\frac{t-m_Z^2}{t-m_H^2}, \tag{2.18}$$

therefore, being t very far from m_H^2, both the interference and the pure Higgs contribution are negligible for the MUonE experiment.

2.2.4 Cross Section at LO

Considering the relevance of all possible LO contributions, we have found the pure QED term to be the dominant one, while the $Z - \gamma$ interference is at the edge of detectability and the remaining contributions are surely negligible. We will therefore focus only on QED diagrams in the remainder of the thesis, and the LO cross section that we will assume is

$$\frac{d\sigma_0}{dt} = \frac{4\pi\alpha^2}{t^2}\frac{(m_\mu^2+m_e^2)^2 - su + t^2/2}{\lambda(s, m_\mu^2, m_e^2)} \tag{2.19}$$

which is related to Eq.(2.10) by virtue of Eq.(2.4).

2.3 QED Corrections at NLO

Having restricted our attention to the QED contributions, in this section we analyze carefully the radiative corrections to $\mu^- e^-$ scattering at NLO. Although these were already derived in previous papers [85–91], we reproduce them independently, as they will be useful in the evaluation of the hadronic contributions at NNLO.

---

[1]Using the Dirac equation, it can be shown that this term is proportional to $\frac{m_\mu m_e}{m_Z^2}$.
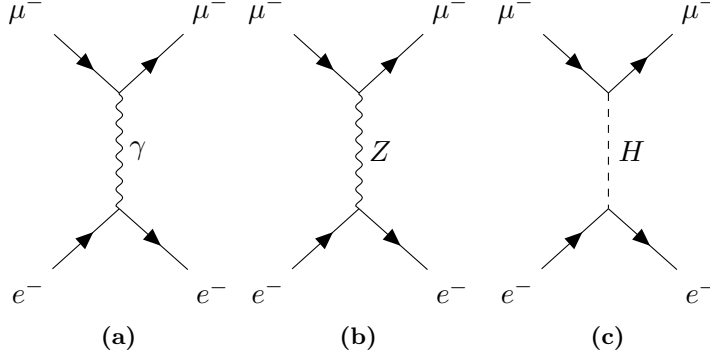
Figure 2.1: diagrams contributing to the tree-level Feynman amplitude for $\mu^- e^-$ scattering: (a) photon contribution; (b) Z boson contribution; (c) Higgs boson contribution.

If the complete Feynman amplitude for the process is

$$\mathcal{M} = \mathcal{M}_0 + \mathcal{M}_1 + \mathcal{O}(\alpha^3)$$

where $\mathcal{M}_0$ and $\mathcal{M}_1$ are the LO ($\mathcal{O}(\alpha)$) and NLO ($\mathcal{O}(\alpha^2)$) contributions, respectively, then the contribution to the cross section at NLO is

$$\frac{d\sigma_1}{dt} = \frac{1}{16\pi} \frac{1}{\lambda(s, m_\mu^2, m_e^2)} \mathcal{X}_1 \tag{2.20}$$

where $\mathcal{X}_1$ is obtained from the interference of the NLO amplitude with the LO one

$$\mathcal{X}_1 = \frac{1}{4} \sum_{\text{spin}} 2 \, \text{Re}(\mathcal{M}_0^* \mathcal{M}_1), \tag{2.21}$$

that is a $\mathcal{O}(\alpha^3)$ quantity.

The QED diagrams contributing to $\mathcal{M}_1$ are depicted in Fig. 2.2: we have to deal with vacuum polarization (VP), in which virtual lepton pairs are created and annihilated, vertex correction (VC) and box diagrams. Also hadronic VP diagrams, consisting of strongly interacting quark pairs, appear at NLO, but they will be considered in Ch. 4, which is specifically devoted to the hadronic contributions to $\mu^- e^-$ scattering.

The diagrams of Fig. 2.2 are related by Feynman rules to loop integrals that are divergent when the loop momentum goes to infinity (UV divergence) and/or to zero (IR divergence). These divergences can be regularized, in the sense that they can be put in a tractable form; after that, UV divergences are dealt with renormalization, while the cancellation of IR divergences is ensured by the Bloch-Nordsieck theorem [99].[2]

In this thesis we use dimensional regularization for UV divergences, setting the dimension of space-time to $D = 4 - \varepsilon$, with $\varepsilon > 0$, and then taking the limit $\varepsilon \to 0$ at the end of calculations: the divergences appear in the form of $1/\varepsilon$ poles. The renormalization of UV divergences is then performed in the framework of renormalized perturbation theory (RPT), which is described and applied to the case of QED corrections to $\mu^- e^-$ scattering in Sect.2.3.1. Concerning IR divergences, these are regularized by giving the photon a small mass λ and taking the limit $\lambda \to 0$ at the end of calculations: the divergences appear in $\log(\lambda)$ terms. We will check the validity of the Bloch-Nordsieck theorem at NLO in Sect.2.4.

Calculations for VP and VC diagrams were first performed in explicit analytic form. The standard procedure for calculating loop integrals consists in the following steps:

1. Feynman parametrization (see App. A.3) is used in order to have an integrand with a single denominator;

---

[2]A more general result concerning the cancellation of IR divergences is the Kinoshita-Lee-Nauenberg (KLN) theorem [100, 101], but in this thesis we will consider only QED contributions, to which the Bloch-Nordsieck theorem applies.

2. the integration over the loop momentum is carried out by going in Euclidean space (some useful results are collected in App. A.3);

3. finally, the integration over Feynman parameters is performed.

The results obtained with the above approach were checked with the ones from the `Mathematica` package `FeynCalc`[3] [102, 103], which makes use of the technique of Passarino-Veltman (PV) decomposition, described in App. B. Box diagrams were evaluated using `FeynCalc` only, given the complexity of the related integrals. We performed the calculations with `FeynCalc` through the following steps:

1. The amplitude for a given diagram is defined in D-dimensions.

2. Using the `FeynCalc` command `TID`, the one-loop integral is decomposed in a linear combination of tensor integrals. The option `UsePaVeBasis` expresses the results in terms of the PV coefficient functions, while `ToPaVe` converts scalar integrals in PV notation.

3. The command `PaVeReduce` further simplifies the result, expressing it in terms of the scalar PV functions (B_0, C_0, D_0) only.

4. When a scalar PV function contains a UV-divergent part, this is made explicit, together with terms depending on the scale μ introduced in dimensional regularization. For example $B_0(0, m^2, m^2)$ is rewritten as
$$B_0(0, m^2, m^2) = \Delta_\varepsilon + \log(\mu^2) + \bar{B}_0(0, m^2, m^2)$$
where $\bar{B}_0(0, m^2, m^2)$ is defined as the UV-finite part of the function.

5. When a UV-divergent scalar PV function is multiplied by a rational function of D, $f(D)$, we expand the latter as
$$f(D) = f(4) - \varepsilon f'(4) + \mathcal{O}(\varepsilon^2)$$
and then take the limit $\varepsilon \to 0$ where possible: this ensures to include finite terms possibly arising from the simplification
$$\lim_{\varepsilon \to 0} \varepsilon \Delta_\varepsilon = \lim_{\varepsilon \to 0} \varepsilon \left[\frac{2}{\varepsilon} - \gamma_E + \log(4\pi) \right] = 2 \; .$$

We make use of the results obtained with `FeynCalc` in the numerical evaluation of the contributions to the cross section, and a complete list of them will be given in App. C. Numerical results are obtained using `LoopTools` [104, 105].

2.3.1 Renormalized Perturbation Theory

Before embarking in the discussion of the various contributions to the cross section, we present here a brief practical account of the renormalization of QED in the framework of renormalized perturbation theory. Let the *bare* lagrangian for a given lepton be defined as[4]

$$\mathcal{L} = -\frac{1}{4} F^{0\mu\nu} F^0_{\mu\nu} + \bar{\psi}^0 (i \slashed{\partial} - m^0) \psi^0 - e^0 \bar{\psi}^0 \slashed{A}^0 \psi^0 \tag{2.22}$$

where $F^0_{\mu\nu} = (\partial_\mu A^0_\nu - \partial_\nu A^0_\mu)$, A^0_μ is the electromagnetic field and ψ^0 is the Dirac spinor associated with the lepton. This lagrangian is capable of giving finite predictions at tree level if m^0 ad e^0 are chosen to be the lepton's experimentally measured mass and charge, but the same lagrangian is known to produce divergent results in the computation of the observable Green's functions at quantum level (i.e. one-loop and higher). However, these divergences can be eliminated by a proper rescaling of the free parameters of the lagrangian, namely the fields, the coupling constant and the mass. If we assume

---

[3]Vers.9.2.0

[4]Being QED an abelian gauge theory, a priori different coupling constants should be considered for different lepton species. However, in the SM lepton flavor universality is assumed, therefore in this thesis we will take e as the universal electromagnetic coupling.
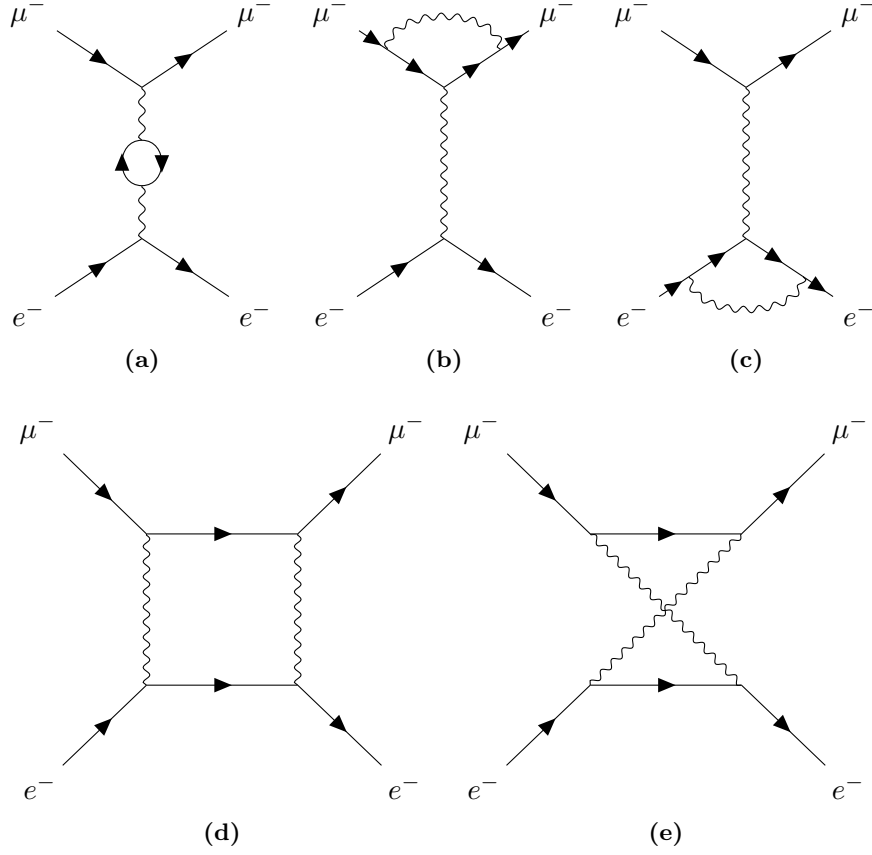
Figure 2.2: One-loop QED diagrams contributing to the NLO amplitude for $\mu^- e^-$ scattering. (a): vacuum polarization through lepton pairs. (b) and (c): muonic and electronic vertex correction. (d) and (e): direct and crossed box.

that the bare parameters are unphysical and define the renormalized parameters via the following relations

$$
\begin{aligned}
A_\mu^0 &= Z_3^{\frac{1}{2}} A_\mu \\
\psi^0 &= Z_2^{\frac{1}{2}} \psi \\
e^0 &= Z_1 Z_2^{-1} Z_3^{-\frac{1}{2}} e[\mu^{\frac{\varepsilon}{2}}] \\
m^0 &= Z_m Z_2^{-1} m
\end{aligned}
\tag{2.23}
$$

we wind up with the *renormalized* lagrangian

$$
\mathcal{L}^{\mathrm{ren}} = -\frac{1}{4} Z_3 F^{\mu\nu} F_{\mu\nu} + Z_2 i \bar{\psi} \slashed{\partial} \psi - m Z_m \bar{\psi}\psi - e[\mu^{\frac{\varepsilon}{2}}] Z_1 \bar{\psi} \slashed{A} \psi
\tag{2.24}
$$

where μ is an arbitrary scale of mass dimension 1, introduced in dimensional regularization in order to leave e dimensionless. The formally infinite renormalization constants Z_i are defined as a perturbative expansion in terms of the renormalized coupling constant e, around a classical tree-level value

$$
Z_i = 1 + \delta_i
$$

with the *counterterms* δ_i starting at $\mathcal{O}(e^2)$. The lagrangian of Eq.(2.24) can then be made explicit

$$
\begin{aligned}
\mathcal{L}^{\mathrm{ren}} = &-\frac{1}{4} F^{\mu\nu} F_{\mu\nu} + i \bar{\psi} \slashed{\partial} \psi - m \bar{\psi}\psi - e[\mu^{\frac{\varepsilon}{2}}] \bar{\psi} \slashed{A} \psi \\
&-\frac{1}{4} \delta_3 F^{\mu\nu} F_{\mu\nu} + \delta_2 i \bar{\psi} \slashed{\partial} \psi - m \delta_m \bar{\psi}\psi - e[\mu^{\frac{\varepsilon}{2}}] \delta_1 \bar{\psi} \slashed{A} \psi
\end{aligned}
\tag{2.25}
$$

where the first line is formally equivalent to the bare lagrangian and the counterterms appear as new interactions in the second line: they are suitably chosen in order to cancel the divergent contributions coming from the lagrangian in the first line.

While the divergent part of the counterterms is fixed (once a regularization procedure has been chosen), their finite part is still arbitrary, and must be set through a renormalization scheme. In this thesis the *on-shell scheme* will be followed. In this scheme, the renormalized mass m and coupling e in Eq.(2.25) are defined as the observed classical parameters for a given lepton, therefore allowing a straightforward physical interpretation of our results.

2.3.2 Vacuum Polarization

In order to deal with diagram (a) of Fig. 2.2 it is convenient to remind the usual presentation of the vacuum polarization as a modification of the tree-level photon propagator. This will allow to relate diagram (a) to the tree-level QED diagram of Fig. 2.1 in a simple way.

Correction to the Photon Propagator

The full exact photon propagator[5] can be expanded in a diagrammatic series of subsequent 1-particle irreducible (1PI) insertions

where each 1PI insertion is in turn given by the sum of all possible 1PI diagrams, namely diagrams which cannot be separated into two subdiagrams by cutting a single internal line

---

[5]Also called *dressed* propagator. It receives contributions from diagrams at all orders in perturbation theory.

Defining a single 1PI insertion as $-i\Pi^{\mu\nu}(q)$, where q is the momentum carried by the photon, the full photon propagator can then be written as

$$iD_{\mathrm{F}}^{\alpha\beta}(q) = \frac{-ig^{\alpha\beta}}{q^2} + \frac{-ig^{\alpha\mu}}{q^2}\left[-i\Pi_{\mu\nu}(q)\right]\frac{-ig^{\nu\beta}}{q^2}$$
$$+ \frac{-ig^{\alpha\mu}}{q^2}\left[-i\Pi_{\mu\nu}(q)\right]\frac{-ig^{\nu\rho}}{q^2}\left[-i\Pi_{\rho\sigma}(q)\right]\frac{-ig^{\sigma\beta}}{q^2} + \dots \tag{2.26}$$

The above expression can be simplified to a more illuminating one. First, using Lorentz decomposition and Ward Identity, we can infer the transversality of $\Pi^{\mu\nu}(q)$

$$\Pi^{\mu\nu}(q) = (q^2 g^{\mu\nu} - q^\mu q^\nu)\Pi(q^2) \tag{2.27}$$

where $\Pi(q^2)$ is a scalar function with no poles at $q^2 = 0$. We may then rewrite Eq.(2.26) as

$$iD_{\mathrm{F}}^{\alpha\beta}(q) = \frac{-ig^{\alpha\beta}}{q^2} + \frac{-ig^{\alpha\mu}}{q^2}\Delta_\mu{}^\beta\left[-\Pi(q^2) + \Pi^2(q^2) + \dots\right]$$
$$= \frac{-ig^{\alpha\beta}}{q^2}\left[1 - \Pi(q^2) + \Pi^2(q^2) + \dots\right] + \frac{iq^\alpha q^\beta}{q^4}\left[-\Pi(q^2) + \Pi^2(q^2) + \dots\right] \tag{2.28}$$

where we have used the idempotence of the quantity

$$\Delta_\mu{}^\beta = i(q^2 g_{\mu\lambda} - q_\mu q_\lambda)\frac{-ig^{\lambda\beta}}{q^2} = \delta_\mu{}^\beta - \frac{q_\mu q^\beta}{q^2}.$$

Now we observe that the $q^\alpha q^\beta$ term in Eq.(2.28) will couple necessarily to a conserved electromagnetic current and so the relative contribution will be zero. Therefore the full photon propagator takes the form

$$iD_{\mathrm{F}}^{\alpha\beta}(q) = \frac{-ig^{\alpha\beta}}{q^2}\left[1 - \Pi(q^2) + \Pi^2(q^2) + \dots\right] \tag{2.29}$$

where we recognize the tree-level photon propagator in Feynman gauge multiplied by the terms in square brackets. We can now regard Eq.(2.29) as a geometric progression of ratio $-\Pi(q^2)$ and write the full propagator in a compact expression

$$iD_{\mathrm{F}}^{\alpha\beta}(q) = \frac{-ig^{\alpha\beta}}{q^2\left[1 + \Pi(q^2)\right]}. \tag{2.30}$$

Function $\Pi(q^2)$, as diagrammatically shown above, receives contributions from diagrams at all orders. However, renormalization can be performed consistently only once an order is fixed in perturbation theory. Since we are interested in diagram (a) of Fig. 2.2 we focus on the $\mathcal{O}(e^2)$ contribution to $\Pi(q^2)$, denoted $\Pi_2(q^2)$ (see also Eq.(2.38)). If we include the counterterm δ_3 from the renormalized lagrangian of Eq.(2.25) we obtain the renormalized 1PI insertion at $\mathcal{O}(e^2)$

$$= \frac{-ig^{\alpha\beta}}{q^2}\left[-\Pi_2(q^2) - \delta_3\right] \tag{2.31}$$

from which we can approximate the full renormalized photon propagator as

$$i\bar{D}_{\mathrm{F}}^{\alpha\beta}(q) = \frac{-ig^{\alpha\beta}}{q^2}\left[1 - \bar{\Pi}_2(q^2) + \bar{\Pi}_2^2(q^2) + \dots\right] = \frac{-ig^{\alpha\beta}}{q^2\left[1 + \bar{\Pi}_2(q^2)\right]} \tag{2.32}$$

where we have defined the renormalized VP function as

$$\bar{\Pi}_2(q^2) = \Pi_2(q^2) + \delta_3. \tag{2.33}$$

Moreover, by multiplying Eq.(2.32) by e^2 we can define the *running charge* $e^2(q^2)$

$$
\begin{aligned}
ie^2 \bar{D}_{\mathrm{F}}^{\alpha\beta}(q) &= \frac{-ig^{\alpha\beta}}{q^2} \frac{e^2}{\left[1 + \bar{\Pi}_2(q^2)\right]} \\
&= \frac{-ig^{\alpha\beta}}{q^2} e^2(q^2) \ .
\end{aligned}
\tag{2.34}
$$

In the on-shell scheme, the renormalization condition is related to the requirement that $e(q^2)$ reduces to the classical charge e in the Thomson limit $q \to 0$, thus implying

$$
\bar{\Pi}_2(0) = 0 \ .
\tag{2.35}
$$

We have now a method to compute the contribution from diagram (a) to the cross section at NLO: we need to calculate $\Pi_2^{\mu\nu}(q)$ and extract the function $\Pi_2(q^2)$; after renormalization, the Feynman amplitude for diagram (a) can be written replacing the tree-level propagator in $\mathcal{M}_0$ (Eq.(2.9)) with the NLO one (i.e. the second term in square brackets in Eq.(2.32))

$$
\frac{-ig^{\alpha\beta}}{q^2} \xrightarrow{\text{NLO}} \frac{-ig^{\alpha\beta}}{q^2} \left[-\bar{\Pi}_2(q^2)\right]
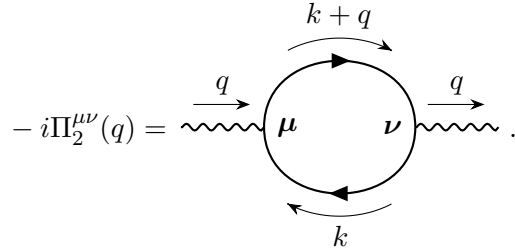\tag{2.36}
$$

yielding

$$
\mathcal{M}_1^{\mathrm{VP}} = \mathcal{M}_0 \left[-\bar{\Pi}_2(q^2)\right] \ .
\tag{2.37}
$$

Finally, $\mathcal{M}_1^{\mathrm{VP}}$ can be substituted in Eq.(2.21). Let us emphasize the importance of the factorization of the VP function showed above, as it will be very useful in evaluating the hadronic contributions at NNLO in Ch. 4.

Computation of $\Pi_2^{\mu\nu}(q)$

Let us define the one-loop vacuum polarization insertion for a photon with momentum q as

$$
-i\Pi_2^{\mu\nu}(q) =
\tag{2.38}
$$

Using the Feynman rules of App. A.1, Eq.(2.38) is equivalent to

$$
-i\Pi_2^{\mu\nu}(q) = (-ie\mu^{\frac{\varepsilon}{2}})^2(-1) \int \frac{d^D k}{(2\pi)^D} \ \mathrm{Tr}\left[\gamma^\mu \frac{i(\slashed{k}+m)}{k^2-m^2}\gamma^\nu \frac{i(\slashed{k}+\slashed{q}+m)}{(k+q)^2-m^2}\right]
\tag{2.39}
$$

where m is the mass of a generic *lepton* running in the loop.

In the specific case of Eq.(2.39) we find again the transversality highlighted in Eq.(2.27) and obtain

$$
\Pi_2^{\mu\nu}(q) = (q^2 g^{\mu\nu} - q^\mu q^\nu)\Pi_2(q^2)
\tag{2.40}
$$

where the (unrenormalized) VP function is

$$
\Pi_2(q^2) = \frac{2\alpha}{\pi} \int_0^1 dx \ x(1-x) \left[\Delta_\varepsilon - \log\left(\frac{m^2 - q^2 x(1-x)}{\mu^2}\right)\right].
\tag{2.41}
$$

We recall that $\Delta_\varepsilon = 2/\varepsilon - \gamma_E + \log(4\pi)$, so $\Pi_2(q^2)$ is UV-divergent. This could also be seen by momentum power-counting in the integral of Eq.(2.39). Having defined the renormalized VP function

by including the counterterm δ_3 as in Eq.(2.33), we fix the latter via the on-shell renormalization condition of Eq.(2.35)

$$\bar{\Pi}_2(0) = 0 \implies \delta_3 = -\Pi_2(0) \tag{2.42}$$

which gives

$$\delta_3 = -\frac{\alpha}{3\pi}\left[\Delta_\varepsilon - \log\left(\frac{m^2}{\mu^2}\right)\right]. \tag{2.43}$$

Note that the counterterm depends on the mass of the lepton flowing in the loop.

We can now write the explicit and `FeynCalc` results for $\bar{\Pi}_2(q^2)$. Here we have considered the case $q^2 < 0$, since the photon in the propagator of diagram (a) carries a momentum $q^\mu = (p_1 - q_1)^\mu$ and so $q^2 = t < 0$ by Eq.(2.1). We then express our results using the t variable. It should be noted that, in the specific case considered, $\bar{\Pi}_2(t)$ does not have an imaginary part, being the argument of the logarithm in Eq.(2.41) always positive. We also recall that we are considering only leptonic contributions to the vacuum polarization.

The equivalence of the two expressions can be checked by looking at the explicit form of the scalar PV functions in App. B.

Explicit Result for $\bar{\Pi}_2(t)$

$$\bar{\Pi}_2(t) = \frac{\alpha}{3\pi}\left[\frac{5}{3} + \frac{4m^2}{t} - \left(1 + \frac{2m^2}{t}\right)\sqrt{1 - \frac{4m^2}{t}}\log\left(\frac{\sqrt{1 - \frac{4m^2}{t}} + 1}{\sqrt{1 - \frac{4m^2}{t}} - 1}\right)\right] \tag{2.44}$$

`FeynCalc` **Result for $\bar{\Pi}_2(t)$**

$$\bar{\Pi}_2(t) = \frac{\alpha}{3\pi}\left[-\frac{1}{3} + \left(1 + \frac{2m^2}{t}\right)\left(\bar{B}_0(t, m^2, m^2) - \bar{B}_0(0, m^2, m^2)\right)\right] \tag{2.45}$$

Contribution to the Cross Section

Let's now consider the entire diagram (a) of Fig. 2.2: if we include the contributions coming from all the three leptons, from Eq.(2.37) we can write the one-loop VP amplitude as

$$\mathcal{M}_1^{\mathrm{VP}} = \mathcal{M}_0\left[-\sum_l \bar{\Pi}_2^{(l)}(t)\right] \tag{2.46}$$

where $\bar{\Pi}_2^{(l)}(t)$ represents the contribution of a given lepton (i.e. we substitute $m \to m_l$ in Eq.(2.44) and (2.45)), and l runs over $\{e, \mu, \tau\}$. Recalling Eq.(2.21), we can finally write the contribution to the cross section as

$$\mathcal{X}_1^{\mathrm{VP}} = \mathcal{X}_0\left[-2\sum_l \bar{\Pi}_2^{(l)}(t)\right]. \tag{2.47}$$

2.3.3 Vertex Correction

We now move to diagrams (b) and (c) of Fig. 2.2, in which the tree-level muonic and electronic vertices are replaced by their one-loop correction. We first analyze separately the general structure of the QED vertex at one-loop, and then use the results to compute the amplitude for diagrams (b) and (c), which can be related formally to the tree-level QED diagram, simplifying the calculations.

General Structure of the QED Vertex

Let's consider the following definition for the one-loop on-shell vertex for a lepton of mass m[6]

$$-ie\,\bar{u}(p_2)\Gamma^\mu(p_1,p_2)u(p_1) = \qquad\qquad\qquad\qquad\qquad\qquad\qquad\qquad (2.48)$$

which is equivalent to

$$-ie\,\bar{u}(p_2)\Gamma^\mu(p_1,p_2)u(p_1) =$$
$$= (-ie\mu^{\frac{\varepsilon}{2}})^3 \int \frac{d^D k}{(2\pi)^D} \frac{-ig_{\alpha\beta}}{k^2 - \lambda^2}\,\bar{u}(p_2)\left[\gamma^\alpha \frac{i[(\slashed{k}+\slashed{p}_2)+m]}{(k+p_2)^2 - m^2}\gamma^\mu \frac{i[(\slashed{k}+\slashed{p}_1)+m]}{(k+p_1)^2 - m^2}\gamma^\beta\right]u(p_1) \quad (2.49)$$

where p_1 and p_2 are the lepton incoming and outgoing momenta, respectively, and $q = (p_2 - p_1)$ is the incoming photon momentum. We have already introduced the regularizing fictitious mass λ in the photon propagator, since the integral is IR-divergent.

Having considered the sandwich between the Dirac spinors in the on-shell definition, we are able to simplify the Dirac term in the numerator using the relations of App. A.2. After the usual steps, the calculation of the integral of Eq.(2.49) yields

$$\bar{u}(p_2)\Gamma^\mu(p_1,p_2)u(p_1) = \bar{u}(p_2)\left[G(q^2)\gamma^\mu + H(q^2)(p_1+p_2)^\mu\right]u(p_1) \qquad (2.50)$$

where we have defined the functions

$$G(q^2) = \frac{\alpha}{4\pi}\left[\Delta_\varepsilon - 2 - 2\int_0^1 dx \int_0^{1-x} dy \,\log\left(\frac{\Delta}{\mu^2}\right)\right.$$
$$\left. + 2\int_0^1 dx \int_0^{1-x} dy\, \frac{q^2(1+xy) - m^2(x+y)^2 - 2m^2 - (x+y)(q^2-4m^2)}{\Delta}\right] \qquad (2.51)$$

$$H(q^2) = \frac{\alpha}{4\pi}\int_0^1 dx \int_0^{1-x} dy\, \frac{2m(x+y)(x+y-1)}{\Delta} \qquad (2.52)$$

and

$$\Delta = m^2(x+y)^2 - q^2 xy + \lambda^2(1-x-y). \qquad (2.53)$$

We note that $G(q^2)$ is UV-divergent because of the Δ_ε term. We then want to impose the renormalization condition for the vertex: in the on-shell scheme, this is expressed by the requirement that in the limit $q \to 0$ the full renormalized vertex is equal to the tree-level one, that is $-ie\gamma^\mu$. Since Γ^μ is defined as the one-loop correction, this means that the renormalized one-loop vertex $\bar{\Gamma}^\mu$ satisfies the relation

$$\bar{\Gamma}^\mu(p_1,p_2) = 0 \quad \text{for } q = (p_2 - p_1) \to 0. \qquad (2.54)$$

The renormalization condition just stated is related to the limit $q \to 0$, thus we rewrite Eq.(2.50) in a more convenient way using the Gordon identity

$$\bar{u}(p_2)(p_2+p_1)^\mu u(p_1) = \bar{u}(p_2)\left[2m\gamma^\mu - i\sigma^{\mu\nu}q_\nu\right]u(p_1) \qquad (2.55)$$

and obtain

$$\bar{u}(p_2)\Gamma^\mu(q)u(p_1) = \bar{u}(p_2)\left[(G(q^2) + 2mH(q^2))\gamma^\mu - iH(q^2)\sigma^{\mu\nu}q_\nu\right]u(p_1) \qquad (2.56)$$

---

[6]The approach followed is that of Romao [106].

where we have stressed that $\Gamma^\mu(p_1, p_2)$ actually depends on the difference $q = p_2 - p_1$ only. As can be seen from Eq.(2.25), the counterterm δ_1 introduced in RPT is proportional to γ^μ, and so the renormalized one-loop vertex takes the form

$$\bar{\Gamma}^\mu(q) = \Gamma^\mu(q) + \delta_1 \gamma^\mu. \tag{2.57}$$

We can now introduce the conventional expression for the renormalized one-loop vertex, in terms of the Dirac and Pauli[7] form factors $F_1(q^2)$ and $F_2(q^2)$

$$\bar{u}(p_2)\bar{\Gamma}^\mu(q)u(p_1) = \bar{u}(p_2)\left[F_1(q^2)\gamma^\mu + \frac{i}{2m}F_2(q^2)\sigma^{\mu\nu}q_\nu\right]u(p_1) \tag{2.58}$$

where

$$F_1(q^2) = G(q^2) + 2mH(q^2) + \delta_1 \tag{2.59}$$

$$F_2(q^2) = -2mH(q^2). \tag{2.60}$$

The renormalization condition of Eq.(2.54) translates into $F_1(0) = 0$, from which we fix the counterterm

$$\delta_1 = -G(0) - 2mH(0). \tag{2.61}$$

Thus, by calculating functions $G(q^2)$ and $H(q^2)$ from Eqs.(2.51 - 2.53), we are able to obtain the vertex form factors for a generic lepton of mass m. As we did for the VP diagram, in our calculation we have analyzed only the case $q^2 = t$ with t negative, therefore Δ in Eq.(2.53) is always positive, and the form factors do not develop an imaginary part.

The expressions for $F_1(t)$, $F_2(t)$ and δ_1 are showed below[8], in terms of the *natural* variable x_t, as in [107, 108]

$$x_t = -\frac{1 - \sqrt{1 - \frac{4m^2}{t}}}{1 + \sqrt{1 - \frac{4m^2}{t}}} \tag{2.62}$$

where $0 < x_t < 1$ for $-\infty < t < 0$. We remark that $F_1(t)$ is still IR-divergent, since $\log(\lambda)$ terms are present for $t \neq 0$. In particular, the scalar PV function $C_0(0, m^2, m^2, m^2, m^2, \lambda^2)$ is divergent in the limit $\lambda \to 0$. Note that $F_1(t)$ in Eq.(2.63) contains a dilogarithm (see App. A.3)

$$\text{Li}_2(z) = \int_z^0 dt\, \frac{\log(1-t)}{t}\ .$$

Explicit Results for the Form Factors

$$\begin{aligned}
F_1(t) = \frac{\alpha}{\pi}\Bigg\{ &-\log\left(\frac{\lambda}{m}\right) - 1 - \frac{3x_t^2 + 2x_t + 3}{4(1 - x_t^2)}\log(x_t) \\
&+ \frac{1 + x_t^2}{1 - x_t^2}\left[-\log\left(\frac{\lambda}{m}\right)\log(x_t) - \frac{1}{4}\log^2(x_t) + \frac{\pi^2}{12} + \text{Li}_2(-x_t) + \log(x_t)\log(1 + x_t)\right]\Bigg\}
\end{aligned} \tag{2.63}$$

$$F_2(t) = \frac{\alpha}{\pi}\left[-\frac{x_t}{1 - x_t^2}\log(x_t)\right] \tag{2.64}$$

$$\delta_1 = \frac{\alpha}{4\pi}\left[-\Delta_\varepsilon + \log\left(\frac{m^2}{\mu^2}\right) - 4 - 4\log\left(\frac{\lambda}{m}\right)\right] \tag{2.65}$$

---

[7] Also known as electric and magnetic form factors, respectively. In the following we will consider only the one-loop form factors, namely the $n = 1$ terms in the perturbative expansion

$$F_1(t) = \sum_{n=1}^\infty \left(\frac{\alpha}{\pi}\right)^n F_1^{(2n)}(t) \qquad F_2(t) = \sum_{n=1}^\infty \left(\frac{\alpha}{\pi}\right)^n F_2^{(2n)}(t)$$

see e.g. Barbieri [107].

[8] In this thesis we always assume the Feynman gauge.

FeynCalc Results for the Form Factors

$$F_1(t) = \frac{1}{16m^2 - 4t}\left[(3t - 8m^2)\left(\bar{B}_0(t, m^2, m^2) - \bar{B}_0(0, m^2, m^2)\right)\right.$$
$$+ 2(8m^4 - 6m^2t + t^2)C_0(t, m^2, m^2, m^2, m^2, \lambda^2)$$
$$\left. + 2(2m^2t - 8m^4)C_0(0, m^2, m^2, m^2, m^2, \lambda^2) - 2t\right] \tag{2.66}$$

$$F_2(t) = -\frac{m^2}{4m^2 - t}\left(\bar{B}_0(t, m^2, m^2) - \bar{B}_0(m^2, m^2, 0)\right) \tag{2.67}$$

$$\delta_1 = \frac{\alpha}{4\pi}\left(-B_0(0, m^2, m^2) - 4 - 4m^2 C_0(0, m^2, m^2, m^2, m^2, \lambda^2)\right) \tag{2.68}$$

Contribution to the Cross Section

We are now able to tackle the VC diagrams of Fig. 2.2. Let's focus on diagram (b), the muonic VC: the contribution to the NLO amplitude is diagrammatically shown below

$$i\mathcal{M}_1^{\text{VC}_\mu} = \qquad + \qquad \tag{2.69}$$

where we have included the counterterm graph in order to obtain a renormalized amplitude. We can write $\mathcal{M}_1^{\text{VC}_\mu}$ in a way that formally resembles the tree-level QED amplitude of Eq.(2.10)

$$\mathcal{M}_1^{\text{VC}_\mu} = e^2\,\frac{\bar{u}(q_1)\bar{\Gamma}^\mu(q_1 - p_1)u(p_1)\,\bar{u}(q_2)\gamma_\mu u(p_2)}{t}, \tag{2.70}$$

where we have replaced the tree-level muonic vertex with the one-loop correction of Eq.(2.58). The relative contribution to the cross section can then be calculated from Eq.(2.21) as

$$\mathcal{X}_1^{\text{VC}_\mu} = \frac{64\pi^2\alpha^2}{t^2}\left[2F_1^{(\mu)}(t)\left[(m_\mu^2 + m_e^2)^2 - su + t^2/2\right] + F_2^{(\mu)}(t)\,t(2m_e^2 + t)\right] \tag{2.71}$$
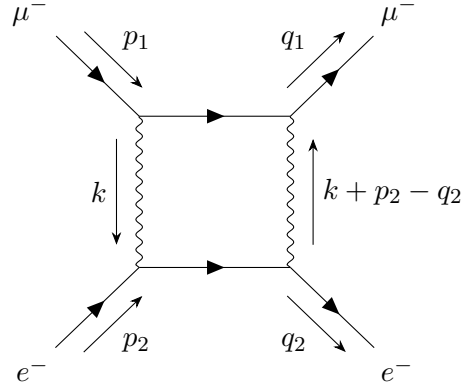
where $F_1^{(\mu)}(t)$ and $F_2^{(\mu)}(t)$ are the form factors for the muonic vertex, in the sense that they depend on m_μ. Note that the first term in square brackets differs from the tree-level QED contribution of Eq.(2.10) only by a factor of 2 (coming from the interference formula of Eq.(2.21)) and by $F_1^{(\mu)}(t)$: this is expected since the Lorentz-structure of the two contributions is the same.

An analogous result for the electronic VC can be obtained by the substitutions $m_e \to m_\mu$, $m_\mu \to m_e$ and $F_i^{(\mu)}(t) \to F_i^{(e)}(t)$ in Eq.(2.71). We give detailed results for the contribution to the cross section in App. C.

2.3.4   Box Diagrams

Moving to the analysis of box diagrams, we have to calculate the amplitude for the *direct* (or *planar*) and the *crossed* box. The amplitude of the former diagram is given by
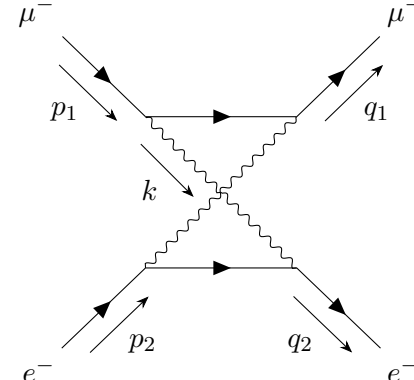

$$i\mathcal{M}_1^{\mathrm{BD}} =$$

$$= (e\mu^{\frac{\varepsilon}{2}})^4 \int \frac{d^D k}{(2\pi)^D} \frac{\mathcal{N}^{\mathrm{BD}}}{[(p_1 - k)^2 - m_\mu^2][(k + p_2)^2 - m_e^2][k^2 - \lambda^2][(k + p_2 - q_2)^2 - \lambda^2]} \tag{2.72}$$

with

$$\mathcal{N}^{\mathrm{BD}} = \bar{u}(q_1)\gamma^\alpha[(\not{p}_1 - \not{k}) + m_\mu]\gamma^\beta u(p_1)\ \bar{u}(q_2)\gamma_\alpha[(\not{k} + \not{p}_2) + m_e]\gamma_\beta u(p_2) \tag{2.73}$$

while for the crossed box we have

$$i\mathcal{M}_1^{\mathrm{BC}} =$$

$$= (e\mu^{\frac{\varepsilon}{2}})^4 \int \frac{d^D k}{(2\pi)^D} \frac{\mathcal{N}^{\mathrm{BC}}}{[(p_1 - k)^2 - m_\mu^2][(q_2 - k)^2 - m_e^2][k^2 - \lambda^2][(k + p_2 - q_2)^2 - \lambda^2]} \tag{2.74}$$

with

$$\mathcal{N}^{\mathrm{BC}} = \bar{u}(q_1)\gamma^\alpha[(\not{p}_1 - \not{k}) + m_\mu]\gamma^\beta u(p_1)\ \bar{u}(q_2)\gamma_\beta[(\not{q}_2 - \not{k}) + m_e]\gamma_\alpha u(p_2)\ . \tag{2.75}$$

As anticipated, calculations for box diagrams were performed using `FeynCalc`, and we include the results for the contribution to the cross section $\mathcal{X}_1^{\mathrm{BD}}$ and $\mathcal{X}_1^{\mathrm{BC}}$ in App. C. Here we make some important remarks.

- It is legitimate to set $D = 4$ in Eqs.(2.72) and (2.74) already, since by momentum power-counting it can be seen that the integrals are UV-finite. Anyway in our calculations we followed the procedure described at the beginning of this section and started with $D < 4$, crudely setting $D = 4$ after the computation of the amplitude and checking that Δ_ε and $\log(\mu)$ terms canceled each other out without the need for a renormalization counterterm[9].

---

[9]The motivation for this choice is that the command TID automatically converts amplitudes in D dimensions, whatever the input.

- Compared to the previous cases, results for the box diagrams include scalar PV functions with the *timelike* variable s as an argument. Therefore they present an imaginary part. However, since there are no products between PV functions in the box amplitudes (just a linear combination of them), and since the tree-level amplitude of Eq.(2.21) is a real quantity, it suffices to take the real part of each PV function in order to calculate the contributions to the cross section.

- The following crossing symmetry relation holds

$$\mathcal{M}_1^{\text{BD}} = -\mathcal{M}_1^{\text{BC}}[s \leftrightarrow u]$$

  and it has been verified as a consistency check.

- The integrals in Eqs.(2.72) and (2.74) are IR-divergent. In particular, the scalar PV functions that are divergent in the limit $\lambda \to 0$ (as shown in [109]) are

$$C_0(m_e^2, m_\mu^2, s, m_e^2, \lambda^2, m_\mu^2) \qquad \text{(Direct Box)}$$
$$D_0(m_\mu^2, m_e^2, m_e^2, m_\mu^2, s, t, m_\mu^2, \lambda^2, m_e^2, \lambda^2)$$

$$C_0(m_e^2, m_\mu^2, u, m_e^2, \lambda^2, m_\mu^2) \qquad \text{(Crossed Box)}$$
$$D_0(m_\mu^2, m_e^2, m_e^2, m_\mu^2, u, t, m_\mu^2, \lambda^2, m_e^2, \lambda^2)$$

2.3.5 Results

We present the complete results for the QED virtual radiative corrections at NLO in App. C. These are UV-finite, but still IR-divergent: this particular issue is analyzed in the next section, devoted to bremsstrahlung. As stated before, these results will be of use in dealing with the hadronic contributions at NNLO, thanks to the factorization property of the VP function showed in Eq.(2.37).

2.4 Soft Bremsstrahlung

In this section we describe an important check of consistency for our previous calculations: we verify that the IR divergences arisen in the computation of the virtual corrections to the $2 \to 2$ process of $\mu^- e^-$ elastic scattering cancel with the ones coming from the same process in which the emission of an additional photon is considered, namely the $2 \to 3$ *bremsstrahlung* process
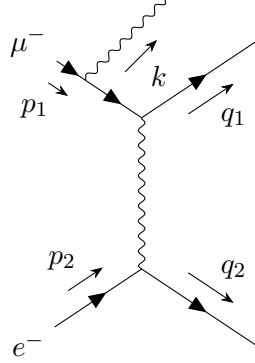
$$\mu^-(p_1) + e^-(p_2) \to \mu^-(q_1) + e^-(q_2) + \gamma(k) \ .$$

This is the content of the Bloch-Nordsieck theorem [99]. In particular, we assume *soft bremsstrahlung*, i.e. we consider a photon with very small energy, since IR divergences arise in the limit $k \to 0$. The choice of this limit has a physical explanation, related to the actual impossibility to resolve a pure elastic process from soft bremsstrahlung in a real experiment, if the emitted photon has an energy so small that it escapes experimental detection. To be consistent with the regularization of IR divergences used previously, also in this section we give the photon a small mass λ.

The diagrams contributing to the soft bremsstrahlung amplitude at LO are given below

$$i\mathcal{M}_0^{\text{Brem}} = \qquad + \qquad + \qquad + \qquad \qquad (2.76)$$

If we analyze the amplitude for the first diagram, in which the photon is emitted by the muon in the initial state, the Feynman rules give

$$i\mathcal{M}_0^{\text{Brem}(\mu \text{ i})} = \qquad\qquad\qquad\qquad\qquad\qquad\qquad\qquad\qquad\qquad (2.77)$$

$$= ie^3 \frac{\bar{u}(q_1)\gamma^\mu(\slashed{p}_1 - \slashed{k} + m_\mu)\gamma^\alpha u(p_1)\ \bar{u}(q_2)\gamma_\mu u(p_2)}{[(p_1 - k)^2 - m_\mu^2][(p_1 - q_1 - k)^2 - \lambda^2]}\varepsilon_\alpha^*(k)\ . \qquad (2.78)$$

Considering the limit $k \to 0$, it is possible to simplify Eq.(2.78) through the following approximations

- We can neglect k terms appearing in the numerator.

- We can neglect λ^2 terms in the denominator, since they are of higher order in k.

Moreover, the numerator of Eq.(2.78) can be further simplified, using some Dirac algebra and the Dirac equation, noting that

$$\bar{u}(q_1)\gamma^\mu(\slashed{p}_1 + m_\mu)\gamma^\alpha u(p_1) = 2p_1^\alpha\ \bar{u}(q_1)\gamma^\mu u(p_1) \qquad (2.79)$$

and the amplitude then becomes

$$\begin{aligned}
\mathcal{M}_0^{\text{Brem}(\mu \text{ i})} &= \frac{e^3}{t}\bar{u}(q_1)\gamma^\mu u(p_1)\bar{u}(q_2)\gamma_\mu u(p_2)\left[\varepsilon_\alpha^*(k)\left(-\frac{p_1^\alpha}{p_1 \cdot k}\right)\right] \\
&= \mathcal{M}_0\ e\left[\varepsilon_\alpha^*(k)\left(-\frac{p_1^\alpha}{p_1 \cdot k}\right)\right]
\end{aligned} \qquad (2.80)$$

where we have noted that the quantity multiplying the term in square brackets is e times the tree-level QED amplitude of Eq.(2.9).

The remaining diagrams in Eq.(2.76) can be dealt with in an analogous way, and the complete amplitude for soft bremsstrahlung is then

$$\mathcal{M}_0^{\text{Brem}} = \mathcal{M}_0\ e\ \varepsilon_\alpha^*(k)\left(\frac{q_1}{q_1 \cdot k} - \frac{p_1}{p_1 \cdot k} + \frac{q_2}{q_2 \cdot k} - \frac{p_2}{p_2 \cdot k}\right)^\alpha\ . \qquad (2.81)$$

After taking the squared modulus and summing over all polarizations we obtain

$$\mathcal{X}_0^{\text{Brem}} = -\mathcal{X}_0\ e^2\left(\frac{q_1}{q_1 \cdot k} - \frac{p_1}{p_1 \cdot k} + \frac{q_2}{q_2 \cdot k} - \frac{p_2}{p_2 \cdot k}\right)^2 \qquad (2.82)$$

where we used

$$\sum_{\text{pol}} \varepsilon_\alpha^*(k)\varepsilon_\beta(k) = -g_{\alpha\beta} \qquad (2.83)$$

We move now to the cross section for the $2 \to 3$ process: comparing to $\mu^- e^-$ elastic scattering, we have to consider an additional phase-space integration over the photon momentum k. However, in the soft bremsstrahlung limit the k in the delta function $\delta^{(4)}(p_1 + p_2 - q_1 - q_2 - k)$, ensuring momentum

conservation, can be neglected and as a result we are able to factorize the cross section for the $2 \to 2$ scattering

$$\left(\frac{d\sigma_0}{dt}\right)_{2\to3} = \left(\frac{d\sigma_0}{dt}\right)_{2\to2} \mathscr{I}(p_1, q_1, p_2, q_2) \tag{2.84}$$

where

$$\mathscr{I}(p_1, q_1, p_2, q_2) = -\frac{e^2}{(2\pi)^3} \int' \frac{d^3k}{2k_0} \left(\frac{q_1}{q_1 \cdot k} - \frac{p_1}{p_1 \cdot k} + \frac{q_2}{q_2 \cdot k} - \frac{p_2}{p_2 \cdot k}\right)^2 \tag{2.85}$$

and the integral $\int'$ is intended over the region $\lambda < k_0 < \omega$, with $\omega \ll m_e$ representing the energy resolution of a particular experiment Following 't Hooft and Veltman [110] we define the integral

$$\mathcal{I}(p_i, p_j) = \int' \frac{d^3k}{k_0} \frac{1}{(p_i \cdot k)(p_j \cdot k)} \tag{2.86}$$

and Eq.(2.85) becomes

$$\begin{aligned}
\mathscr{I}(p_1, q_1, p_2, q_2) = \frac{e^2}{(2\pi)^3} \frac{1}{2} \Bigg[&-m_\mu^2 \Big(\mathcal{I}(q_1, q_1) + \mathcal{I}(p_1, p_1)\Big) - m_e^2 \Big(\mathcal{I}(q_2, q_2) + \mathcal{I}(p_2, p_2)\Big) \\
&+ 2(q_1 \cdot p_1)\mathcal{I}(q_1, p_1) - 2(q_1 \cdot q_2)\mathcal{I}(q_1, q_2) + 2(q_1 \cdot p_2)\mathcal{I}(q_1, p_2) \\
&+ 2(p_1 \cdot q_2)\mathcal{I}(p_1, q_2) - 2(p_1 \cdot p_2)\mathcal{I}(p_1, p_2) + 2(q_2 \cdot p_2)\mathcal{I}(q_2, p_2) \Bigg].
\end{aligned} \tag{2.87}$$

The expression above is valid in every reference frame, but can be simplified in the CM frame, where the following equalities hold

$$\mathcal{I}(q_1, q_1) = \mathcal{I}(p_1, p_1) \qquad\qquad \mathcal{I}(q_2, q_2) = \mathcal{I}(p_2, p_2)$$
$$\mathcal{I}(p_1, q_2) = \mathcal{I}(q_1, p_2) \qquad\qquad \mathcal{I}(p_1, p_2) = \mathcal{I}(q_1, q_2)$$

so in the CM frame we have

$$\begin{aligned}
\left(\frac{d\sigma_0}{dt}\right)_{2\to3} = \left(\frac{d\sigma_0}{dt}\right)_{2\to2} \frac{\alpha}{2\pi^2} \Bigg[&-m_\mu^2 \mathcal{I}(p_1, p_1) - m_e^2 \mathcal{I}(p_2, p_2) \\
&+ \frac{(2m_\mu^2 - t)}{2}\mathcal{I}(q_1, p_1) + \frac{(2m_e^2 - t)}{2}\mathcal{I}(q_2, p_2) \\
&- (s - (m_\mu^2 + m_e^2))\mathcal{I}(p_1, p_2) - (u - (m_\mu^2 + m_e^2))\mathcal{I}(q_1, p_2) \Bigg]
\end{aligned} \tag{2.88}$$

where it must be noted that the soft photon energy ω in the expression for the bremsstrahlung integrals is not a Lorentz-invariant quantity, therefore $\omega_{\text{lab}} \neq \omega_{\text{CM}}$.

2.4.1 Cancellation of IR Divergences

In order to check the validity of the Bloch-Nordsieck theorem (and therefore of our calculations) we extracted the $\log(\lambda)$ terms from Eq.(2.88) (see App.B) and from the IR-divergent PV scalar functions appearing in the results for the virtual radiative corrections and verified that they are equal and opposite.[10] In a concise form, we obtained the following relation

$$\left(\frac{d\sigma_0}{dt}\right)_{\text{IR}}^{\text{Soft Brem}} + \left(\frac{d\sigma_1}{dt}\right)_{\text{IR}}^{\text{VC}\mu} + \left(\frac{d\sigma_1}{dt}\right)_{\text{IR}}^{\text{VCe}} + \left(\frac{d\sigma_1}{dt}\right)_{\text{IR}}^{\text{BD}} + \left(\frac{d\sigma_1}{dt}\right)_{\text{IR}}^{\text{BC}} = 0. \tag{2.89}$$

We remark that there is a specific pattern in the cancellation, which can be better appreciated looking at the diagrams.

---

[10]The IR-divergent part of the relevant PV scalar functions can be taken from the expressions in [111].

VC Diagrams   The cancellation of IR divergences between soft bremsstrahlung and VC diagrams is shown below [11], in the case of the muonic vertex

$$
\left| \quad + \quad \right|^2_{\text{IR}} + 2\text{Re}\left(\quad \times \quad \right)_{\text{IR}} = 0 \qquad (2.90)
$$

with an analogous result for the electronic vertex. Note that for the VC the cancellation comes from diagrams with bremsstrahlung on the same lepton line.

Box Diagrams   For the box, bremsstrahlung diagrams with mixed lepton lines are involved. Considering the direct box we have

$$
2\text{Re}\left(\quad \times \quad + \quad \times \quad \right)_{\text{IR}}
$$

$$
+ 2\text{Re}\left(\quad \times \quad \right)_{\text{IR}} = 0 \quad (2.91)
$$

while for the crossed box the cancellation is given by

$$
2\text{Re}\left(\quad \times \quad + \quad \times \quad \right)_{\text{IR}}
$$

$$
+ 2\text{Re}\left(\quad \times \quad \right)_{\text{IR}} = 0 \ . \quad (2.92)
$$

---

[11]Sum over polarizations is understood in the diagrammatic representation.

Chapter 3

Dispersive Approach to Feynman Amplitudes

Before we proceed to analyze the cross section at NNLO, we need to consider some technical results that go beyond perturbation theory. As stated in Sect. 1.2.3, hadronic contributions cannot be treated perturbatively at low energies because of strong-interaction effects. Therefore the perturbative expansion in α, used in the previous chapter for the evaluation of diagrams involving leptons only, breaks down when strongly interacting quarks are considered in virtual corrections. However, there exist a non-perturbative approach based on dispersion relations (Sect. 3.1) and the optical theorem (Sect. 3.2), which exploits the properties of *causality* and *unitarity* of Quantum Field Theory (QFT) to circumvent this problem. This approach is introduced in the present chapter and applied to the case of the hadronic vacuum polarization (HVP) function in Sect. 3.3, where we show its importance in the evaluation of the hadronic leading order (HLO) contribution to the muon $g - 2$. Moreover, the same non-perturbative method will be useful in dealing with the hadronic contributions to $\mu^- e^-$ scattering at NNLO .

3.1 Dispersion Relations

Let us consider a function $F(z)$ which is analytic in the complex plane, except for a branch cut starting at point s_0 on the positive real s-axis (we use s for later convenience). If we consider a closed path $\mathcal{C}_R$ excluding the branch cut as that of Fig.3.1, $F(z)$ admits the Cauchy integral representation

$$F(z) = \frac{1}{2\pi i} \oint_{\mathcal{C}_R} dz' \frac{F(z')}{z' - z} \tag{3.1}$$

for any z included in the region defined by $\mathcal{C}_R$. If we set $R \to \infty$, we can write $F(z)$ for the whole complex plane, excluding the cut, as

$$F(z) = \frac{1}{2\pi i} \oint_{\mathcal{C}_\infty} dz' \frac{F(z')}{z' - z} + \frac{1}{2\pi i} \int_{s_0}^{\infty} ds \frac{F(s + i0) - F(s - i0)}{s - z} \tag{3.2}$$

where the second term represents the contribution in the vicinity of the cut. Moreover, if $F(z)$ is a continuous real function for $z \in \mathbb{R}$, by the Schwarz reflection principle it satisfies the relation

$$F^*(z) = F(z^*)$$

in its domain of analyticity, and the contribution in the vicinity of the cut can be written as[1]

$$F(s + i0) - F(s - i0) = 2i \operatorname{Im} F(s + i0) \qquad (s \in \mathbb{R}, \ s > s_0). \tag{3.3}$$

Now if $F(z)$ vanishes sufficiently rapidly for $|z| \to \infty$, then the $\mathcal{C}_\infty$ contour integral in Eq.(3.2) is zero and we obtain the *dispersion relation*

$$F(z) = \frac{1}{\pi} \int_{s_0}^{\infty} ds \frac{\operatorname{Im} F(s)}{s - z} \tag{3.4}$$

---

[1] The positive orientation of the path is conventionally defined as the one that leaves on its left the enclosed region.
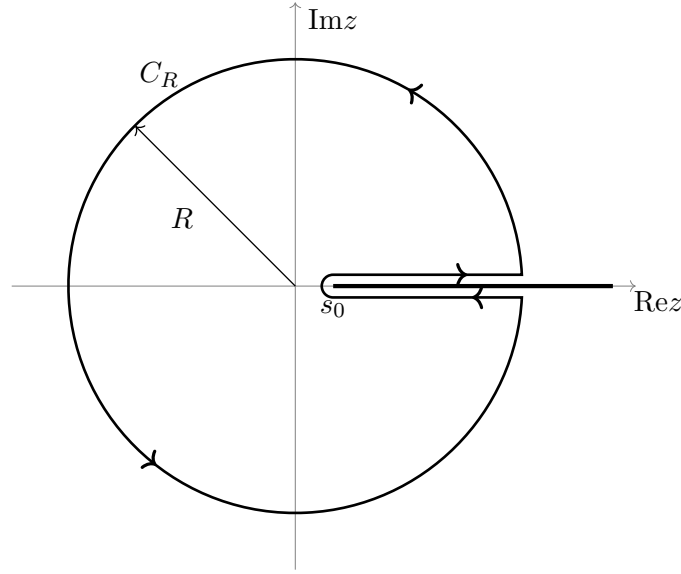
Figure 3.1: analyticity region of $F(z)$ and closed path C_R. The branch cut starts at s_0.

where $\mathrm{Im}F(s)$ actually stands for $\mathrm{Im}F(s + i0)$.

We can also retrieve a result valid for a point on the cut $s > s_0$ by considering the limit

$$
\begin{aligned}
F(s) &= \lim_{\varepsilon \to 0} F(s + i\varepsilon) \\
&= \lim_{\varepsilon \to 0} \frac{1}{\pi} \int_{s_0}^{\infty} ds' \frac{\mathrm{Im}F(s')}{s' - s - i\varepsilon} \ .
\end{aligned}
\tag{3.5}
$$

Therefore, the knowledge of only the imaginary part of $F(s)$ allows to reconstruct the entire function. In particular, recalling the formal relation

$$
\frac{1}{s' - s - i\varepsilon} = \mathcal{P} \frac{1}{s' - s} + i\pi \delta(s' - s)
$$

the real part of $F(s)$ can be extracted as

$$
\mathrm{Re}F(s) = \frac{1}{\pi} \mathcal{P} \int_{s_0}^{\infty} ds' \frac{\mathrm{Im}F(s')}{s' - s}
\tag{3.6}
$$

where $\mathcal{P}$ represents the principal value of the integral.

If $F(z)$ does not satisfy the fall-off condition mentioned above, but is such that

$$
\lim_{z \to \infty} \frac{F(z)}{z} = 0
\tag{3.7}
$$

then, to ensure the convergence of the previous integrals, it suffices to know the value of $F(z)$ for $z = a$, with a lying on the real axis outside the cut, and to consider the function

$$
G(z) = \frac{F(z) - F(a)}{z - a}
\tag{3.8}
$$

which has a better asymptotic behavior for $|z| \to \infty$. This allows one to write a dispersion relation like Eq.(3.4)

$$
G(z) = \frac{1}{\pi} \int_{s_0}^{\infty} ds \frac{\mathrm{Im}G(s)}{s - z}
\tag{3.9}
$$

where the imaginary part of $G(z)$ is

$$
\mathrm{Im}G(s) = \frac{\mathrm{Im}F(s)}{s - a}
\tag{3.10}
$$

30

and again $\text{Im}G(s)$ stands for $\text{Im}G(s + i0)$. Therefore, going back to $F(z)$, we have

$$\frac{F(z) - F(a)}{z - a} = \frac{1}{\pi} \int_{s_0}^{\infty} ds \, \frac{\text{Im}F(s)}{(s - a)(s - z)} \tag{3.11}$$

which is known as a *subtracted dispersion relation*. Finally the contribution on the cut is obtained as

$$\frac{F(s) - F(a)}{s - a} = \frac{1}{\pi} \lim_{\varepsilon \to 0} \int_{s_0}^{\infty} ds' \, \frac{\text{Im}F(s')}{(s' - a)(s' - s - i\varepsilon)} \; . \tag{3.12}$$

Dispersion relations are particularly useful in the evaluation of Feynman amplitudes, since their imaginary part can be extracted using the optical theorem. That's the strategy that will be followed in dealing with the hadronic vacuum polarization contributions.

3.2 The Optical Theorem

The second ingredient needed for our future calculations is the optical theorem, which exploits the unitarity of the S-matrix to relate one-loop amplitudes to tree-level cross sections.[2]

If T is the non-trivial part of the S-matrix, the unitarity of the latter is expressed as

$$\begin{aligned} \mathbf{1} &= S^\dagger S \\ &= (\mathbf{1} - iT^\dagger)(\mathbf{1} + iT) \end{aligned} \tag{3.13}$$

from which

$$i(T^\dagger - T) = T^\dagger T. \tag{3.14}$$

We can sandwich Eq.(3.14) between some initial and final quantum states, and inserting a completeness relation[3] in the r.h.s. we obtain

$$i \langle f | (T^\dagger - T) | i \rangle = \sum_n \int d\Pi_n \, \langle f | T^\dagger | n \rangle \langle n | T | i \rangle \; . \tag{3.15}$$

Finally, recalling the definition of the Feynman amplitude $\mathcal{M}(i \to f)$

$$\langle f | T | i \rangle = (2\pi)^4 \delta^4(p_i - p_f) \mathcal{M}(i \to f) \tag{3.16}$$

we find the generalized relation

$$\mathcal{M}(i \to f) - \mathcal{M}^*(f \to i) = i \sum_n \int d\Pi_n (2\pi)^4 \delta^4(p_i - p_f) \mathcal{M}(i \to n) \mathcal{M}^*(f \to n). \tag{3.17}$$

If now we consider the special case $|i\rangle = |f\rangle = |A\rangle$, which will be of interest for our purposes, then Eq.(3.17) turns into

$$2\text{Im}\mathcal{M}(A \to A) = \sum_n \int d\Pi_n (2\pi)^4 \delta^4(p_A - p_n) |\mathcal{M}(A \to n)|^2 \; . \tag{3.18}$$

In particular, if $\mathcal{M}(A \to A)$ is proportional to g^2, where g is the coupling constant of the theory, this forces $\mathcal{M}(A \to n)$ to be $\propto g$: in other words, the imaginary part of a given one-loop ($\mathcal{O}(g^2)$) amplitude can be linked to an *inclusive* tree-level ($\mathcal{O}(g)$) cross section, where all the physically allowed final states are considered in the r.h.s. of Eq.(3.18).

---

[2]We follow Schwartz [112].

[3]The completeness relation is defined as

$$\mathbf{1} = \sum_n \int d\Pi_n \, |n\rangle \langle n|$$

where the sum is carried over all the possible (single- and multi-particle) states allowed by the theory and

$$d\Pi_n = \prod_{j \in n} \frac{d^3 p_j}{(2\pi)^3} \frac{1}{2E_j},$$

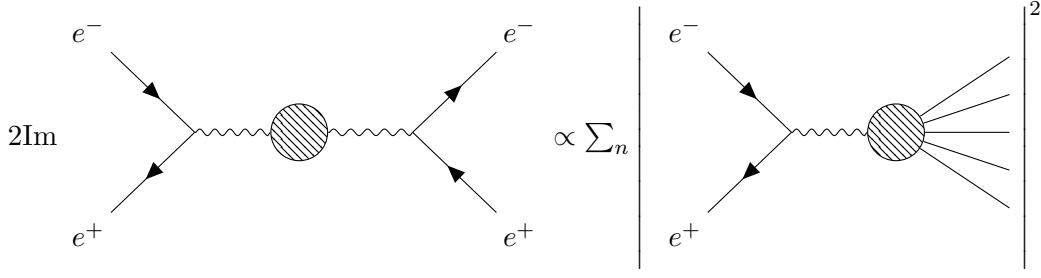where j labels a particle in the state $|n\rangle$.

Figure 3.2: the optical theorem for the VP function.

3.3 Dispersive Approach for Vacuum Polarization

We can now combine the results discussed in the previous two sections. Consider the Standard Model 1PI vacuum polarization (VP) function $\Pi(q^2)$ introduced in Sect. 2.3.2. Since its analyticity is ensured by causality, it satisfies a subtracted dispersion relation like the one of Eq.(3.12)

$$\Pi(q^2) - \Pi(0) = \frac{q^2}{\pi} \int_{4m_e^2}^{\infty} ds \frac{\text{Im}\Pi(s)}{s(s - q^2 - i\varepsilon)} \tag{3.19}$$

where $\Pi(q^2) - \Pi(0)$ is exactly the renormalized VP function $\bar{\Pi}(q^2)$ defined in the on-shell scheme (it is the generalization to all orders of Eq.(2.33)), and the starting point of the branch cut is $4m_e^2$, since m_e is the mass of the lightest particles that can be pair-produced.

Moreover, using the optical theorem the imaginary part of the VP function can be related to the inclusive cross section

$$\sigma(e^+ e^- \to \gamma^* \to \text{anything})$$

as diagrammatically shown in Fig.3.2. In particular, using the cross section $\sigma(e^+ e^- \to \gamma^* \to \mu^+ \mu^-)$ in the limit $s \gg 4m_\mu^2$ as a normalization factor, the following relation holds

$$\text{Im}\Pi(s) = \frac{\alpha}{3} R(s) \tag{3.20}$$

where

$$R(s) = \frac{\sigma(e^+ e^- \to \gamma^* \to \text{anything})}{\sigma(e^+ e^- \to \gamma^* \to \mu^+ \mu^-)} = \left(\frac{3}{4\pi} \frac{s}{\alpha^2} \right) \sigma(e^+ e^- \to \gamma^* \to \text{anything}) \tag{3.21}$$

and $\alpha(s)$ is the running fine-structure constant.

Thus, the $\bar{\Pi}(q^2)$ function is connected to the inclusive cross section $\sigma(e^+ e^- \to \gamma^* \to \text{anything})$ by combining DRs and the optical theorem. This is an important result, since whenever the theory fails to provide information about $\bar{\Pi}(q^2)$, one can rely on the experimental data coming from the measurement of the above cross section.

If we want to apply this result specifically to the hadronic part of the VP function, we have to consider only hadronic final states in the inclusive cross section, therefore

$$\bar{\Pi}_{\text{had}}(q^2) = \frac{\alpha q^2}{3\pi} \int_{m_\pi^2}^{\infty} ds \frac{R_{\text{had}}(s)}{s(s - q^2 - i\varepsilon)} \tag{3.22}$$

where

$$R_{\text{had}}(s) = \left(\frac{3}{4\pi} \frac{s}{\alpha^2} \right) \sigma(e^+ e^- \to \gamma^* \to \text{hadrons}) \tag{3.23}$$

is also known as the *hadronic ratio* (see Fig.3.3). Note that the cut starting point for the HVP function in Eq.(3.22) is m_π^2, since the channel $\gamma^* \to \pi^0 \gamma$ is the one with the lowest hadronic threshold.
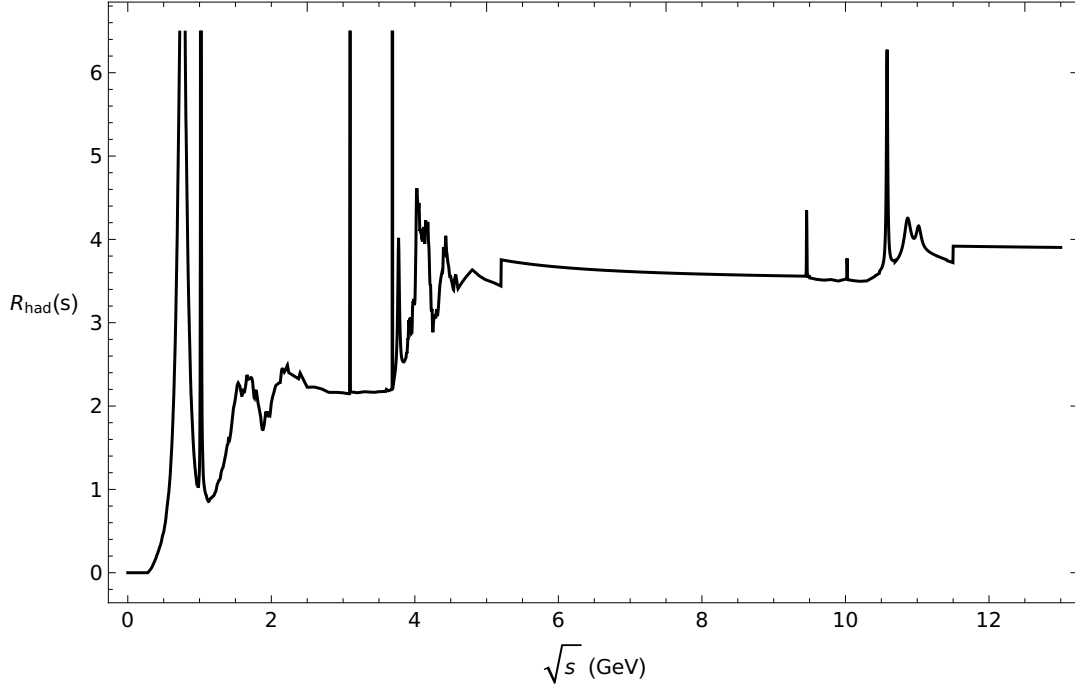
Figure 3.3: hadronic ratio $R_{\text{had}}(s)$ in the non-perturbative region $\sqrt{s} \in [0, 13]$GeV, as obtained from the `alphaQED16` package. Note the many resonances in correspondence of meson production thresholds. The region $\sqrt{s} \gtrsim 13$GeV is well reproduced by perturbative QCD.

3.3.1 Hadronic Contributions to a_μ

As an application of the dispersive approach just described, we present how this is employed to evaluate the LO hadronic contribution to the anomalous magnetic moment of the muon, a_μ^{HLO}, showing how Eq.(1.31) is obtained. First, we look at the contribution of the whole 1PI VP insertion, labeled X in the muonic vertex diagram (a) of Fig. 3.4.

If we recall the expression for the full propagator Eq.(2.29) and consider the renormalized VP function at all orders $\bar{\Pi}(q^2)$, we can write the amplitude for the diagram simply by substituting

$$\frac{-ig_{\alpha\beta}}{k^2} \;\rightarrow\; \frac{-ig_{\alpha\beta}}{k^2}\left[-\bar{\Pi}(k^2)\right]$$

in the definition for the vertex correction of Eq.(2.49), obtaining

$$
\begin{aligned}
-ie\,\bar{u}(p_2)\Gamma^\mu_{(\text{X})}(p_1,p_2)u(p_1) = (-ie\mu^{\frac{\varepsilon}{2}})^3 \int \frac{d^D k}{(2\pi)^D}\,\frac{-ig_{\alpha\beta}}{k^2}\left[-\bar{\Pi}(k^2)\right] \\
\times\,\bar{u}(p_2)\left[\gamma^\alpha\frac{i[(\slashed{k}+\slashed{p}_2)+m_\mu]}{(k+p_2)^2-m_\mu^2}\gamma^\mu\frac{i[(\slashed{k}+\slashed{p}_1)+m_\mu]}{(k+p_1)^2-m_\mu^2}\gamma^\beta\right]u(p_1)
\end{aligned}
\tag{3.24}
$$

Now we use the DR of Eq.(3.19) and find

$$
\begin{aligned}
-ie\,\bar{u}(p_2)\Gamma^\mu_{(\text{X})}(p_1,p_2)u(p_1) = (-ie\mu^{\frac{\varepsilon}{2}})^3\frac{1}{\pi}\int_{4m_e^2}^\infty\frac{ds}{s}\,\text{Im}\Pi(s)\times \\
\times \int\frac{d^D k}{(2\pi)^D}\,\frac{-ig_{\alpha\beta}}{k^2-s}\,\bar{u}(p_2)\left[\gamma^\alpha\frac{i[(\slashed{k}+\slashed{p}_2)+m_\mu]}{(k+p_2)^2-m_\mu^2}\gamma^\mu\frac{i[(\slashed{k}+\slashed{p}_1)+m_\mu]}{(k+p_1)^2-m_\mu^2}\gamma^\beta\right]u(p_1)\;.
\end{aligned}
\tag{3.25}
$$

Note that the last integral is formally equal to the one of Eq.(2.49), in the sense that the photon seems to develop a non-zero mass $\sqrt{s}$. Calculations can then be carried out in the same way as for the one-loop QED vertex, with the only important difference that here s is not an IR regulator, therefore
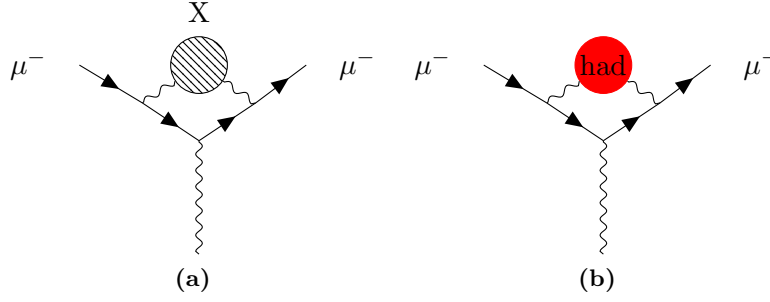
Figure 3.4: two-loop muonic vertex diagrams contributing to a_μ: the complete 1PI VP is shown in diagram (a), while only the hadronic part of the latter is depicted as a red blob in diagram (b).

it cannot be neglected (no limit to zero must be taken). Obtaining an analogous of Eq(2.58), we find for the renormalized vertex

$$\bar{u}(p_2)\bar{\Gamma}^\mu_{(\mathrm{X})}(q)u(p_1) = \frac{1}{\pi}\int_{4m_e^2}^\infty \frac{ds}{s}\,\mathrm{Im}\Pi(s)\,\bar{u}(p_2)\left[F_1(q^2,s)\gamma^\mu + \frac{i}{2m_\mu}F_2(q^2,s)\sigma^{\mu\nu}q_\nu\right]u(p_1) \qquad (3.26)$$

where we have stressed that the form factors depend both on q^2 and on the integration variable s. The expressions for $F_1(q^2,s)$ and $F_2(q^2,s)$ can be obtained starting from functions $G(q^2,s)$ and $H(q^2,s)$, i.e. Eqs.(2.51-2.53) with the substitution $\lambda^2 \to s$ in the formula for Δ. Considering now the anomalous magnetic moment of the muon, we have to look at $F_2(q^2=0)$ and the contribution of a single 1PI VP insertion to a_μ is found to be

$$a_\mu^{(\mathrm{X})} = \frac{1}{\pi}\int_{4m_e^2}^\infty \frac{ds}{s}\,\mathrm{Im}\Pi(s)K_\mu^{(2)}(s) \qquad (3.27)$$

where the kernel

$$K_\mu^{(2)}(s) = \frac{\alpha}{\pi}\int_0^1 dx\,\frac{x^2(1-x)}{x^2+(s/m_\mu^2)(1-x)} \qquad (3.28)$$

is nothing but $F_2(0,s)$, and it's equal to the Schwinger term $\alpha/2\pi$ for $s=0$, as expected.

The result just obtained in Eq.(3.27) is valid for the full VP contribution, and allows a non-perturbative approach to the computation of radiative corrections. Indeed, DRs and the optical theorem are a consequence of analyticity and unitarity, respectively, two very general properties of QFT. Therefore Eq.(3.27) can be used both as a check of perturbative calculations (as in the case of leptonic VP contributions to a_μ) and as a way out whenever these are not reliable: as said before, this is the case for hadronic contributions. If we restart from Eq.(3.24) and focus on the contribution coming from $\bar{\Pi}_{\mathrm{had}}(k^2)$, recalling Eq.(3.22) we wind up with

$$a_\mu^{\mathrm{had}} = \frac{\alpha}{\pi}\int_{m_\pi^2}^\infty \frac{ds}{s}\int_0^1 dx\,\frac{x^2(1-x)}{x^2+(s/m_\mu^2)(1-x)}\frac{\alpha}{3\pi}R_{\mathrm{had}}(s) \qquad (3.29)$$

where $R_{\mathrm{had}}(s)$ can't be computed perturbatively at low s, because of strong interaction effects (as can be seen in Fig.3.3) and it is rather extracted by experiment.

Depending on which integration is performed first, there are two possible representations for a_μ^{had}

- Integrating over x first yields the *time-like* representation

$$a_\mu^{\mathrm{had}} = \frac{\alpha}{3\pi}\int_{m_\pi^2}^\infty \frac{ds}{s}K_\mu^{(2)}(s)R_{\mathrm{had}}(s) \qquad (3.30)$$

- Integrating over s and defining $t(x) = -\frac{x^2}{1-x}m_\mu^2 < 0$ results in the *space-like* representation [74]

$$a_\mu^{\mathrm{had}} = \frac{\alpha}{\pi}\int_0^1 dx\,(1-x)\Delta\alpha_{\mathrm{had}}^{(5)}[t(x)] \qquad (3.31)$$

which is the keystone of the MUonE experiment.

We finally present a rough estimate of the LO hadronic contribution to a_μ, namely the $\mathcal{O}(\alpha^2)$ contribution given by diagram (b) of Fig. 3.4. Using the function $\mathrm{Im}\Pi_{\mathrm{had}}(s)$ provided by the package `alphaQED16` [113], we performed the two-fold numerical integral (3.30) and obtained $a_\mu^{\mathrm{HLO}} = 687.53 \times 10^{-10}$, which is very close to Jegerlehner's latest result $a_\mu^{\mathrm{HLO}} = 688.07 \pm 4.14 \times 10^{-10}$ (Eq.(5.29) of [27]).
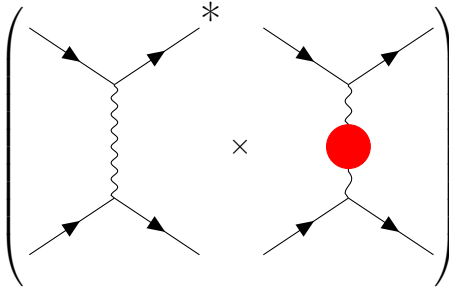
Chapter 4

Hadronic Contributions to Muon-Electron Scattering

Having discussed all the tools needed for our task, we are now able to evaluate the hadronic contributions to $\mu^- e^-$ scattering, which start to appear at NLO. The key diagram here is the same hadronic vacuum polarization (HVP) insertion appearing in diagram (b) of Fig. 3.4. At NNLO, we will show that with all the results obtained in the previous chapters, namely the QED contributions to the NLO cross section and the dispersive approach, we succeeded in calculating these hadronic contributions.

4.1 NLO Contribution

The only hadronic contribution to the NLO amplitude is a LO QED diagram with one HVP insertion in the virtual photon propagator. Remembering Eq.(2.21) it contributes to the NLO cross section as

This contribution can be evaluated easily by recalling the factorization property for the VP function found in Eq.(2.46), which holds both for leptonic and hadronic VP

$$\mathcal{M}_1^{\text{HVP}} = \mathcal{M}_0 \left[-\bar{\Pi}_{\text{had}}(t) \right] \ . \tag{4.1}$$

As a result, the HVP contribution can be expressed in terms of the LO one

$$\begin{aligned} \mathcal{X}_1^{\text{had}} &= \mathcal{X}_0 \left[-2\bar{\Pi}_{\text{had}}(t) \right] \\ &= \mathcal{X}_0 \times \delta_1^{\text{had}} \end{aligned} \tag{4.2}$$

where $\bar{\Pi}_{\text{had}}(t)$ is automatically real, since it depends on the space-like quantity $t < 0$.[1]

---

[1]Note that the $\bar{\Pi}_{\text{had}}(q^2)$ used in our calculations comes from the package `alphaQED16`. This includes also higher order terms, since radiative corrections are added in the experimental data [27, 32, 114]. Therefore the contribution to the NNLO cross section coming from a diagram like the one below
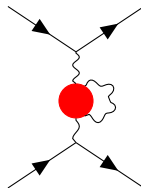
is already included in the hadronic NLO term computed here.

4.2 NNLO Contributions

We now focus on the hadronic contributions to $\mu^- e^-$ scattering at NNLO: these are $\mathcal{O}(\alpha^4)$ contributions to the cross section arising from (the product of) diagrams containing at least one HVP insertion, i.e. one red blob. We identify four classes of contributions, depending on the different kinds of diagrams considered, which we proceed to discuss in the following.

Class I

Class I contributions to the cross section arise from products of diagrams involving two VP insertions (only hadronic or hadronic and leptonic). These include the squared modulus of the $\mathcal{O}(\alpha^2)$ NLO HVP diagram, the interference of the same diagram with the NLO leptonic VP and the interference of the LO QED amplitude with the $\mathcal{O}(\alpha^3)$ two-loop diagrams containing two VPs. They are represented below (the sum over polarizations is understood in the products of diagrams)

In order to evaluate these contributions, we exploit the factorization property Eq.(2.46). As a result, the contribution to the cross section can be easily evaluated in terms of $\mathcal{X}_0$

$$\begin{aligned} \mathcal{X}_\text{I} &= \mathcal{X}_0 \; 3\bar{\Pi}_\text{had}(t) \left[\bar{\Pi}_\text{had}(t) + 2\bar{\Pi}_\text{lep}(t) \right] \\ &= \mathcal{X}_0 \times \delta_\text{I} \end{aligned} \tag{4.3}$$

where both the hadronic and leptonic VP functions are real, as they depend on t.

Class II

The contributions to the cross section from Class II diagrams are depicted below: these include products of diagrams involving one HVP insertion and a QED loop as those of Sect. 2.3.3 and 2.3.4.

As for Class I diagrams, factorizing the HVP function allows us to express the contribution to the cross section in terms of the results for the NLO contributions obtained in Sect. 2.3. In particular, we find

$$
\begin{aligned}
\mathcal{X}_{\mathrm{II}} &= -\bar{\Pi}_{\mathrm{had}}(t) \left[2\mathcal{X}_1^{\mathrm{VC}_\mu} + 2\mathcal{X}_1^{\mathrm{VC}_e} + \mathcal{X}_1^{\mathrm{BD}} + \mathcal{X}_1^{\mathrm{BC}} \right] \\
&= -\bar{\Pi}_{\mathrm{had}}(t)\, \mathcal{X}_0 \times \left[2\delta_{\mathrm{VC}_\mu} + 2\delta_{\mathrm{VC}_e} + \delta_{\mathrm{BD}} + \delta_{\mathrm{BC}} \right] \\
&= \mathcal{X}_0 \times \delta_{\mathrm{II}} \ .
\end{aligned}
\tag{4.4}
$$

Note that the NLO loops computed in Sect. 2.3.3 and 2.3.4 are IR-divergent, but here we have already assumed the validity of the Bloch-Nordsieck theorem (we will prove the cancellation of IR divergences for the hadronic NNLO contributions in the next section).

Class III

Class III contributions are related to the bremsstrahlung cross section at NLO: they arise from the interference of the $\mathcal{O}\left(\alpha^{\frac{3}{2}}\right)$ LO amplitude with the $\mathcal{O}\left(\alpha^{\frac{5}{2}}\right)$ NLO diagrams containing one HVP in the virtual photon propagator. For example, if the photon is emitted from the initial muon line we have the contribution

The complete analysis of these contributions requires the calculation of hard bremsstrahlung, which will not be treated in this thesis. However, by restricting our discussion to the soft-photon limit, in the next section we will be able to prove the cancellation of the IR divergences for the entire set of hadronic NNLO contributions. Here we note that in the soft limit the factorization of the HVP function for the NLO bremsstrahlung diagrams allows us to write

$$
\left(\frac{d\sigma_1}{dt} \right)_{\mathrm{IR}}^{\mathrm{Soft\ Brem}} = \left(\frac{d\sigma_0}{dt} \right)_{\mathrm{IR}}^{\mathrm{Soft\ Brem}} \left[-2\bar{\Pi}_{\mathrm{had}}(t) \right]
\tag{4.5}
$$

a relation that will be useful in the following section.

Class IV

The contributions to the cross section from Class IV diagrams are

where both the direct and crossed box diagrams can present the HVP either in their left (BDL and BCL) or in their right (BDR and BCR) photon propagator.

Note that in this case the factorization of the VP function cannot be exploited, since the HVP is now inside a loop itself, and $\bar{\Pi}_{\text{had}}(k^2)$ depends on the loop-momentum k. However, the dispersive approach introduced in Sect. 3.3 can be employed in the evaluation of these contributions, in much the same way as for the computation of $a_\mu^{(\text{X})}$.

VC Diagrams In Sect. 3.3.1 we found that the VP insertion modifies the vertex correction amplitude as in Eq.(3.25), leading to Eq.(3.26). In the same way, focusing on the HVP yields

$$\bar{u}(p_2)\Gamma^\mu_{\text{had}}(q)u(p_1) = \frac{1}{\pi}\int_{m_\pi^2}^\infty \frac{dz}{z}\,\text{Im}\Pi_{\text{had}}(z)\,\bar{u}(p_2)\left[F_1(q^2,z)\gamma^\mu + \frac{i}{2m}F_2(q^2,z)\sigma^{\mu\nu}q_\nu\right]u(p_1) \qquad (4.6)$$

where m is the mass of a generic lepton and we have used z instead of s to avoid confusion with the Mandelstam variable introduced for the scattering process. We emphasize that the form factors in the above equation are actually different from the ones of Sect. 2.3.3, since here z is not a small variable. Indeed, no IR divergences arise in the evaluation of the VC diagrams of Class IV. Moreover, the dispersive approach allows us to deal with one-loop integrals only, as for the NLO diagrams, despite the fact that we are considering contributions of higher order in α.

The expressions for $F_1(t,z)$ and $F_2(t,z)$ were calculated using `FeynCalc` and are given below.[2] In particular, note that a new counterterm $\delta_1(z)$ has to be introduced: this depends on the integration variable z, and the on-shell renormalization condition is now expressed as

$$F_1(0,z) = 0 \;\forall z, \qquad (4.7)$$

therefore the counterterm is fixed as

$$\delta_1(z) = -G(0,z) - 2mH(0,z). \qquad (4.8)$$

As a consistency check, we considered our results in the limit $z \to 0$ and verified that the NNLO form factors reproduce exactly the NLO ones from Sect. 2.3.3.

---

[2]Again, the squared momentum transfer q^2 is equal to the t variable in our analysis.

Modified Form Factors

$$F_1(t,z) = \frac{\alpha}{4\pi} \frac{1}{(mt - 4m^3)^2} \Big\{ a_0 + a_1 \bar{B}_0(0,z,z) + a_2 \bar{B}_0\left(t, m^2, m^2\right) + a_3 \bar{B}_0\left(0, m^2, m^2\right)$$
$$+ a_4 \bar{B}_0\left(m^2, m^2, z\right) + a_5 C_0\left(0, m^2, m^2, m^2, m^2, z\right) \tag{4.9}$$
$$+ a_6 C_0\left(m^2, m^2, t, m^2, z, m^2\right) \Big\}$$

with

$$a_0 = t\left(4m^2 - t\right)\left(2m^2 - z\right) \qquad\qquad a_1 = -tz\left(4m^2 - t\right)$$
$$a_2 = -m^2\left(32m^4 - 4m^2(5t - 4z) + t(3t + 2z)\right) \qquad a_3 = \left(4m^2 - t\right)\left(8m^4 - m^2(t - 4z) - tz\right)$$
$$a_4 = 2t\left(-4m^4 + m^2(t + 7z) - tz\right) \qquad a_5 = -\left(t - 4m^2\right)^2\left(2m^2 - z\right)\left(2m^2 + z\right)$$
$$a_6 = 2m^2\left(32m^6 - 32m^4 t + 2m^2\left(5t^2 + 4tz - 4z^2\right) - t(t + z)^2\right)$$

$$F_2(t,z) = \frac{\alpha}{\pi} \frac{1}{(t - 4m^2)^2} \Big\{ b_0 + b_1 \bar{B}_0(0,z,z) + b_2 \bar{B}_0(t, m^2, m^2) + b_3 \bar{B}_0(0, m^2, m^2)$$
$$+ b_4 \bar{B}_0(m^2, m^2, z) + b_5 C_0\left(m^2, m^2, t, m^2, z, m^2\right) \Big\} \tag{4.10}$$

with

$$b_0 = -\left(4m^2 - t\right)\left(2m^2 - z\right) \qquad\qquad b_1 = z\left(4m^2 - t\right)$$
$$b_2 = -m^2\left(4m^2 - t - 6z\right) \qquad\qquad b_3 = -m^2\left(4m^2 - t\right)$$
$$b_4 = 8m^4 - 2m^2(t + 5z) + tz \qquad\qquad b_5 = -2m^2 z\left(8m^2 - 2t - 3z\right)$$

$$\delta_1(z) = -\frac{\alpha}{4\pi m^2} \Big\{ -z - z B_0(0,z,z) - \left(z + m^2\right) B_0\left(0, m^2, m^2\right)$$
$$+ 2\left(z + m^2\right) B_0\left(m^2, m^2, z\right) + \left(4m^4 - z^2\right) C_0\left(0, m^2, m^2, m^2, m^2, z\right) \Big\} \tag{4.11}$$

Now we can proceed as in Sect. 2.3.3 for the evaluation of the contribution to the cross section, by joining the hadronic VC just discussed together with the remaining tree-level part of the diagram. For the muonic vertex the two-loop amplitude reads

$$\mathcal{M}_2^{\text{VC}_\mu} = e^2 \frac{\bar{u}(q_1)\bar{\Gamma}_{\text{had}}^\mu(q_1 - p_1)u(p_1)\,\bar{u}(q_2)\gamma_\mu u(p_2)}{t} \tag{4.12}$$

and finally taking the interference with the LO diagram we obtain

$$\mathcal{X}_{\text{IV}}^{\text{VC}_\mu} = \frac{1}{\pi}\int_{m_\pi^2}^{\infty} \frac{dz}{z} \text{Im}\Pi_{\text{had}}(z)\,\mathcal{X}_1^{\text{VC}_\mu}(z) \tag{4.13}$$

where $\mathcal{X}_1^{\text{VC}_\mu}(z)$ is obtained[3] substituting $F_1^{(\mu)}(t) \to F_1^{(\mu)}(t,z)$ and $F_2^{(\mu)}(t) \to F_2^{(\mu)}(t,z)$ in Eq.(2.71). An analogous result can be readily calculated for the electronic vertex. Detailed results for $\mathcal{X}_1^{\text{VC}_\mu}(z)$ and $\mathcal{X}_1^{\text{VC}_e}(z)$ are presented in App. D.

To compute the relative contribution $\delta_{\text{IV}}^{\text{VC}}$ from both the muonic and electronic vertex, we factorize the quantity $\mathcal{X}_0$ and take it out of the integral in Eq.(4.13), since it does not depend on z, obtaining

$$\mathcal{X}_{\text{IV}}^{\text{VC}} = \mathcal{X}_0 \times \delta_{\text{IV}}^{\text{VC}} \tag{4.14}$$

---

[3]The subscript 1 in $\mathcal{X}_1^{\text{VC}_\mu}(z)$ emphasizes that it is a NLO result.

where

$$\delta_{\mathrm{IV}}^{\mathrm{VC}} = \frac{1}{\mathcal{X}_0} \frac{1}{\pi} \int_{m_\pi^2}^{\infty} \frac{dz}{z} \mathrm{Im}\Pi_{\mathrm{had}}(z) \, \mathcal{X}_1^{\mathrm{VC}}(z). \tag{4.15}$$

The last integration has to be performed numerically. Note, however, that the integration over z provides a result for a single, fixed value of t. In order to recover the cross section in the entire t-range, we subdivided the latter in bins, and calculated the mean value for a given bin.

Box Diagrams If the HVP is inserted in one of the two photon propagators in the box diagrams, we can still use the dispersive approach to calculate their contribution. However, being the other photon propagator a tree-level one, these box diagrams are IR-divergent.

Consider the amplitude for the direct box with the HVP in the left photon line (BDL): using the DR we express it as

$$i\mathcal{M}_2^{\mathrm{BDL}} = \frac{1}{\pi} \int_{m_\pi^2}^{\infty} \frac{dz}{z} \mathrm{Im}\Pi_{\mathrm{had}}(z)$$
$$\times (e\mu^{\frac{\varepsilon}{2}})^4 \int \frac{d^D k}{(2\pi)^D} \frac{\mathcal{N}^{\mathrm{BD}}}{[(p_1 - k)^2 - m_\mu^2][(k + p_2)^2 - m_e^2][k^2 - z][(k + p_2 - q_2)^2 - \lambda^2]} \tag{4.16}$$

where $\mathcal{N}^{\mathrm{BD}}$ is the same numerator as the NLO direct box one of Eq.(2.73), z on the third denominator comes from the DR and λ in the fourth denominator is the usual IR regulator. Note the different roles that the two photon "masses" play simultaneously in the calculations for the box diagrams.

Moving to the crossed boxes, we have the analogous contribution for the BCL diagram

$$i\mathcal{M}_2^{\mathrm{BCL}} = \frac{1}{\pi} \int_{m_\pi^2}^{\infty} \frac{dz}{z} \mathrm{Im}\Pi_{\mathrm{had}}(z)$$
$$\times (e\mu^{\frac{\varepsilon}{2}})^4 \int \frac{d^D k}{(2\pi)^D} \frac{\mathcal{N}^{\mathrm{BC}}}{[(p_1 - k)^2 - m_\mu^2][(q_2 - k)^2 - m_e^2][k^2 - z][(k + p_2 - q_2)^2 - \lambda^2]} \tag{4.17}$$

with the same $\mathcal{N}^{\mathrm{BC}}$ of Eq.(2.75). The amplitudes for BDR and BCR are straightforwardly obtained by interchanging z with λ^2 in Eqs.(4.16) and (4.17), respectively. The dispersive evaluation of the amplitudes proceeds analogously to that of the VC diagrams previously analyzed. Taking the BDL diagram as an example, after the re-evaluation of the one-loop integral in Eq.(4.16), neglecting λ terms (when possible) but keeping all dependence on z, we consider the interference with LO and wind up with

$$\mathcal{X}_{\mathrm{IV}}^{\mathrm{BDL}} = \frac{1}{\pi} \int_{m_\pi^2}^{\infty} \frac{dz}{z} \mathrm{Im}\Pi_{\mathrm{had}}(z) \, \mathcal{X}_1^{\mathrm{BDL}}(z) \tag{4.18}$$

and so on for the other box diagrams. Detailed results for $\mathcal{X}_1^{\mathrm{BD}}(z) = \mathcal{X}_1^{\mathrm{BDL}}(z) + \mathcal{X}_1^{\mathrm{BDR}}(z)$ and $\mathcal{X}_1^{\mathrm{BC}}(z) = \mathcal{X}_1^{\mathrm{BCL}}(z) + \mathcal{X}_1^{\mathrm{BCR}}(z)$ are collected in Appendix D.

4.3 Cancellation of IR Divergences

We now discuss the IR divergences of the hadronic contributions to the cross section at NNLO, verifying that these cancel each other out as stated by the Bloch-Nordsieck theorem. The result found at NLO was

$$\left(\frac{d\sigma_0}{dt}\right)_{\mathrm{IR}}^{\mathrm{Soft\ Brem}} + \left(\frac{d\sigma_1}{dt}\right)_{\mathrm{IR}}^{\mathrm{VC\mu}} + \left(\frac{d\sigma_1}{dt}\right)_{\mathrm{IR}}^{\mathrm{VCe}} + \left(\frac{d\sigma_1}{dt}\right)_{\mathrm{IR}}^{\mathrm{BD}} + \left(\frac{d\sigma_1}{dt}\right)_{\mathrm{IR}}^{\mathrm{BC}} = 0 \tag{4.19}$$

where the soft-photon limit was taken when considering the bremsstrahlung contribution.

Looking at the IR-divergent contributions at NNLO, we observe that

- Class I contributions are IR-finite.

- Class II contributions are all IR-divergent, and their IR divergences are inherited from the NLO virtual contributions, as can be seen in Eq.(4.4).

- Class III contributions are all IR-divergent, and their divergences are inherited from the LO bremsstrahlung contributions, as can be seen in Eq.(4.5).

- Only the four box diagrams of Class IV yield IR-divergent contributions.

The total IR-divergent contribution to the cross section would be then

$$
\left(\frac{d\sigma_2}{dt}\right)^{\text{had}}_{\text{IR}} = \left[-\bar{\Pi}_{\text{had}}(t)\right]\left\{2\left(\frac{d\sigma_0}{dt}\right)^{\text{Soft Brem}}_{\text{IR}} + 2\left(\frac{d\sigma_1}{dt}\right)^{\text{VC}\mu}_{\text{IR}} + 2\left(\frac{d\sigma_1}{dt}\right)^{\text{VCe}}_{\text{IR}} + \left(\frac{d\sigma_1}{dt}\right)^{\text{BD}}_{\text{IR}} + \left(\frac{d\sigma_1}{dt}\right)^{\text{BC}}_{\text{IR}}\right\}
$$
$$
+ \left(\frac{d\sigma_2}{dt}\right)^{\text{BDL}}_{\text{IR}} + \left(\frac{d\sigma_2}{dt}\right)^{\text{BDR}}_{\text{IR}} + \left(\frac{d\sigma_2}{dt}\right)^{\text{BCL}}_{\text{IR}} + \left(\frac{d\sigma_2}{dt}\right)^{\text{BCR}}_{\text{IR}}
$$

$$(4.20)$$

where the terms in curly brackets are the known LO (bremsstrahlung) and NLO (virtual corrections) contributions.

In order to verify that Eq.(4.20) is actually zero, let us consider the sum of the amplitudes for the left and right direct box diagrams. We can write

$$
\mathcal{M}_2^{\text{BDL}} + \mathcal{M}_2^{\text{BDR}} = \frac{1}{\pi}\int_{m_\pi^2}^{\infty}\frac{dz}{z}\,\text{Im}\Pi_{\text{had}}(z)\int\frac{d^4k}{(2\pi)^4}\frac{(-ie^4)\mathcal{N}^{\text{BD}}}{\left[(p_1-k)^2-m_\mu^2\right]\left[(k+p_2)^2-m_e^2\right]}
$$
$$
\times\left[\frac{1}{k^2-z}\frac{1}{(k+p_2-q_2)^2} + \frac{1}{k^2}\frac{1}{\left[(k+p_2-q_2)^2-z\right]}\right]
$$
$$
= \frac{1}{\pi}\int_{m_\pi^2}^{\infty}\frac{dz}{z}\,\text{Im}\Pi_{\text{had}}(z)\int\frac{d^4k}{(2\pi)^4}\frac{(-ie^4)\mathcal{N}^{\text{BD}}}{\left[(p_1-k)^2-m_\mu^2\right]\left[(k+p_2)^2-m_e^2\right]k^2(k+p_2-q_2)^2}
$$
$$
\times\left[\frac{k^2}{k^2-z} + \frac{(k+p_2-q_2)^2}{(k+p_2-q_2)^2-z}\right]
$$

$$(4.21)$$

where we have set $D=4$ (the integral is UV finite) and $\lambda=0$. Now we note that excluding the term in square brackets, the integral in d^4k in the third line of Eq.(4.21) is nothing but the one-loop direct box amplitude, $\mathcal{M}_1^{\text{BD}}$. When the IR limit $k\to 0$ is considered, the term in square brackets becomes

$$
\lim_{k\to 0}\left[\frac{k^2}{k^2-z} + \frac{(k+p_2-q_2)^2}{(k+p_2-q_2)^2-z}\right] = \frac{t}{t-z}
$$

$$(4.22)$$

and the IR-divergent part of the sum of the two amplitudes is

$$
\left(\mathcal{M}_2^{\text{BDL}} + \mathcal{M}_2^{\text{BDR}}\right)_{\text{IR}} = \frac{1}{\pi}\int_{m_\pi^2}^{\infty}\frac{dz}{z}\,\text{Im}\Pi_{\text{had}}(z)\frac{t}{t-z}\left(\mathcal{M}_1^{\text{BD}}\right)_{\text{IR}}
$$
$$
= \left[-\bar{\Pi}_{\text{had}}(t)\right]\left(\mathcal{M}_1^{\text{BD}}\right)_{\text{IR}}
$$

$$(4.23)$$

where in the second line we have used a DR similar to Eq.(3.19) and $\left(\mathcal{M}_1^{\text{BD}}\right)_{\text{IR}}$ is already known from the analysis of Sect. 2.3.4. Moving to the cross section, the result is

$$
\left(\frac{d\sigma_2}{dt}\right)^{\text{BDL}}_{\text{IR}} + \left(\frac{d\sigma_2}{dt}\right)^{\text{BDR}}_{\text{IR}} = \left[-\bar{\Pi}_{\text{had}}(t)\right]\left(\frac{d\sigma_1}{dt}\right)^{\text{BD}}_{\text{IR}}.
$$

$$(4.24)$$

The same reasoning applied to the crossed box diagrams yields

$$
\left(\frac{d\sigma_2}{dt}\right)^{\text{BCL}}_{\text{IR}} + \left(\frac{d\sigma_2}{dt}\right)^{\text{BCR}}_{\text{IR}} = \left[-\bar{\Pi}_{\text{had}}(t)\right]\left(\frac{d\sigma_1}{dt}\right)^{\text{BC}}_{\text{IR}}.
$$

$$(4.25)$$

Finally, using Eqs.(4.24) and (4.25) we can now express the total IR-divergent hadronic contribution to the NNLO cross section as

$$
\left(\frac{d\sigma_2}{dt}\right)^{\text{had}}_{\text{IR}} = 2\left[-\bar{\Pi}_{\text{had}}(t)\right]\left\{\left(\frac{d\sigma_0}{dt}\right)^{\text{Soft Brem}}_{\text{IR}} + \left(\frac{d\sigma_1}{dt}\right)^{\text{VC}\mu}_{\text{IR}} + \left(\frac{d\sigma_1}{dt}\right)^{\text{VCe}}_{\text{IR}} + \left(\frac{d\sigma_1}{dt}\right)^{\text{BD}}_{\text{IR}} + \left(\frac{d\sigma_1}{dt}\right)^{\text{BC}}_{\text{IR}}\right\}
$$

$$(4.26)$$

and the term in curly brackets is zero by Eq.(4.19). Again, the NLO results turned out to be very useful for the analysis of the higher-order contributions.

Chapter 5

Conclusions

The leading hadronic contribution is a key element in the SM prediction for the anomalous magnetic moment of the muon. However, the precision of the dispersive approach, usually employed in its evaluation, will soon be challenged by the upcoming results of the E989 Muon g-2 experiment at Fermilab.

In this thesis we discussed the recently proposed MUonE experiment at CERN [1, 2] as a possible solution to this problem: the leading hadronic contribution to a_μ could be extracted from the experimental measurement of the differential cross section $d\sigma/dt$ for elastic muon-electron scattering in the space-like region. The expected relative precision in the determination of $d\sigma/dt$ is of the order of 10 ppm, and the knowledge of the radiative corrections to this cross section is therefore required up to NNLO for a correct interpretation of the experiment's results.

We focused on the calculation of the hadronic contributions to the cross section at NNLO, which does not appear in the literature. These $\mathcal{O}(\alpha^4)$ terms are related to hadronic vacuum polarization (HVP) insertions in diagrams contributing to the amplitude at NLO and NNLO. We identified four classes of contributions. Those from Class I arise from products of diagrams involving two vacuum polarization (VP) insertions (only hadronic or hadronic and leptonic), while Class II contributions involve one-loop QED diagrams with one HVP insertion in the t-channel photon. The contributions from these two classes were calculated using the factorization property of the VP function, and were expressed in terms of the QED corrections to the cross section at NLO, which were obtained in Ch. 2. The bremsstrahlung contributions of Class III were analyzed in the soft-photon limit and were employed in the proof of the cancellation of IR divergences for the entire set of these hadronic contributions. Finally, the most challenging terms were the irreducible two-loop diagrams of Class IV, arising from one-loop QED vertex and box diagrams with a HVP insertion appearing inside the loop. These contributions were evaluated using the dispersive approach presented in Ch. 3.

The results of this thesis will be implemented in a Monte Carlo code and will be essential for the interpretation of the future results of the MUonE experiment.

Appendix A

Conventions and Useful Formulas

A.1 Relevant Feynman Rules

External Lines

$$\text{Incoming lepton}: u(p) \qquad \xrightarrow{\quad p \quad} \bullet \qquad\qquad \text{Outgoing lepton}: \bar{u}(p) \qquad \bullet \xrightarrow{\quad p \quad} \qquad (A.1)$$

$$\text{Incoming photon}: \varepsilon_\alpha(k) \qquad \xrightarrow{\quad k \quad} \alpha \qquad\qquad \text{Outgoing photon}: \varepsilon_\alpha^*(k) \qquad \alpha \xrightarrow{\quad k \quad} \qquad (A.2)$$

Propagators

Feynman gauge is assumed. The $i\varepsilon$ prescription is omitted.

$$
\begin{aligned}
\text{Photon}: \quad & \mu \xrightarrow{\quad k \quad} \nu \;=\; \frac{-ig_{\mu\nu}}{k^2} \\[2mm]
\text{Fermion}: \quad & \xrightarrow{\quad p \quad} \;=\; \frac{i(\not{p}+m)}{p^2-m^2} \\[2mm]
\text{Massive Vector Boson}: \quad & \mu \xrightarrow{\quad k \quad} \nu \;=\; \frac{i\left(-g_{\mu\nu}+\frac{k_\mu k_\nu}{m^2}\right)}{k^2-m^2} \\[2mm]
\text{Scalar}: \quad & \xrightarrow{\quad p \quad} \;=\; \frac{i}{p^2-m^2}
\end{aligned}
\qquad (A.3)
$$

Vertices

$$= -ie\gamma^\mu$$

$$= \frac{-ig\gamma^\mu}{2\cos\theta_W}(g_V - g_A\gamma^5) \tag{A.4}$$

$$= \frac{-im_f}{v^2}$$

Counterterms

$$= -i\delta_3 k^2 g^{\mu\nu}$$

$$= -ie\delta_1\gamma^\mu \tag{A.5}$$

A.2 Dirac Algebra

$$\{\gamma^\mu, \gamma^\nu\} = 2g^{\mu\nu} \tag{A.6}$$

$$\gamma^5 = i\gamma^0\gamma^1\gamma^2\gamma^3 \tag{A.7}$$

with

$$\{\gamma^\mu, \gamma^5\} = 0, \qquad \left(\gamma^5\right)^2 = \mathbf{1}, \qquad \gamma^{5\dagger} = \gamma^5 \tag{A.8}$$

and

$$\sigma^{\mu\nu} = \frac{i}{2}\left[\gamma^\mu, \gamma^\nu\right] \tag{A.9}$$

Traces

$$\mathrm{Tr}\left[\gamma^\mu\gamma^\nu\right] = 4g^{\mu\nu}$$
$$\mathrm{Tr}\left[\gamma^\mu\gamma^\nu\gamma^\rho\gamma^\sigma\right] = 4\left(g^{\mu\nu}g^{\rho\sigma} - g^{\mu\rho}g^{\nu\sigma} + g^{\mu\sigma}g^{\nu\rho}\right)$$
$$\mathrm{Tr}\left[\text{odd numer of }\gamma\text{'s}\right] = 0$$
$$\mathrm{Tr}\left[\gamma^5\right] = 0$$
$$\mathrm{Tr}\left[\gamma^\mu\gamma^5\right] = 0$$
$$\mathrm{Tr}\left[\gamma^\mu\gamma^\nu\gamma^5\right] = 0$$
$$\mathrm{Tr}\left[\gamma^\mu\gamma^\nu\gamma^\rho\gamma^5\right] = 0$$
$$\mathrm{Tr}\left[\gamma^\mu\gamma^\nu\gamma^\rho\gamma^\sigma\gamma^5\right] = -4i\varepsilon^{\mu\nu\rho\sigma}$$

$$\tag{A.10}$$

Contraction Identities in D-dimensions

$$g^{\mu\nu}g_{\mu\nu} = D$$
$$\gamma^\mu\gamma_\mu = D$$
$$\gamma^\mu\gamma^\nu\gamma_\mu = (2-D)\gamma^\nu \tag{A.11}$$
$$\gamma^\mu\gamma^\nu\gamma^\rho\gamma_\mu = 4g^{\nu\rho} + (D-4)\gamma^\nu\gamma^\rho$$
$$\gamma^\mu\gamma^\nu\gamma^\rho\gamma^\sigma\gamma_\mu = -2\gamma^\sigma\gamma^\rho\gamma^\nu + (4-D)\gamma^\nu\gamma^\rho\gamma^\sigma$$

Dirac Equation in Momentum Space

$$(\not{p} - m)u(p) = 0 \qquad\qquad \bar{u}(p)(\not{p} - m) = 0 \tag{A.12}$$
$$(\not{p} + m)v(p) = 0 \qquad\qquad \bar{v}(p)(\not{p} + m) = 0 \tag{A.13}$$

A.3 Standard Results for Loop Integrals

Feynman Parametrization

$$\frac{1}{a_1 a_2 \ldots a_n} = \Gamma(n) \int_0^1 dx_1 \int_0^{1-x_1} dx_2 \ldots$$
$$\cdots \int_0^{1-x_1-\cdots-x_{n-1}} dx_{n-1} \frac{1}{[a_1 x_1 + a_2 x_2 + \cdots + a_n(1-x_1-\cdots-x_{n-1})]^n} \tag{A.14}$$

Relevant Integrals in D-dimensions

$$\int \frac{d^D k}{(2\pi)^D} \frac{1}{(k^2 - \Delta)} = \frac{(-1)^n i}{(4\pi)^{\frac{D}{2}}} \frac{\Gamma(n - \frac{D}{2})}{\Gamma(n)} \left(\frac{1}{\Delta}\right)^{n-\frac{D}{2}}$$
$$\int \frac{d^D k}{(2\pi)^D} \frac{k^2}{(k^2 - \Delta)} = \frac{(-1)^{n-1} i}{(4\pi)^{\frac{D}{2}}} \frac{D}{2} \frac{\Gamma(n - \frac{D}{2} - 1)}{\Gamma(n)} \left(\frac{1}{\Delta}\right)^{n-\frac{D}{2}-1} \tag{A.15}$$
$$\int \frac{d^D k}{(2\pi)^D} \frac{k^\mu k^\nu}{(k^2 - \Delta)} = \frac{(-1)^{n-1} i}{(4\pi)^{\frac{D}{2}}} \frac{g^{\mu\nu}}{2} \frac{\Gamma(n - \frac{D}{2} - 1)}{\Gamma(n)} \left(\frac{1}{\Delta}\right)^{n-\frac{D}{2}-1}$$

where, for $\varepsilon \to 0$,

$$\Gamma(\varepsilon) = \frac{1}{\varepsilon} - \gamma_E + \mathcal{O}(\varepsilon) \tag{A.16}$$

with γ_E the Euler-Mascheroni constant.

Dilogarithms

Dilogarithms or *Spence functions* are defined by the following equation

$$\text{Li}_2(z) = \int_z^0 dt \frac{\log(1-t)}{t} \tag{A.17}$$

and if the logarithm is defined with a cut along the negative real axis, the dilogarithm presents a cut for $z > 1$, with z real. Useful results are

$$\text{Li}_2(1) = \frac{\pi^2}{6}$$
$$\text{Li}_2(z) = \text{Li}_2(1-z) + \frac{\pi^2}{6} - \log(z)\log(1-z) \tag{A.18}$$
$$\text{Li}_2(z) = -\text{Li}_2\left(\frac{1}{z}\right) - \frac{\pi^2}{6} - \frac{1}{2}\log^2(-z)$$

see e.g. Lewin [115]

Appendix B

Scalar Integrals

Passarino-Veltman Decomposition

We give here a brief introduction to the technique of PV decomposition [116] for one-loop integrals, following the conventions used in [102,117]. For a broader presentation we also refer the reader to [106].

Assuming dimensional regularization $D = 4 - \varepsilon$, a generic one-loop tensor integral is defined as

$$T_n^{\mu_1\cdots\mu_p} = \frac{(2\pi\mu)^{4-D}}{i\pi^2} \int d^D k \, \frac{k^{\mu_1}\cdots k^{\mu_p}}{D_0 D_1 D_2 \cdots D_{n-1}} \tag{B.1}$$

where a denominator D_i is given (omitting the $i\varepsilon$ prescription) by

$$D_i = (k + r_i)^2 - m_i^2 \tag{B.2}$$

and if p_i are the external momenta entering in the loop, then

$$\begin{aligned}
r_j &= \sum_{i=1}^{j} p_i \qquad (j = 1, \ldots, n-1) \\
r_0 &= \sum_{i=1}^{n} p_i = 0 \;.
\end{aligned} \tag{B.3}$$

Exploiting the Lorentz covariance of the tensor integrals, these can be written as a linear combination of the external momenta and the metric tensor $g^{\mu\nu}$ using a set of coefficient functions. Moreover, it is shown that all the tensor integrals can be decomposed in terms of only four independent scalar integrals with one, two, three or four denominators, denoted as

$$\begin{aligned}
A_0(m_0^2) &= \frac{(2\pi\mu)^\varepsilon}{i\pi^2} \int d^D k \, \frac{1}{k^2 - m_0^2} \\
B_0(r_{10}^2, m_0^2, m_1^2) &= \frac{(2\pi\mu)^\varepsilon}{i\pi^2} \int d^D k \, \prod_{i=0}^{1} \frac{1}{[(k+r_i)^2 - m_i^2]} \\
C_0(r_{10}^2, r_{12}^2, r_{20}^2, m_0^2, m_1^2, m_2^2) &= \frac{(2\pi\mu)^\varepsilon}{i\pi^2} \int d^D k \, \prod_{i=0}^{2} \frac{1}{[(k+r_i)^2 - m_i^2]} \\
D_0(r_{10}^2, r_{12}^2, r_{23}^2, r_{30}^2, r_{20}^2, r_{13}^2, m_0^2, m_1^2, m_2^2, m_3^2) &= \frac{(2\pi\mu)^\varepsilon}{i\pi^2} \int d^D k \, \prod_{i=0}^{3} \frac{1}{[(k+r_i)^2 - m_i^2]}
\end{aligned} \tag{B.4}$$

where

$$r_{ij}^2 = (r_i - r_j)^2 \qquad \forall i, j = (0, n-1) \;. \tag{B.5}$$

The scalar integrals of Eq.(B.4) have been classified and computed by 't Hooft and Veltman [110]. The expression for some of the simplest PV scalar functions appearing in our calculations are listed below, where $\Delta_\varepsilon = 2/\varepsilon - \gamma_E + \log(4\pi)$.

Explicit expressions for scalar PV functions

Function A_0

$$A_0(m^2) = m^2 \left(\Delta_\varepsilon + 1 - \log\left(\frac{m^2}{\mu^2}\right) \right)$$

Function B_0

$$B_0(q^2, m^2, m^2) = \Delta_\varepsilon - \log\left(\frac{m^2}{\mu^2}\right) + 2 - \sqrt{1 - \frac{4m^2}{q^2}} \log\left(\frac{\sqrt{1 - \frac{4m^2}{q^2}} + 1}{\sqrt{1 - \frac{4m^2}{q^2}} - 1} \right) \qquad (q^2 < 0)$$

$$B_0(0, m_0^2, m_1^2) = \Delta_\varepsilon + 1 - \frac{m_0^2 \log(m_0^2) - m_1^2 \log(m_1^2)}{m_0^2 - m_1^2}$$

$$B_0(0, m^2, m^2) = \Delta_\varepsilon - \log\left(\frac{m^2}{\mu^2}\right)$$

$$B_0(m^2, 0, m^2) = B_0(0, m^2, m^2) + 2 \ .$$

(B.6)

The relation

$$B_0(0, 0, m^2) = \Delta_\varepsilon + 1 - \log\left(\frac{m^2}{\mu^2}\right) = \frac{A_0(m^2)}{m^2}$$

(B.7)

allows us to avoid using A_0 functions in our results.

Function C_0

One important case is $C_0(0, m^2, m^2, m^2, m^2, \lambda^2)$, which is divergent in the IR limit $\lambda \to 0$

$$C_0(0, m^2, m^2, m^2, m^2, \lambda^2) = \frac{1}{2m^2} \log\left(\frac{\lambda^2}{m^2}\right)$$

(B.8)

Soft Bremsstrahlung Scalar Integrals

Another kind of integrals involved in the calculation of the muon-electron scattering cross section are the bremsstrahlung integrals defined in [110] and in Eq.(2.86)

$$\mathcal{I}(p_i, p_j) = \int' \frac{d^3k}{k_0} \frac{1}{(p_i \cdot k)(p_j \cdot k)}$$

(B.9)

where p_i, p_j are the external momenta of the particles emitting the soft photon and k is the photon momentum, with $\lambda < k_0 < \omega$. The external momenta can be redefined as $p = \rho p_i$ and $q = p_j$, where ρ is chosen to satisfy $(p - q)^2 = 0$ and such that $p_0 - q_0$ has the same sign of q_0. Thanks to this redefinition the calculation is simplified but is still rather lengthy, therefore we only quote the result

$$\mathcal{I}(p_i, p_j) = -\frac{2\pi\rho}{vl} \left[\frac{1}{2} \log\left(\frac{p^2}{q^2}\right) \log\left(\frac{4\omega^2}{\lambda^2}\right) \right.$$
$$\left. + \left\{ \frac{1}{4} \log^2\left(\frac{u_0 - |\mathbf{u}|}{u_0 + |\mathbf{u}|}\right) + \mathrm{Li}_2\left(\frac{v + u_0 + |\mathbf{u}|}{v}\right) + \mathrm{Li}_2\left(\frac{v + u_0 - |\mathbf{u}|}{v}\right) \right\}_{u=q}^{u=p} \right]$$

(B.10)

with

$$l = p_0 - q_0 \qquad\qquad v = (p^2 - q^2)/2l \qquad\qquad \lambda \to 0 \ .$$

Note that the integral is IR divergent. The case $p_i = p_j = p$ is simpler to calculate and one finds

$$\mathcal{I}(p, p) = \frac{2\pi}{m^2} \left[\log\left(\frac{4\omega^2}{\lambda^2}\right) + \frac{1}{\beta} \log\left(\frac{1 - \beta}{1 + \beta}\right) \right]$$

(B.11)

where $p^2 = m^2$, $\beta = |\mathbf{p}|/p_0$ and the limit $\lambda \to 0$ has been taken.

Appendix C

Detailed Results for the NLO Cross Section

The virtual radiative corrections to the $\mu^- e^-$ elastic scattering at NLO can be expressed as

$$\frac{d\sigma_1}{dt} = \frac{1}{16\pi} \frac{1}{\lambda(s, m_\mu^2, m_e^2)} \mathcal{X}_1 \tag{C.1}$$

where $\mathcal{X}_1$ includes the corrections

$$\mathcal{X}_1 = \mathcal{X}_1^{\mathrm{VP}} + \mathcal{X}_1^{\mathrm{VC}\mu} + \mathcal{X}_1^{\mathrm{VC}e} + \mathcal{X}_1^{\mathrm{BD}} + \mathcal{X}_1^{\mathrm{BC}} \tag{C.2}$$

Vacuum Polarization

$$\mathcal{X}_1^{\mathrm{VP}} = \mathcal{X}_0 \left\{ -2 \sum_l \frac{\alpha}{3\pi} \left[-\frac{1}{3} + \left(1 + \frac{2m_l^2}{t} \right) \left(\bar{B}_0(t, m_l^2, m_l^2) - \bar{B}_0(0, m_l^2, m_l^2) \right) \right] \right\} \tag{C.3}$$

with l running over $\{e, \mu, \tau\}$.

Muon Vertex Correction

$$\mathcal{X}_1^{\mathrm{VC}\mu} = \frac{16\pi\alpha^3}{t^2} \left\{ a_0 + a_1 \bar{B}_0(0, m_\mu^2, m_\mu^2) + a_2 \bar{B}_0(t, m_\mu^2, m_\mu^2) \right.$$
$$\left. + a_3 \log(m_\mu) + a_4 \log(\lambda) + a_5 C_0(t, m_\mu^2, m_\mu^2, m_\mu^2, m_\mu^2, \lambda^2) \right\} \tag{C.4}$$

with

$$a_0 = -\frac{2t}{4m_\mu^2 - t} \left[2m_e^4 + 2m_\mu^4 + 2s^2 - 4m_e^2(m_\mu^2 + s) + 2st + t^2 - 4m_\mu^2(s + t) \right]$$

$$a_1 = \frac{4}{4m_\mu^2 - t} \left[6m_\mu^2(m_e^2 + m_\mu^2 - s)^2 - 2\left(m_e^4 + m_\mu^4 + m_e^2(m_\mu^2 - 2s) - 5m_\mu^2 s + s^2\right)t + 2(2m_\mu^2 - s)t^2 - t^3 \right]$$

$$a_2 = -\frac{1}{4m_\mu^2 - t} \left[16m_\mu^2(m_e^2 + m_\mu^2 - s)^2 - 2\left(3m_e^4 + 3m_\mu^4 + 2m_e^2(m_\mu^2 - 3s) - 14m_\mu^2 s + 3s^2\right)t \right.$$
$$\left. + 6(2m_\mu^2 - s)t^2 - 3t^3 \right]$$

$$a_3 = 6\left[2(m_e^2 + m_\mu^2 - s)^2 + 2st + t^2 \right]$$

$$a_4 = -4\left[2(m_e^2 + m_\mu^2 - s)^2 + 2st + t^2 \right]$$

$$a_5 = 2(2m_\mu^2 - t)\left(2(m_e^2 + m_\mu^2 - s)^2 + 2st + t^2 \right)$$

Electron Vertex Correction

$$\mathcal{X}_1^{\text{VC}_e} = \frac{16\pi\alpha^3}{t^2}\left\{ b_0 + b_1\bar{B}_0(0, m_e^2, m_e^2) + b_2\bar{B}_0(t, m_e^2, m_e^2) \right.$$

$$\left. + b_3\log(m_e) + b_4\log(\lambda) + b_5 C_0(t, m_e^2, m_e^2, m_e^2, m_e^2, \lambda^2) \right\} \quad \text{(C.5)}$$

with

$$b_0 = -\frac{2t}{4m_e^2 - t}\left[2m_e^4 + 2(m_\mu^2 - s)^2 + 2st + t^2 - 4m_e^2(m_\mu^2 + s + t) \right]$$

$$b_1 = \frac{4}{4m_e^2 - t}\left[6m_e^2(m_e^2 + m_\mu^2 - s)^2 - 2\big(m_e^4 + m_e^2(m_\mu^2 - 5s) + (m_\mu^2 - s)^2\big)t + 2(2m_e^2 - s)t^2 - t^3 \right]$$

$$b_2 = -\frac{1}{4m_e^2 - t}\left[16m_e^2(m_e^2 + m_\mu^2 - s)^2 - 2\big(3m_e^4 + 2m_e^2(m_\mu^2 - 7s) + 3(m_\mu^2 - s)^2\big)t \right.$$

$$\left. + 6(2m_e^2 - s)t^2 - 3t^3 \right]$$

$$b_3 = 6\left[2(m_e^2 + m_\mu^2 - s)^2 + 2st + t^2 \right]$$

$$b_4 = -4\left[2(m_e^2 + m_\mu^2 - s)^2 + 2st + t^2 \right]$$

$$b_5 = 2(2m_e^2 - t)\big(2(m_e^2 + m_\mu^2 - s)^2 + 2st + t^2 \big)$$

Direct Box

$$\mathcal{X}_1^{\mathrm{BD}} = \frac{16\pi\alpha^3}{t}\mathrm{Re}\bigg\{ c_0 + c_1\bar{B}_0(0, m_e^2, m_e^2) + c_2\bar{B}_0(0, m_\mu^2, m_\mu^2) + c_3\bar{B}_0(s, m_e^2, m_\mu^2) + c_4\bar{B}_0(t, 0, 0)$$

$$+ c_5 C_0(m_e^2, m_e^2, t, \lambda^2, m_e^2, \lambda^2) + c_6 C_0(m_\mu^2, m_\mu^2, t, \lambda^2, m_\mu^2, \lambda^2) + c_7 C_0(m_e^2, m_\mu^2, s, m_e^2, \lambda^2, m_\mu^2) \quad \text{(C.6)}$$

$$+ c_8 D_0(m_\mu^2, m_e^2, m_e^2, m_\mu^2, s, t, m_\mu^2, \lambda^2, m_e^2, \lambda^2)\bigg\}$$

with

$$c_0 = \frac{8}{(4m_e^2 - t)(4m_\mu^2 - t)\big((m_e - m_\mu)^2 - s\big)\big((m_e + m_\mu)^2 - s\big)}\bigg[-t^2\big(m_e^2 + m_\mu^2\big)\big(-2s\big(m_e^2 + m_\mu^2\big) + 3\big(m_e^2 - m_\mu^2\big)^2 - s^2\big)$$

$$+ t^3\big(\big(m_e^2 - m_\mu^2\big)^2 - s\big(m_e^2 + m_\mu^2\big)\big) + 16m_e^2 m_\mu^2\big((m_e - m_\mu)^2 - s\big)\big(m_e^2 + m_\mu^2 - s\big)\big((m_e + m_\mu)^2 - s\big)$$

$$+ 2t\Big(s^3\big(m_e^2 + m_\mu^2\big) - s^2\big(3m_e^2 + m_\mu^2\big)\big(m_e^2 + 3m_\mu^2\big) - \big(m_e^2 - m_\mu^2\big)^4 + s\big(m_e^2 + m_\mu^2\big)\big(3m_e^4 + 2m_e^2 m_\mu^2 + 3m_\mu^4\big)\Big)\bigg]$$

$$c_1 = \frac{4m_e^2}{(4m_e^2 - t)\big((m_e - m_\mu)^2 - s\big)\big((m_e + m_\mu)^2 - s\big)}\bigg[t^2\big(-m_e^2 + m_\mu^2 + s\big)$$

$$+ 2\big((m_e - m_\mu)^2 - s\big)\big(m_e^2 + m_\mu^2 - s\big)\big((m_e + m_\mu)^2 - s\big) + t\big(3m_e^4 - 2m_e^2(m_\mu^2 + s) - (m_\mu^2 - s)^2\big)\bigg]$$

$$c_2 = \frac{4m_\mu^2}{(4m_\mu^2 - t)\big((m_e - m_\mu)^2 - s\big)\big((m_e + m_\mu)^2 - s\big)}\bigg[t^2\big(m_e^2 - m_\mu^2 + s\big)$$

$$+ 2\big((m_e - m_\mu)^2 - s\big)\big(m_e^2 + m_\mu^2 - s\big)\big((m_e + m_\mu)^2 - s\big) - t\big(m_e^4 + 2m_e^2(m_\mu^2 - s) - 3m_\mu^4 + 2m_\mu^2 s + s^2\big)\bigg]$$

$$c_3 = -\frac{2\big[m_e^6 + m_e^4\big(-m_\mu^2 - 3s + t\big) - m_e^2\big(m_\mu^4 + 2m_\mu^2(s + t) - 3s^2\big) + t\big(m_\mu^4 - s^2\big) + \big(m_\mu^2 - s\big)^3\big]}{\big((m_e - m_\mu)^2 - s\big)\big((m_e + m_\mu)^2 - s\big)}$$

$$c_4 = \frac{2\big[t^2\big(s - 3\big(m_e^2 + m_\mu^2\big)\big) + 16m_e^2 m_\mu^2\big(m_e^2 + m_\mu^2 - s\big) + t^3\big]}{\big(t - 4m_e^2\big)\big(4m_\mu^2 - t\big)}$$

$$c_5 = -\frac{4m_e^4\big(4m_\mu^2 - 4s + t\big) + 2m_e^2\big(8\big(m_\mu^2 - s\big)^2 + 4st + t^2\big) + t\big(-4\big(m_\mu^2 - s\big)^2 - 2st - t^2\big)}{4m_e^2 - t}$$

$$c_6 = -\frac{16m_\mu^2\big(m_e^2 - s\big)\big(m_e^2 + m_\mu^2 - s\big) - 4t\big(m_e^4 - 2s\big(m_e^2 + m_\mu^2\big) - m_\mu^4 + s^2\big) + 2t^2\big(m_\mu^2 - s\big) - t^3}{4m_\mu^2 - t}$$

$$c_7 = -2(2s + t)\big(m_e^2 + m_\mu^2 - s\big)$$

$$c_8 = -\big(m_e^2 + m_\mu^2 - s\big)\big(4\big(m_e^2 + m_\mu^2 - s\big)^2 + 2st + t^2\big)$$

Crossed Box

$$\mathcal{X}_1^{\mathrm{BC}} = \frac{16\pi\alpha^3}{t}\mathrm{Re}\Big\{ d_0 + d_1\bar{B}_0(0, m_e^2, m_e^2) + d_2\bar{B}_0(0, m_\mu^2, m_\mu^2) + d_3\bar{B}_0(u, m_e^2, m_\mu^2) + d_4\bar{B}_0(t, 0, 0)$$

$$+ d_5 C_0(m_e^2, m_e^2, t, \lambda^2, m_e^2, \lambda^2) + d_6 C_0(m_\mu^2, m_\mu^2, t, \lambda^2, m_\mu^2, \lambda^2) + d_7 C_0(m_e^2, m_\mu^2, u, m_e^2, \lambda^2, m_\mu^2) \quad (C.7)$$

$$+ d_8 D_0(m_\mu^2, m_e^2, m_e^2, m_\mu^2, u, t, m_\mu^2, \lambda^2, m_e^2, \lambda^2) \Big\}$$

with

$$d_0 = -\frac{8}{\left(4m_e^2 - t\right)\left(t - 4m_\mu^2\right)\left((m_e - m_\mu)^2 - s - t\right)\left((m_e + m_\mu)^2 - s - t\right)}$$

$$\Big[t^3\big(3s(m_e^2 + m_\mu^2) + (m_e^2 - m_\mu^2)^2\big) + 16m_e^2 m_\mu^2\big((m_e - m_\mu)^2 - s\big)\big(m_e^2 + m_\mu^2 - s\big)\big((m_e + m_\mu)^2 - s\big)$$

$$+ t^2\big(5s^2(m_e^2 + m_\mu^2) + (m_e^2 + m_\mu^2)(m_e^2 - m_\mu^2)^2$$

$$- 2s(3m_e^4 + 22m_e^2 m_\mu^2 + 3m_\mu^4)\big) - 2t\big(m_e^8 + 3m_e^6(4m_\mu^2 - s)$$

$$+ m_e^4(-26m_\mu^4 - 37m_\mu^2 s + 3s^2) + m_e^2(m_\mu^2 - s)(12m_\mu^4 - 25m_\mu^2 s + s^2) + m_\mu^2(m_\mu^2 - s)^3\big)\Big]$$

$$d_1 = \frac{4m_e^2}{\left(4m_e^2 - t\right)\left((m_e - m_\mu)^2 - s - t\right)\left((m_e + m_\mu)^2 - s - t\right)}\Big[t^2\big(-m_e^2 + m_\mu^2 - 3s\big)$$

$$+ 2\big((m_e - m_\mu)^2 - s\big)\big(m_e^2 + m_\mu^2 - s\big)\big((m_e + m_\mu)^2 - s\big) - t\big(m_e^4 - 6m_e^2(m_\mu^2 + s) + 5(m_\mu^2 - s)^2\big)\Big]$$

$$d_2 = \frac{4m_\mu^2}{\left(4m_\mu^2 - t\right)\left((m_e - m_\mu)^2 - s - t\right)\left((m_e + m_\mu)^2 - s - t\right)}\Big[2m_e^6 - m_e^4\big(2m_\mu^2 + 6s + 5t\big)$$

$$+ m_e^2\big(-2m_\mu^4 + m_\mu^2(6t - 4s) + 6s^2 + 10st + t^2\big) + (m_\mu^2 - s - t)\big(t(m_\mu^2 + 3s) + 2(m_\mu^2 - s)^2\big)\Big]$$

$$d_3 = -\frac{2}{\left((m_e - m_\mu)^2 - s - t\right)\left((m_e + m_\mu)^2 - s - t\right)}\Big[m_e^6 - m_e^4(m_\mu^2 + 3s)$$

$$- m_e^2\big(m_\mu^4 + 2m_\mu^2(s - 4t) - 3s^2 - 2st + t^2\big) - t^2(m_\mu^2 + s) + 2st(m_\mu^2 - s) + (m_\mu^2 - s)^3\Big]$$

$$d_4 = \frac{2\big[16m_e^4 m_\mu^2 + m_e^2\big(16m_\mu^4 - 16m_\mu^2(s + t) + t^2\big) + t^2(m_\mu^2 + s)\big]}{\left(t - 4m_e^2\right)\left(4m_\mu^2 - t\right)}$$

$$d_5 = \frac{1}{4m_e^2 - t}\Big[2t^2\big(11m_e^2 + 2m_\mu^2 - 3s\big) + 16m_e^2\big(m_e^2 + m_\mu^2 - s\big)\big(2m_e^2 + m_\mu^2 - s\big)$$

$$- 4t\big(11m_e^4 + 2m_e^2(4m_\mu^2 - 5s) + (m_\mu^2 - s)^2\big) - 3t^3\Big]$$

$$d_6 = \frac{1}{4m_\mu^2 - t}\Big[2t^2\big(2m_e^2 + 11m_\mu^2 - 3s\big) + 16m_\mu^2\big(m_e^2 + m_\mu^2 - s\big)\big(m_e^2 + 2m_\mu^2 - s\big)$$

$$- 4t\big(m_e^4 - 2s(m_e^2 + 5m_\mu^2) + 8m_e^2 m_\mu^2 + 11m_\mu^4 + s^2\big) - 3t^3\Big]$$

$$d_7 = -2\big(4m_e^2 + 4m_\mu^2 - 2s - t\big)\big(m_e^2 + m_\mu^2 - s - t\big)$$

$$d_8 = -\big(m_e^2 + m_\mu^2 - s - t\big)\big(4(m_e^2 + m_\mu^2 - s)^2 - 4t(m_e^2 + m_\mu^2) + 6st + 3t^2\big)$$

Appendix D

Detailed Results for Class IV at NNLO

Muonic Vertex Correction

$$
\mathcal{X}_1^{\mathrm{VC}_\mu}(t,z) = \frac{16\pi\alpha^3}{m_\mu^2 t^2 z \left(t - 4m_\mu^2\right)^2} \Bigg\{ e_0 + e_1 \bar{B}_0(0,z,z) + e_2 \bar{B}_0(t, m_\mu^2, m_\mu^2) + e_3 \bar{B}_0(0, m_\mu^2, m_\mu^2)
$$
$$
+ e_4 \bar{B}_0(m_\mu^2, m_\mu^2, z) + e_5 C_0(0, m_\mu^2, m_\mu^2, m_\mu^2, m_\mu^2, z) \tag{D.1}
$$
$$
+ e_6 C_0(m_\mu^2, m_\mu^2, t, m_\mu^2, z, m_\mu^2) \Bigg\}
$$

with

$$
e_0 = t \left(4m_\mu^2 - t\right)\left(2m_\mu^2 - z\right)\left(2m_e^4 - 4m_e^2\left(m_\mu^2 + s\right) + 2m_\mu^4 - 4m_\mu^2(s+t) + 2s^2 + 2st + t^2\right)
$$

$$
e_1 = -tz\left(4m_\mu^2 - t\right)\left(2m_e^4 - 4m_e^2\left(m_\mu^2 + s\right) + 2m_\mu^4 - 4m_\mu^2(s+t) + 2s^2 + 2st + t^2\right)
$$

$$
e_2 = -m_\mu^2 \Big[m_e^4\left(64m_\mu^4 + 8m_\mu^2(4z - 5t) + 2t(3t + 2z)\right) + 4m_e^2\big(32m_\mu^6 - 4m_\mu^4(8s + 3t - 4z)
$$
$$
+ m_\mu^2(t(20s + t) - 2z(8s + 5t)) - st(3t + 2z)\big) + \left(4m_\mu^2 - t\right)\big(16m_\mu^6 - 2m_\mu^4(16s + 3t)
$$
$$
+ 4m_\mu^2(s+t)(4s+3t) - 3t\left(2s^2 + 2st + t^2\right)\big) + 2z\Big(16\left(m_\mu^3 - m_\mu s\right)^2 + 2t^2\left(s - 2m_\mu^2\right)
$$
$$
+ 2t\left(m_\mu^4 + 6m_\mu^2 s + s^2\right) + t^3\Big) \Big]
$$

$$
e_3 = \left(4m_\mu^2 - t\right)\Big[z\left(4m_\mu^2 - t\right)\left(2\left(m_e^2 + m_\mu^2 - s\right)^2 + 2st + t^2\right) + m_\mu^2\Big(16m_\mu^2\left(m_e^2 + m_\mu^2 - s\right)^2
$$
$$
- 2t\left(m_e^4 - 2s\left(m_e^2 + 5m_\mu^2\right) + 6m_e^2 m_\mu^2 + m_\mu^4 + s^2\right) + 2t^2\left(2m_\mu^2 - s\right) - t^3\Big)\Big]
$$

$$
e_4 = 2t\Big[2m_e^4\left(-4m_\mu^4 + m_\mu^2(t + 7z) - tz\right) + 4m_e^2\left(4m_\mu^6 + m_\mu^4(4s - t - 3z) - m_\mu^2 s(t + 7z) + stz\right)
$$
$$
- m_\mu^2\left(4m_\mu^2 - t\right)\left(2m_\mu^4 - 4m_\mu^2(s+t) + 2s^2 + 2st + t^2\right) + z\Big(14\left(m_\mu^3 - m_\mu s\right)^2 + t^2\left(9m_\mu^2 - 2s\right)
$$
$$
- 2t\left(11m_\mu^4 - 9m_\mu^2 s + s^2\right) - t^3\Big)\Big]
$$

$$
e_5 = -\left(t - 4m_\mu^2\right)^2\left(2m_\mu^2 - z\right)\left(2m_\mu^2 + z\right)\left(2\left(m_e^2 + m_\mu^2 - s\right)^2 + 2st + t^2\right)
$$

$$
e_6 = 2m_\mu^2\Big[\left(2m_\mu^2 - t\right)\left(t - 4m_\mu^2\right)^2\left(2\left(m_e^2 + m_\mu^2 - s\right)^2 + 2st + t^2\right)
$$
$$
+ 2tz\left(4m_\mu^2 - t\right)\left(2m_e^4 - 4m_e^2\left(m_\mu^2 + s\right) + 2m_\mu^4 - 4m_\mu^2(s+t) + 2s^2 + 2st + t^2\right)
$$
$$
- z^2\Big(16m_\mu^2\left(m_e^2 + m_\mu^2 - s\right)^2 + 2t\left(m_e^4 - 2m_e^2\left(5m_\mu^2 + s\right) + m_\mu^4 + 6m_\mu^2 s + s^2\right) + 2t^2\left(s - 2m_\mu^2\right) + t^3\Big)\Big]
$$

Electronic Vertex Correction

$$
\mathcal{X}_1^{\mathrm{VC}_e}(t,z) = \frac{16\pi\alpha^3}{m_e^2 t^2 z \,(t-4m_e^2)^2}\Big\{ f_0 + f_1 \bar{B}_0(0,z,z) + f_2 \bar{B}_0(t,m_e^2,m_e^2) + f_3 \bar{B}_0(0,m_e^2,m_e^2)
$$
$$
+ f_4 \bar{B}_0(m_e^2,m_e^2,z) + f_5 C_0(0,m_e^2,m_e^2,m_e^2,m_e^2,z) \tag{D.2}
$$
$$
+ f_6 C_0(m_e^2,m_e^2,t,m_e^2,z,m_e^2)\Big\}
$$

with

$$
f_0 = t\left(4m_e^2 - t\right)\left(2m_e^2 - z\right)\left(2m_e^4 - 4m_e^2\left(m_\mu^2 + s + t\right) + 2\left(m_\mu^2 - s\right)^2 + 2st + t^2\right)
$$

$$
f_1 = -tz\left(4m_e^2 - t\right)\left(2m_e^4 - 4m_e^2\left(m_\mu^2 + s + t\right) + 2\left(m_\mu^2 - s\right)^2 + 2st + t^2\right)
$$

$$
f_2 = -m_e^2\Big[64m_e^8 + 8m_e^6\left(16m_\mu^2 - 16s - 5t + 4z\right) + 2m_e^4\big(32m_\mu^4 - 8m_\mu^2(8s + 3t - 4z)
$$
$$
+ 32s^2 + 72st - 32sz + 27t^2 + 2tz\big) + 4m_e^2\Big(t\left(t\left(m_\mu^2 - 13s\right) - 10\left(m_\mu^2 - s\right)^2 - 6t^2\right)
$$
$$
- 2z\left(t\left(5m_\mu^2 - 3s\right) - 4\left(m_\mu^2 - s\right)^2 + t^2\right)\Big) + t(3t + 2z)\left(2\left(m_\mu^2 - s\right)^2 + 2st + t^2\right)\Big]
$$

$$
f_3 = \left(4m_e^2 - t\right)\Big[16m_e^8 + m_e^6\left(32m_\mu^2 - 32s - 2t + 8z\right) + 2m_e^4\big(8m_\mu^4 - 2m_\mu^2(8s + 3t - 4z)
$$
$$
- z(8s + t) + 2(s + t)(4s + t)\big) + m_e^2\Big(t\left(-2\left(m_\mu^2 - s\right)^2 - 2st - t^2\right)
$$
$$
+ 4z\left(2m_\mu^4 - m_\mu^2(4s + t) + (s + t)(2s + t)\right)\Big) - tz\left(2\left(m_\mu^2 - s\right)^2 + 2st + t^2\right)\Big]
$$

$$
f_4 = 2t\Big[-8m_e^8 + 2m_e^6\left(8m_\mu^2 + 8s + 9t + 7z\right) - 2m_e^4\big(4m_\mu^4 + 2m_\mu^2(-4s + t + 3z) + 4s^2
$$
$$
+ 6st + 14sz + 4t^2 + 11tz\big) + m_e^2\left(z\left(14\left(m_\mu^2 - s\right)^2 + 18st + 9t^2\right) + t\left(2\left(m_\mu^2 - s\right)^2 + 2st + t^2\right)\right)
$$
$$
- tz\left(2\left(m_\mu^2 - s\right)^2 + 2st + t^2\right)\Big]
$$

$$
f_5 = -\left(t - 4m_e^2\right)^2\left(2m_e^2 - z\right)\left(2m_e^2 + z\right)\left(2\left(m_e^2 + m_\mu^2 - s\right)^2 + 2st + t^2\right)
$$

$$
f_6 = 2m_e^2\Big[\left(2m_e^2 - t\right)\left(t - 4m_e^2\right)^2\left(2\left(m_e^2 + m_\mu^2 - s\right)^2 + 2st + t^2\right)
$$
$$
+ 2tz\left(4m_e^2 - t\right)\left(2m_e^4 - 4m_e^2\left(m_\mu^2 + s + t\right) + 2\left(m_\mu^2 - s\right)^2 + 2st + t^2\right)
$$
$$
- z^2\left(16m_e^2\left(m_e^2 + m_\mu^2 - s\right)^2 + 2t^2\left(s - 2m_e^2\right) + 2t\left(m_\mu^4 + m_e^2\left(6s - 10m_\mu^2\right) + \left(m_\mu^2 - s\right)^2\right) + t^3\right)\Big]
$$

Direct Box (Left and Right)

$$
\mathcal{X}_1^{\mathrm{BDL}}(t,z) + \mathcal{X}_1^{\mathrm{BDR}}(t,z) = \frac{8\pi\alpha^3}{t}\mathrm{Re}\Big\{ g_0 + g_1\bar{B}_0(0,m_e^2,m_e^2) + g_2\bar{B}_0(0,m_\mu^2,m_\mu^2) + g_3\bar{B}_0(m_e^2,m_e^2,z)
$$
$$
+ g_4\bar{B}_0(m_\mu^2,m_\mu^2,z) + g_5\bar{B}_0(s,m_e^2,m_\mu^2) + g_6\bar{B}_0(t,0,z) + g_7 C_0(m_e^2,m_e^2,t,0,m_e^2,z) + g_8 C_0(m_\mu^2,m_\mu^2,t,0,m_\mu^2,z)
$$
$$
+ g_9 C_0(m_e^2,m_\mu^2,s,m_e^2,0,m_\mu^2) + g_{10}C_0(m_e^2,m_\mu^2,s,m_e^2,z,m_\mu^2) + g_{11}D_0(m_e^2,m_e^2,m_\mu^2,m_\mu^2,t,s,z,m_e^2,0,m_\mu^2)\Big\}
$$
$$
\tag{D.3}
$$

with

$$g_0 = \frac{16}{(4m_e^2 - t)(4m_\mu^2 - t)(m_e^2 - 2m_em_\mu + m_\mu^2 - s)(m_e^2 + 2m_em_\mu + m_\mu^2 - s)}\Big[2m_e^8(8m_\mu^2 - t)$$

$$+ m_e^6\left(-16m_\mu^4 + 8m_\mu^2(t - 6s) + 3t(2s - t)\right) + m_e^4\left(-16m_\mu^6 - 4m_\mu^4(8s + 3t) + m_\mu^2\left(48s^2 + 10st + 3t^2\right)\right.$$

$$\left. + t\left(-6s^2 + 2st + t^2\right)\right) + m_e^2\left(16m_\mu^8 + 8m_\mu^6(t - 6s) + m_\mu^4\left(48s^2 + 10st + 3t^2\right)\right.$$

$$\left. - 2m_\mu^2\left(8s^3 + 10s^2t - 2st^2 + t^3\right) + st\left(2s^2 + st - t^2\right)\right) - m_\mu^2 t\left(m_\mu^2 - s\right)\left(2m_\mu^4 + m_\mu^2(3t - 4s) + 2s^2 + st - t^2\right)\Big]$$

$$g_1 = \frac{1}{(4m_e^2 - t)(m_e^2 - 2m_em_\mu + m_\mu^2 - s)(m_e^2 + 2m_em_\mu + m_\mu^2 - s)}\Big[8m_e^2\Big(2m_e^6 + m_e^4\left(-2m_\mu^2 - 6s + 3t\right)$$

$$- m_e^2\left(2m_\mu^4 + 2m_\mu^2(2s + t) - 6s^2 + 2st + t^2\right) + 2m_\mu^6 - m_\mu^4(6s + t) + m_\mu^2\left(6s^2 + 2st + t^2\right)$$

$$+ s\left(-2s^2 - st + t^2\right)\Big)\Big]$$

$$g_2 = \frac{1}{(4m_\mu^2 - t)(m_e^2 - 2m_em_\mu + m_\mu^2 - s)(m_e^2 + 2m_em_\mu + m_\mu^2 - s)}\Big[8m_\mu^2\Big(2m_e^6 - m_e^4\left(2m_\mu^2 + 6s + t\right)$$

$$+ m_e^2\left(-2m_\mu^4 - 2m_\mu^2(2s + t) + 6s^2 + 2st + t^2\right) + \left(m_\mu^2 - s\right)\left(2m_\mu^4 + m_\mu^2(3t - 4s) + 2s^2 + st - t^2\right)\Big)\Big]$$

$$g_3 = g1$$

$$g_4 = g2$$

$$g_5 = -\frac{8\left[m_e^6 + m_e^4\left(-m_\mu^2 - 3s + t\right) - m_e^2\left(m_\mu^4 + 2m_\mu^2(s + t) - 3s^2\right) + \left(m_\mu^2 - s\right)\left(m_\mu^4 + m_\mu^2(t - 2s) + s(s + t)\right)\right]}{\left(m_e^2 - 2m_em_\mu + m_\mu^2 - s\right)\left(m_e^2 + 2m_em_\mu + m_\mu^2 - s\right)}$$

$$g_6 = \frac{8\left[16m_e^4 m_\mu^2 + m_e^2\left(16m_\mu^4 - 16m_\mu^2 s - 3t^2\right) + t^2\left(-3m_\mu^2 + s + t\right)\right]}{\left(4m_e^2 - t\right)\left(t - 4m_\mu^2\right)}$$

$$g_7 = -\frac{4}{4m_e^2 - t}\Big[4m_e^4\left(4m_\mu^2 - 4s + t - z\right) + 2m_e^2\left(8m_\mu^4 - 2m_\mu^2(8s + z) + 8s^2 + 4st + 2sz + t^2 - tz\right)$$

$$- t\left(4m_\mu^4 - 8m_\mu^2 s + 4s^2 + 2st + t^2 - tz\right)\Big]$$

$$g_8 = -\frac{4}{4m_\mu^2 - t}\Big[4m_e^4\left(4m_\mu^2 - t\right) + 4m_e^2\left(4m_\mu^4 - m_\mu^2(8s + z) + 2st\right) - 4m_\mu^4(4s - t + z)$$

$$+ 2m_\mu^2\left(8s^2 + 4st + 2sz + t^2 - tz\right) - t\left(4s^2 + 2st + t^2 - tz\right)\Big]$$

$$g_9 = -4\left(m_e^2 + m_\mu^2 - s\right)(2s + t + z)$$

$$g_{10} = -\frac{1}{\left(m_e^2 - 2m_em_\mu + m_\mu^2 - s\right)\left(m_e^2 + 2m_em_\mu + m_\mu^2 - s\right)}4\Big[m_e^6(2s + t + z)$$

$$- m_e^4\left(m_\mu^2(2s + t + z) + 6s^2 + 3s(t + z) - 2tz\right) - m_e^2\left(m_\mu^4(2s + t + z) + 2m_\mu^2\left(2s^2 + s(t + z) + 2tz\right)\right.$$

$$\left. - s\left(6s^2 + 3s(t + z) - 2tz\right)\right) + \left(m_\mu^2 - s\right)\left(m_\mu^4(2s + t + z) - 2m_\mu^2\left(2s^2 + s(t + z) - tz\right) + s^2(2s + t + z)\right)\Big]$$

$$g_{11} = -4\left(m_e^2 + m_\mu^2 - s\right)\left(4m_e^4 + 8m_e^2\left(m_\mu^2 - s\right) + 4m_\mu^4 - 8m_\mu^2 s + 4s^2 + 2st + 2sz + t^2 + z^2\right)$$

Crossed Box (Left and Right)

$$\mathcal{X}_1^{\text{BCL}}(t, z) + \mathcal{X}_1^{\text{BCR}}(t, z) = \frac{32\pi\alpha^3}{t}\text{Re}\Big\{h_0 + h_1\bar{B}_0(0, m_e^2, m_e^2) + h_2\bar{B}_0(0, m_\mu^2, m_\mu^2) + h_3\bar{B}_0(m_e^2, m_e^2, z)$$

$$+ h_4\bar{B}_0(m_\mu^2, m_\mu^2, z) + h_5\bar{B}_0(u, m_e^2, m_\mu^2) + h_6\bar{B}_0(t, 0, z) + h_7C_0(m_e^2, m_e^2, t, 0, m_e^2, z) + h_8C_0(m_\mu^2, m_\mu^2, t, 0, m_\mu^2, z)$$

$$+ h_9C_0(m_e^2, m_\mu^2, u, m_e^2, 0, m_\mu^2) + h_{10}C_0(m_e^2, m_\mu^2, u, m_e^2, z, m_\mu^2) + h_{11}D_0(m_e^2, m_e^2, m_\mu^2, m_\mu^2, t, u, z, m_e^2, 0, m_\mu^2)\Big\}$$

$$\text{(D.4)}$$

$$h_0 = -\frac{4}{(4m_e^2 - t)(t - 4m_\mu^2)(m_e^2 - 2m_e m_\mu + m_\mu^2 - s - t)(m_e^2 + 2m_e m_\mu + m_\mu^2 - s - t)}\Big[2m_e^8\left(8m_\mu^2 - t\right)$$
$$+ m_e^6\left(-16m_\mu^4 - 24m_\mu^2(2s + t) + t(6s + t)\right) + m_e^4\left(-16m_\mu^6 + m_\mu^4(52t - 32s) + m_\mu^2\left(48s^2 + 74st - t^2\right)\right.$$
$$+ t\left(-6s^2 - 6st + t^2\right)\big) + m_e^2\big(16m_\mu^8 - 24m_\mu^6(2s + t) + m_\mu^4\left(48s^2 + 74st - t^2\right)$$
$$- 2m_\mu^2\left(8s^3 + 26s^2t + 22st^2 + t^3\right) + st\left(2s^2 + 5st + 3t^2\right)\big)$$
$$+ m_\mu^2 t\left(-2m_\mu^6 + m_\mu^4(6s + t) + m_\mu^2\left(-6s^2 - 6st + t^2\right) + s\left(2s^2 + 5st + 3t^2\right)\right)\Big]$$

$$h_1 = \frac{2m_e^2}{(4m_e^2 - t)(m_e^2 - 2m_e m_\mu + m_\mu^2 - s - t)(m_e^2 + 2m_e m_\mu + m_\mu^2 - s - t)}\Big[2m_e^6 - m_e^4\left(2m_\mu^2 + 6s + t\right)$$
$$- m_e^2\left(2m_\mu^4 + m_\mu^2(4s - 6t) - 6s^2 - 6st + t^2\right) + 2m_\mu^6 - m_\mu^4(6s + 5t) + m_\mu^2\left(6s^2 + 10st + t^2\right)$$
$$- s\left(2s^2 + 5st + 3t^2\right)\Big]$$

$$h_2 = \frac{2m_\mu^2}{(4m_\mu^2 - t)(m_e^2 - 2m_e m_\mu + m_\mu^2 - s - t)(m_e^2 + 2m_e m_\mu + m_\mu^2 - s - t)}\Big[2m_e^6 - m_e^4\left(2m_\mu^2 + 6s + 5t\right)$$
$$+ m_e^2\left(-2m_\mu^4 + m_\mu^2(6t - 4s) + 6s^2 + 10st + t^2\right) + 2m_\mu^6 - m_\mu^4(6s + t) + m_\mu^2\left(6s^2 + 6st - t^2\right)$$
$$- s\left(2s^2 + 5st + 3t^2\right)\Big]$$

$$h_3 = h_1$$
$$h_4 = h_2$$

$$h_5 = \frac{2}{(m_e^2 - 2m_e m_\mu + m_\mu^2 - s - t)(m_e^2 + 2m_e m_\mu + m_\mu^2 - s - t)}\Big[-m_e^6 + m_e^4\left(m_\mu^2 + 3s\right)$$
$$+ m_e^2\left(m_\mu^4 + 2m_\mu^2(s - 4t) - 3s^2 - 2st + t^2\right) - m_\mu^6 + 3m_\mu^4 s + m_\mu^2\left(-3s^2 - 2st + t^2\right) + s(s + t)^2\Big]$$

$$h_6 = \frac{2\left(16m_e^4 m_\mu^2 + m_e^2\left(16m_\mu^4 - 16m_\mu^2(s + t) + t^2\right) + t^2\left(m_\mu^2 + s\right)\right)}{(4m_e^2 - t)(t - 4m_\mu^2)}$$

$$h_7 = \frac{1}{4m_e^2 - t}\Big[32m_e^6 + 4m_e^4\left(12m_\mu^2 - 12s - 11t + z\right) + 2m_e^2\left(8m_\mu^4 + 2m_\mu^2(z - 8(s + t)) + 8s^2\right.$$
$$- z(2s + 3t) + 20st + 11t^2\big) + t\left(-4m_\mu^4 + 4m_\mu^2(2s + t) - 4s^2 - 6st + t(z - 3t)\right)\Big]$$

$$h_8 = \frac{1}{4m_\mu^2 - t}\Big[4m_e^4\left(4m_\mu^2 - t\right) + 4m_e^2\left(12m_\mu^4 + m_\mu^2(z - 8(s + t)) + t(2s + t)\right) + 32m_\mu^6$$
$$+ 4m_\mu^4(-12s - 11t + z) + 2m_\mu^2\left(8s^2 + 20st - 2sz + 11t^2 - 3tz\right) + t\left(-4s^2 - 6st + t(z - 3t)\right)\Big]$$

$$h_9 = -\left(m_e^2 + m_\mu^2 - s - t\right)\left(4m_e^2 + 4m_\mu^2 - 2s - t + z\right)$$

$$h_{10} = -\frac{1}{(m_e^2 - 2m_e m_\mu + m_\mu^2 - s - t)(m_e^2 + 2m_e m_\mu + m_\mu^2 - s - t)}\Big[4m_e^8 + m_e^6(-14s - 13t + z)$$
$$- m_e^4\left(8m_\mu^4 + m_\mu^2(18s + 19t + z) - 3\left(6s^2 + 11st + 5t^2\right) + z(3s + t)\right) + m_e^2\Big(-m_\mu^4(18s + 19t + z)$$
$$+ 2m_\mu^2\left(14s^2 + 27st - sz + 13t^2 + 5tz\right) + (s + t)\left(-10s^2 + s(3z - 17t) + t(z - 7t)\right)\Big)$$
$$+ \left(m_\mu^2 - s - t\right)\left(4m_\mu^6 + m_\mu^4(-10s - 9t + z) + 2m_\mu^2\left(4s^2 + 7st - sz + 3t^2\right) + (s + t)^2(-2s - t + z)\right)\Big]$$

$$h_{11} = \left(m_e^2 + m_\mu^2 - s - t\right)\Big((t - z)\left(4m_e^2 + 4m_\mu^2 - 2s - t + z\right)$$
$$- 2\left(2m_e^4 + 4m_e^2\left(m_\mu^2 - s\right) + 2m_\mu^4 - 4m_\mu^2 s + 2s^2 + 2st + t^2\right)\Big)$$

Bibliography

[1] C. M. Carloni Calame, M. Passera, L. Trentadue and G. Venanzoni, *A new approach to evaluate the leading hadronic corrections to the muon g-2*, *Phys. Lett. B* **746** (2015) 325 [1504.02228v2].

[2] G. Abbiendi et al., *Measuring the leading hadronic contribution to the muon $g - 2$ via μe scattering*, *Eur. Phys. J.* **C77** (2017) 139 [1609.08987].

[3] S. A. Goudsmit and G. E. Uhlenbeck, *Ersetzung der hypothese vom unmechanischen zwang durch eine forderung bezüglich des inneren verhaltens jedes einzelnen elektrons*, *Die Naturwissenschaften* **47** (1925) 953.

[4] G. E. Uhlenbeck and S. A. Goudsmit, *Spinning electrons and the structure of spectra*, *Nature* **117** (1926) 264.

[5] P. A. M. Dirac, *The quantum theory of the electron*, *Proc. Roy. Soc. Lond.* **A117** (1928) 610.

[6] P. Kusch and H. M. Foley, *The Magnetic Moment of the Electron*, *Phys. Rev.* **74** (1948) 250.

[7] J. S. Schwinger, *On Quantum electrodynamics and the magnetic moment of the electron*, *Phys. Rev.* **73** (1948) 416.

[8] W. E. Lamb and R. C. Retherford, *Fine structure of the hydrogen atom by a microwave method*, *Phys. Rev.* **72** (1947) 241.

[9] D. Hanneke, S. Fogwell and G. Gabrielse, *New Measurement of the Electron Magnetic Moment and the Fine Structure Constant*, *Phys. Rev. Lett.* **100** (2008) 120801 [0801.1134].

[10] T. Aoyama, M. Hayakawa, T. Kinoshita and M. Nio, *Tenth-Order QED Contribution to the Electron g-2 and an Improved Value of the Fine Structure Constant*, *Phys. Rev. Lett.* **109** (2012) 111807 [1205.5368].

[11] V. B. Berestetskii, O. N. Krokhin and A. K. Khlebnikov, *The radiative correction to the magnetic moment of the μ-meson*, *Zh. Eksp. Teor. Fiz* **30** (1956) 788.

[12] V. B. Berestetskii, O. N. Krokhin and A. K. Khlebnikov, *Concerning the radiative correction to the mu-meson magnetic moment*, *Sov. Phys. JETP* .

[13] W. Cowland, *On Schwinger's theory of the muon*, *Nucl. Phys.* **8** (1958) 397 .

[14] G. F. Giudice, P. Paradisi and M. Passera, *Testing new physics with the electron g-2*, *JHEP* **11** (2012) 113 [1208.6583].

[15] T. D. Lee and C. N. Yang, *Question of Parity Conservation in Weak Interactions*, *Phys. Rev.* **104** (1956) 254.

[16] R. L. Garwin, L. M. Lederman and M. Weinrich, *Observations of the Failure of Conservation of Parity and Charge Conjugation in Meson Decays: The Magnetic Moment of the Free Muon*, *Phys. Rev.* **105** (1957) 1415.

[17] J. I. Friedman and V. L. Telegdi, *Nuclear Emulsion Evidence for Parity Nonconservation in the Decay Chain* $\pi^+ \to \mu^+ \to e^+$, *Phys. Rev.* **106** (1957) 1290.

[18] G. Charpak, P. J. M. Farley, E. L. Garwin, T. Muller, J. C. Sens and A. Zichichi, *The anomalous magnetic moment of the muon*, *Nuovo Cim.* **37** (1965) 1241.

[19] J. Bailey et al., *Precise Measurement of the Anomalous Magnetic Moment of the Muon*, *Nuovo Cim.* **A9** (1972) 369.

[20] CERN-Mainz-Daresbury collaboration, J. Bailey et al., *Final Report on the CERN Muon Storage Ring Including the Anomalous Magnetic Moment and the Electric Dipole Moment of the Muon, and a Direct Test of Relativistic Time Dilation*, *Nucl. Phys.* **B150** (1979) 1.

[21] Muon g-2 collaboration, G. W. Bennett et al., *Measurement of the negative muon anomalous magnetic moment to 0.7 ppm*, *Phys. Rev. Lett.* **92** (2004) 161802 [`hep-ex/0401008`].

[22] Muon g-2 collaboration, J. Grange et al., *Muon (g-2) Technical Design Report*, `1501.06858`.

[23] D. W. Hertzog, *Next Generation Muon g2 Experiments*, *EPJ Web Conf.* **118** (2016) 01015 [`1512.00928`].

[24] J-PARC g-2/EDM collaboration, N. Saito, *A novel precision measurement of muon g-2 and EDM at J-PARC*, *AIP Conf. Proc.* **1467** (2012) 45.

[25] F. Jegerlehner, *Muon g-2 theory: The hadronic part*, *EPJ Web Conf.* **166** (2018) 00022 [`1705.00263`].

[26] Muon g-2 collaboration, G. W. Bennett et al., *Final Report of the Muon E821 Anomalous Magnetic Moment Measurement at BNL*, *Phys. Rev.* **D73** (2006) 072003 [`hep-ex/0602035`].

[27] F. Jegerlehner, *The anomalous magnetic moment of the muon*, vol. 274. Springer, 2017.

[28] T. Kinoshita and W. J. Marciano, *Theory of the muon anomalous magnetic moment*, *Adv. Ser. Direct. High Energy Phys.* **7** (1990) 419.

[29] A. Petermann, *Fourth order magnetic moment of the electron*, *Nucl. Phys.* **5** (1958) 677 .

[30] C. M. Sommerfield, *Magnetic dipole moment of the electron*, *Phys. Rev.* **107** (1957) 328.

[31] H. H. Elend, *On the anomalous magnetic moment of the muon*, *Phys. Lett.* **20** (1966) 682.

[32] M. Passera, *The Standard model prediction of the muon anomalous magnetic moment*, *J. Phys.* **G31** (2005) R75 [`hep-ph/0411168`].

[33] T. Kinoshita, *Quantum electrodynamics*, pp. 218–321. World Scientific, Singapore.

[34] J. A. Mignaco and E. Remiddi, *Fourth-order vacuum polarization contribution to the sixth-order electron magnetic moment*, *Il Nuovo Cimento A (1965-1970)* **60** (1969) 519.

[35] R. Barbieri and E. Remiddi, *Sixth Order electron and Muon (g-2) / 2 from Second Order Vacuum Polarization Insertion*, *Phys. Lett.* **49B** (1974) 468.

[36] R. Barbieri and E. Remiddi, *Electron and Muon (g-2)/2 from Vacuum Polarization Insertions*, *Nucl. Phys.* **B90** (1975) 233.

[37] R. Barbieri, M. Caffo and E. Remiddi, *A Sixth Order Contribution to the electron Anomalous Magnetic Moment*, *Phys. Lett.* **57B** (1975) 460.

[38] M. J. Levine, E. Remiddi and R. Roskies, *Analytic Contributions to the g Factor of the Electron in Sixth Order*, *Phys. Rev.* **D20** (1979) 2068.

[39] S. Laporta and E. Remiddi, *The Analytic value of the light-light vertex graph contributions to the electron (g-2) in QED*, *Phys. Lett.* **B265** (1991) 182.

[40] S. Laporta, *Analytical value of some sixth order graphs to the electron (g-2) in QED*, *Phys. Rev.* **D47** (1993) 4793.

[41] S. Laporta, *The Analytical value of the corner ladder graphs contribution to the electron (g-2) in QED*, *Phys. Lett.* **B343** (1995) 421 [`hep-ph/9410248`].

[42] S. Laporta and E. Remiddi, *Progress in the analytical evaluation of the electron (g-2) in QED: The Scalar part of the triple cross graphs*, *Phys. Lett.* **B356** (1995) 390.

[43] S. Laporta and E. Remiddi, *The Analytical value of the electron (g-2) at order α^3 in QED*, *Phys. Lett.* **B379** (1996) 283 [`hep-ph/9602417`].

[44] S. Laporta, *The analytical contribution of the sixth-order graphs with vacuum polarization insertions to the muon (g-2) in qed*, *Il Nuovo Cimento A (1965-1970)* **106** (1993) 675.

[45] S. Laporta and E. Remiddi, *The Analytical value of the electron light-light graphs contribution to the muon (g-2) in QED*, *Phys. Lett.* **B301** (1993) 440.

[46] M. Passera, *Precise mass-dependent QED contributions to leptonic g-2 at order α^2 and α^3*, *Phys. Rev.* **D75** (2007) 013002 [`hep-ph/0606174`].

[47] A. Czarnecki and M. Skrzypek, *The muon anomalous magnetic moment in qed: three-loop electron and tau contributions*, *Phys. Lett. B* **449** (1999) 354.

[48] T. Aoyama, M. Hayakawa, T. Kinoshita and M. Nio, *Tenth-Order Electron Anomalous Magnetic Moment — Contribution of Diagrams without Closed Lepton Loops*, *Phys. Rev.* **D91** (2015) 033006 [`1412.8284`].

[49] S. Laporta, *High-precision calculation of the 4-loop contribution to the electron g-2 in QED*, *Phys. Lett.* **B772** (2017) 232 [`1704.06996`].

[50] T. Aoyama, M. Hayakawa, T. Kinoshita and M. Nio, *Complete Tenth-Order QED Contribution to the Muon g-2*, *Phys. Rev. Lett.* **109** (2012) 111808 [`1205.5370`].

[51] T. Aoyama, M. Hayakawa, T. Kinoshita and M. Nio, *Tenth-order qed contribution to the electron $g-2$ and an improved value of the fine structure constant*, *Phys. Rev. Lett.* **109** (2012) 111807.

[52] R. Jackiw and S. Weinberg, *Weak interaction corrections to the muon magnetic moment and to muonic atom energy levels*, *Phys. Rev.* **D5** (1972) 2396.

[53] I. Bars and M. Yoshimura, *Muon magnetic moment in a finite theory of weak and electromagnetic interaction*, *Phys. Rev.* **D6** (1972) 374.

[54] G. Altarelli, N. Cabibbo and L. Maiani, *The Drell-Hearn sum rule and the lepton magnetic moment in the Weinberg model of weak and electromagnetic interactions*, *Phys. Lett.* **40B** (1972) 415.

[55] W. A. Bardeen, R. Gastmans and B. E. Lautrup, *Static quantities in Weinberg's model of weak and electromagnetic interactions*, *Nucl. Phys.* **B46** (1972) 319.

[56] K. Fujikawa, B. W. Lee and A. I. Sanda, *Generalized Renormalizable Gauge Formulation of Spontaneously Broken Gauge Theories*, *Phys. Rev.* **D6** (1972) 2923.

[57] T. V. Kukhto, E. A. Kuraev, Z. K. Silagadze and A. Schiller, *The Dominant two loop electroweak contributions to the anomalous magnetic moment of the muon*, *Nucl. Phys.* **B371** (1992) 567.

[58] A. Czarnecki, B. Krause and W. J. Marciano, *Electroweak Fermion loop contributions to the muon anomalous magnetic moment*, *Phys. Rev.* **D52** (1995) R2619 [`hep-ph/9506256`].

[59] A. Czarnecki, B. Krause and W. J. Marciano, *Electroweak corrections to the muon anomalous magnetic moment*, *Phys. Rev. Lett.* **76** (1996) 3267 [`hep-ph/9512369`].

[60] A. Czarnecki, W. J. Marciano and A. Vainshtein, *Triangle anomaly and the muon g-2*, *Acta Phys. Polon.* **B34** (2003) 5669 [`hep-ph/0310276`].

[61] Bouchiat, C. and Michel, L., *La résonance dans la diffusion méson méson le moment magnétique anormal du méson*, *J. Phys. Radium* **22** (1961) 121.

[62] L. Durand, *Pionic Contributions to the Magnetic Moment of the Muon*, *Phys. Rev.* **128** (1962) 441.

[63] S. J. Brodsky and E. De Rafael, *Suggested Boson - Lepton Pair Couplings and the Anomalous Magnetic Moment of the Muon*, *Phys. Rev.* **168** (1968) 1620.

[64] M. Gourdin and E. De Rafael, *Hadronic contributions to the muon g-factor*, *Nucl. Phys.* **B10** (1969) 667.

[65] F. Jegerlehner, *Variations on Photon Vacuum Polarization*, `1711.06089`.

[66] F. Jegerlehner, *Leading-order hadronic contribution to the electron and muon g2*, *EPJ Web Conf.* **118** (2016) 01016 [`1511.04473`].

[67] F. Jegerlehner and A. Nyffeler, *The Muon g-2*, *Phys. Rept.* **477** (2009) 1 [`0902.3360`].

[68] C. Aubin and T. Blum, *Calculating the hadronic vacuum polarization and leading hadronic contribution to the muon anomalous magnetic moment with improved staggered quarks*, *Phys. Rev.* **D75** (2007) 114502 [`hep-lat/0608011`].

[69] P. Boyle, L. Del Debbio, E. Kerrane and J. Zanotti, *Lattice Determination of the Hadronic Contribution to the Muon $g - 2$ using Dynamical Domain Wall Fermions*, *Phys. Rev.* **D85** (2012) 074504 [`1107.1497`].

[70] X. Feng, K. Jansen, M. Petschlies and D. B. Renner, *Two-flavor QCD correction to lepton magnetic moments at leading-order in the electromagnetic coupling*, *Phys. Rev. Lett.* **107** (2011) 081802 [`1103.4818`].

[71] T. Blum, P. A. Boyle, T. Izubuchi, L. Jin, A. Jttner, C. Lehner et al., *Calculation of the hadronic vacuum polarization disconnected contribution to the muon anomalous magnetic moment*, *Phys. Rev. Lett.* **116** (2016) 232002 [`1512.09054`].

[72] B. Chakraborty, C. T. H. Davies, P. G. de Oliviera, J. Koponen, G. P. Lepage and R. S. Van de Water, *The hadronic vacuum polarization contribution to a_μ from full lattice QCD*, *Phys. Rev.* **D96** (2017) 034516 [`1601.03071`].

[73] D. Giusti, F. Sanfilippo and S. Simula, *The light-quark contribution to the leading HVP term of the muon $g - 2$ from twisted-mass fermions*, `1808.00887`.

[74] B. e. Lautrup, A. Peterman and E. de Rafael, *Recent developments in the comparison between theory and experiments in quantum electrodynamics*, *Phys. Rept.* **3** (1972) 193.

[75] G. Backenstoss, B. D. Hyams, G. Knop, P. C. Marin and U. Stierlin, *Helicity of μ- Mesons from π-Meson Decay*, *Phys. Rev. Lett.* **6** (1961) 415.

[76] G. Backenstoss, B. D. Hyams, D. Knop, P. C. Marin and U. Stierlin, *The scattering of 8 GeV/c μ mesons on electrons*, in *Proceedings, Confrence Internationale d'Aix-en-Provence sur les Particules Elementaires: Aix-en-Provence, France, Sep 14-20, 1961*, vol. Vol.1, pp. 147–150, 1962.

[77] T. B. W. Kirk and S. H. Neddermeyer, *Scattering of high-energy positive and negative muons on electrons*, Phys. Rev. **171** (1968) 1412.

[78] P. L. Jain and N. J. Wixon, *Scattering of high-energy positive and negative muons on electrons*, *Phys. Rev. Lett.* **23** (1969) 715.

[79] R. F. Deery and S. H. Neddermeyer, *Cloud-chamber study of hard collisions of cosmic-ray muons with electrons*, Phys. Rev. **121** (1961) 1803.

[80] I. B. McDiarmid and M. D. Wilson, *The production of high-energy knock-on electrons and bremsstrahlung by μ-mesons*, Canadian J. of Phys. **40** (1962) 698.

[81] N. Chaudhuri and M. S. Sinha, *Production of knock-on electrons by cosmic-ray muons underground (148 m we)*, Nuovo Cim. (1955-1965) **35** (1965) 13.

[82] P. D. Kearney and W. E. Hazen, *Electromagnetic interactions of high-energy muons*, Phys. Rev. **138** (1965) B173.

[83] K. P. Schuler, *A Muon polarimeter based on elastic muon electron scattering*, *AIP Conf. Proc.* **187** (1989) 1401.

[84] D. Adams, B. Adeva, T. Akdogan, E. Arik, A. Arvidson, B. Badelek et al., *Measurement of the SMC muon beam polarisation using the asymmetry in the elastic scattering off polarised electrons*, Nuclear Instruments and Methods in Physics Research Section A **443** (2000) 1.

[85] A. I. Nikishov, *Radiative corrections to the scattering of μ mesons on electrons*, Sov. Phys. JETP **12** (1961) .

[86] K. E. Eriksson, *On radiative corrections due to soft photons*, *Il Nuovo Cimento (1955-1965)* **19** (1961) 1010.

[87] K. E. Eriksson, B. Larsson and G. A. Rinander, *Radiative corrections to muon-electron scattering*, Nuovo Cim. (1955-1965) **30** (1963) 1434.

[88] P. Van Nieuwenhuizen, *Muon-electron scattering cross-section to order α^3*, *Nucl. Phys.* **B28** (1971) 429.

[89] T. V. Kukhto, N. M. Shumeiko and S. I. Timoshin, *Radiative Corrections in Polarized Electron Muon Elastic Scattering*, *J. Phys.* **G13** (1987) 725.

[90] D. Yu. Bardin and L. Kalinovskaya, *QED corrections for polarized elastic μe scattering*, `hep-ph/9712310`.

[91] N. Kaiser, *Radiative corrections to lepton-lepton scattering revisited*, *J. Phys.* **G37** (2010) 115005.

[92] E. Derman and W. J. Marciano, *Parity Violating Asymmetries in Polarized Electron Scattering*, *Ann. Phys.* **121** (1979) 147.

[93] G. D'Ambrosio, *Electron Muon Scattering in the Electroweak Unified Theory*, *Lett. Nuovo Cim.* **38** (1983) 593.

[94] J. C. Montero, V. Pleitez and M. C. Rodriguez, *L - R asymmetries and signals for new bosons*, *AIP Conf. Proc.* **490** (1999) 397 [`hep-ph/9903317`].

[95] P. Mastrolia, M. Passera, A. Primo and U. Schubert, *Master integrals for the NNLO virtual corrections to μe scattering in QED: the planar graphs*, *JHEP* **11** (2017) 198 [`1709.07435`].

[96] P. Mastrolia, M. Passera, A. Primo, U. Schubert and W. J. Torres Bobadilla, *On μe-scattering at NNLO in QED*, *EPJ Web Conf.* **179** (2018) 01014.

[97] S. Di Vita, S. Laporta, P. Mastrolia, A. Primo and U. Schubert, *Master integrals for the NNLO virtual corrections to μe scattering in QED: the non-planar graphs*, `1806.08241`.

[98] M. Fael, *Hadronic corrections to μ-e scattering at NNLO with space-like data*, `1808.08233`.

[99] F. Bloch and A. Nordsieck, *Note on the Radiation Field of the electron*, *Phys. Rev.* **52** (1937) 54.

[100] T. Kinoshita, *Mass singularities of Feynman amplitudes*, *J. Math. Phys.* **3** (1962) 650.

[101] T. D. Lee and M. Nauenberg, *Degenerate Systems and Mass Singularities*, *Phys. Rev.* **133** (1964) B1549.

[102] R. Mertig, M. Böhm and A. Denner, *Feyn Calc - Computer-algebraic calculation of Feynman amplitudes*, *Comp. Phys. Comm.* **64** (1991) 345 .

[103] V. Shtabovenko, R. Mertig and F. Orellana, *New developments in FeynCalc 9.0*, *Comp. Phys. Comm.* **207** (2016) 432 .

[104] T. Hahn and M. Prez-Victoria, *Automated one-loop calculations in four and D dimensions*, *Comp. Phys. Comm.* **118** (1999) 153 .

[105] G. J. van Oldenborgh and J. A. M. Vermaseren, *New algorithms for one-loop integrals*, *Zeitschrift für Physik C* **46** (1990) 425.

[106] J. Romao, *Modern Techniques for One-Loop Calculations*, `https://porthos.tecnico.ulisboa.pt/OneLoop/one-loop.pdf` .

[107] R. Barbieri, J. A. Mignaco and E. Remiddi, *Electron Form Factors up to Fourth Order - I*, *Nuovo Cim.* **11 A** (1972) 824.

[108] M. V. Terent'ev, *Application of the dispersion relations technique to the calculation of the magnetic moment of the electron*, *Sov. JETP* **16** (1963) 444.

[109] R. K. Ellis and G. Zanderighi, *Scalar one-loop integrals for QCD*, *JHEP* **02** (2008) 002 [`0712.1851`].

[110] G. 't Hooft and M. J. G. Veltman, *Scalar One Loop Integrals*, *Nucl. Phys.* **B153** (1979) 365.

[111] W. Beenakker and A. Denner, *Infrared Divergent Scalar Box Integrals With Applications in the Electroweak Standard Model*, *Nucl. Phys.* **B338** (1990) 349.

[112] M. D. Schwartz, *Quantum Field Theory and the Standard Model*. Cambridge University Press, 2014.

[113] `http://www-com.physik.hu-berlin.de/~fjeger/software.html`.

[114] K. Melnikov, *On the theoretical uncertainties in the muon anomalous magnetic moment*, *Int. J. Mod. Phys.* **A16** (2001) 4591 [`hep-ph/0105267`].

[115] L. L., *Polylogarithms and associated functions*. Elsevier, North Holland, Inc., New York, N.Y., 1981.

[116] G. Passarino and M. J. G. Veltman, *One Loop Corrections for $e^+ e^-$ Annihilation Into $\mu^+ \mu^-$ in the Weinberg Model*, *Nucl. Phys.* **B160** (1979) 151.

[117] A. Denner, *Techniques for calculation of electroweak radiative corrections at the one loop level and results for W physics at LEP-200*, *Fortsch. Phys.* **41** (1993) 307 [`0709.1075`].